Diss ETH Nr. 14724

IN SITU REMOVAL OF IRON FROM GROUND WATER: Fe (II) OXYGENATION, AND PRECIPITATION PRODUCTS IN A CALCAREOUS AQUIFER

A dissertation submitted to the
SWISS FEDERAL INSTITUTE OF TECHNOLOGY ZÜRICH

for the degree of
DOCTOR OF NATURAL SCIENCES

presented by
SUZANNE METTLER
Dipl. Natw. ETH
born November 17th, 1968
citizen of Urnäsch (AR), Switzerland

accepted on the recommendation of
Prof. Bernhard Wehrli, examiner
Prof. Wolfgang Kinzelbach, co-examiner
Dr. Urs von Gunten, co-examiner

Zürich 2002

MERCI !

Urs von Gunten danke ich für sein fachliches und persönliches Engagement, das er mir im Lauf der Diss-Zeit und auch während seinem Auslandaufenthalt wiederholt gezeigt hat. Bernhard Wehrli hat mit seiner unkomplizierten Art ein sehr angenehmes, der Forschung dienendes Klima geschaffen. Die Gespräche mit Wolfgang Kinzelbach insbesondere sein schrittweises Vorgehen brachten nicht nur mir mehr Verständnis und Klarheit für das Fachgebiet. Beiden danke ich für ihre verstärkte Unterstützung während der Abwesenheit von Urs. Ebenfalls in dieser Zeit, habe ich die Tips und Anregungen von Stefan Hug als sehr hilfreiche und wichtige Beiträge ganz besonders geschätzt.

Für die Interpretation und die Analyse der Daten, für weiterführende Analysen und anregende Gespräche danke ich Arnold Stahel, Denis Mavrocordatos, Eduard Hoehn, Jürg Zobrist, Mustapha Abdelmoula, Peter Weidler und Silvio Canonica. René Schönenberger hat die sonst langen Arbeitstage an der Glove Box wirkungsvoll verkürzt. Mit David Kistler, Elisabeth Salhi, Jürgen Schindler, Marianne Erbs, Martin Elsner, Stefan Rübli, Hermann Mönch habe ich neues Fachwissen und Techniken lernen oder auffrischen können.

Das Klima in der Trinkwassergruppe mit Yves, Conrad, Hervé, Lisa, Juan, Nadya, Marc & Marc und Pascal war stets freundschaftlich und abwechslungsreich, manchmal auch sehr lustig. Zeitweise brachten wir es sogar zu einer frankophonen Mehrheit. Die erweiterte Gruppe WUT und EAWAG lieferten einen fast unerschöpflichen Rahmen teils für fachlichen Austausch, teils für gemeinsame Aktivitäten und Unterhaltung. Dafür trugen die einzelnen Personen Laura, Martin, Marianne, Thomas, Ignaz, Marianne, Annette, Lukas, Diane, Isabel, Olivier, Ursi, Johannes, Frank, Laurence, Monika, Edith, Annette, Céline, Sebastien, Séverine, Monika erheblich bei. Sei es beim Joggen, Schwimmen in der Badi Dübendorf, Grillen am Greifensee, in der Kaffeepause oder auf dem Flur. Daraus entstanden zum Teil langjährige Freundschaften.

Alles wäre viel schwieriger oder kaum möglich gewesen ohne die liebende und geduldige Unterstützung meiner Eltern. Herzlichen Dank auch meinen Brüdern, meinen Freundinnen und Freunden, sowie meinem lieben Pepe, die alle unsichtbar mitgewirkt haben.

This doctoral thesis was supported by the Comission for Technology and Innovation (KTI grant N° 3443.2).

I thank the Fondation Labor et Pax for its generous support.

ZUSAMMENFASSUNG

Bei der Gewinnung von Grundwasser wird eine Enteisenung und eine Entmanganung empfohlen, wenn die gelösten Höchstkonzentrationen an Eisen (Fe(II)), respektive Mangan (Mn(II)) 0.3 mg/L, bzw. 0.05 mg/L übersteigen. Die Entfernung von Eisen und Mangan wird durch die Oxidation der zweiwertigen Ionen eingeleitet. Die darauf folgende Hydrolyse führt zu gut filtrierbaren Eisen- und Manganoxidausfällungen (Fe- und Mn- Oxid). Im Unterschied zur konventionellen Aufbereitung findet bei der *in situ* Grundwasseraufbereitung die Fe- und Mn-Ausfällung im Aquifer statt. Dafür ist eine Ausfällungszone im Umkreis des Brunnens vorgesehen. Jedoch gibt es Bedenken, dass die zunehmenden Fe- und Mn- Ausfällungen den Aquifer teilweise verstopfen könnten. Zudem sind die Mechanismen, die unter diesen Umständen zu Ausfällungen führen ungenügend geklärt. Eine Optimierung des Betriebs ist damit schwierig. Die vorliegende Untersuchung geht diesen beiden Fragen nach.

In einer Feldstudie in La Neuveville (BE) wurde der kalkhaltige Aquifer einer 10-jährigen Enteisenungs- und Entmanganungsanlage auf Eisen- und Manganausfällungen untersucht. Die Eisen- und Mangankonzentrationen sowie der Oxidationszustand der Metalle wurden mittels selektiver Auflösungsmethoden (saure und reduktive Auflösungen mit Salzsäure, Ascorbinsäure und Ti(III)-EDTA), sowie mit Röntgendiffraktion und Mössbauer Spektroskopie untersucht. Die Manganresultate ergaben, dass Mn(II) zum grössten Teil nicht oxidiert wurde, sondern als Mn(II), vermutlich als Mangancarbonat oder gemischtes Calcit-Mangancarbonat, gefällt wurde. Eine reine Manganphase konnte nicht identifiziert werden. Die Eisenmessungen zeigten, dass 50-80% des Eisens aus kristallinem Fe-oxid bestand, das als Goethit bestimmt werden konnte. Die Verteilung der Eisen- und Mangankonzentrationen zeigte eine deutliche Korngrössenabhängigkeit: Proben aus feinen Partikeln enthielten hohe Konzentrationen und solche aus groben Partikeln geringe Konzentrationen. Diese Tendenz war für

Eisen stärker ausgeprägt als für Mangan; sie weist auf einen oberflächenabhängigen Ausfällungsmechanismus hin.

Die bestimmten Konzentrationen des ausgefällten Fe und Mn stimmten mit einer Schätzung basierend auf der Massenbilanz gut überein. Sie betrugen ca. das Zweifache der Fe- und Mn-Hintergrundkonzentration. Die gleichmässige Konzentrationsverteilung der Proben deutet auf eine homogene Ausfällung von Fe und Mn in der Ausfällungszone hin. Eine gleichmässige Verteilung von Fe und Mn in der Ausfällungszone sowie die Bildung eines dichten kristallinen Fe-oxids wie Goethit sollte das Verstopfungsrisiko minimieren.

Da besonders hohe Goethitkonzentrationen zusammen mit Karbonatmineralien (Calcit und Dolomit) vorkamen, wurde der Einfluss von Calcit auf die Bildung von Fe-Oxiden in Laborexperimenten getestet. Die Wechselwirkung von Fe(II) mit Calcit wurde mit und ohne Sauerstoff untersucht. Verlängerte Reaktionszeiten von Fe(II) mit Calcit führten zur Bildung einer gemischten Fe(II)-Calciumcarbonat Phase, für die ein Molverhältnis, Fe(II)/Ca, von 0.4 % bestimmt wurde. Die Oxidation von Fe(II) mit Sauerstoff lief in Anwesenheit von Calcit schneller ab als unter homogenen Bedingungen (ohne Festphase). In einem System hingegen in dem Eisen und Calcit während längerer Zeit equilibriert wurden (>15 Stunden), konnte keine Beschleunigung beobachtet werden, zudem wurde Fe(II) nicht vollständig oxidiert. Unvollständige Oxidation von Fe(II) wird mit einer Inkorporation des Fe(II) im Calcit erklärt, das eingeschlossene Fe(II) wird damit vor dem Sauerstoff teilweise geschützt. Eine Calcitsuspension, die schrittweise durch wiederholte Fe(II) Zugabe und anschliessende Oxidation mit Fe(III) angereichert wurde, beschleunigte die Fe(II) Oxidation sogar stärker als reines Calcit oder Goethit. Die so entstandenen kleinen Fe(III)-oxide Clusters zeichnen sich durch ein grosses Oberfläche zu Volumen Verhältnis aus, dadurch vermögen sie oberflächenkatalysierte Reaktionen noch stärker zu beschleunigen. Leider konnten diese reaktiven Fe(III)-oxide spektroskopisch nicht identifiziert werden. Mithilfe der selektiver Auflösungsmethoden wurden sie als amorphe Fe(III)-oxide bestimmt.

Ähnliche Experimente wie im Fe(II)-Calcit-O_2 System wurden mit Goethit anstelle von Calcit durchgeführt (Fe(II)-Goethit-O_2). Beide Systeme wurden dann aneinander gegenübergestellt. Goethit wies eine grössere Adsorptionskapazität als Calcit auf (3 versus 0.6 Fe(II) Sites /nm^2). Die Oxidationsrate von Fe(II) in Anwesenheit von Goethit war schneller als mit Calcit (um einen Faktor 100, wenn sich die Rate auf die Masse bezieht oder um einen Faktor 3, wenn sie sich auf die Adsorptionskapazität bezieht).

Aus den Resultaten wird vorgeschlagen, dass heterogene Oxidation mit anschliessender Fällung zu Fe(III)-oxid zur Entfernung von Fe(II) aus dem Grundwasser führt. In einem ersten Schritt wird Fe(II) an einer natürlichen Oberfläche des Aquifers adsorbiert. Durch die darauf folgende Oxidation wird das adsorbierte Fe(II) an Ort zu Fe-Oxid gefällt. Die gebildeten Fe-Oxide haben ein grosse Adsorptionskapazität und beschleunigen die Fe(II) Oxidation. Nach fortgesetztem Betrieb der Anlage entsteht allmählich eine Schicht von Fe-Oxiden auf den Oberflächen des Aquifers, welche die Ausfällungszone in einen effizienten Enteisenungsfilter verwandelt. In einem Grundwassersystem mit reduzierenden Bedingungen werden beschränkte Mengen Sauerstoff schnell durch konkurrierende Oxidationsreaktionen gezehrt. Unter diesen Bedingungen kann eine oxidative Fällung von Fe(II) nur durch eine besonders rasche Fe(II) Oxidation stattfinden.

Die oberflächenkatalysierte Ausfällung von Fe(II) führt zu einem allmählichen Wachstum von Fe-Oxiden auf den natürlichen Oberflächen des Aquifers. Im Gegensatz dazu bildet die homogene Fe(II) Oxidation voluminösere Ausfällungen. Die kontrollierte Ausfällung des Fe(II) zusammen mit einer grosszügigen Dimensionierung der Ausfällungszone in einem homogenen Aquifers sollten ein frühzeitiges Verstopfen des Aquifers verhindern. Mit einer Massenbilanz kann das benötigte Volumen der Ausfällungszone einfach abgeschätzt werden.

ABSTRACT

Iron and manganese removal from ground water is recommended when the dissolved concentrations exceed 0.3 mg/L iron (Fe(II)) and 0.05 mg/L manganese (Mn(II)). Removal is generally achieved by oxidation of the bivalent cation. Consecutive hydrolysis of the oxidized cation and polymerization finally lead to precipitates, which can be removed by filtration. *In situ* ground water treatment differs from conventional ground water treatment because removal of iron and manganese takes place in the underground, in a precipitation zone around the extraction well. The main concern of this treatment method is clogging of the aquifer by the precipitates. Also the mechanisms of the involved processes are not well documented and therefore optimization is difficult. The present study adresses both issues.

A field study was performed on a treatment plant, located in a calcareous aquifer in La Neuveville (BE), which had been operating for 10 years. The aquifer was sampled and analyzed for manganese and iron precipitates. Concentrations and oxidation state of the metals were determined with selective chemical extraction methods like acid dissolution (5M HCl) or reductive dissolution (Ti(III)-EDTA, ascorbic acid) as well as X-ray diffraction and Mössbauer spectroscopy.

Manganese was found predominantly as Mn(II), indicating that it had not been oxidized. No pure manganese phases were identified; it was concluded that manganese is co-precipitated with calcite to carbonate minerals. Most of the analyzed iron (50-80%) consisted of oxidized Fe(III) in the form of goethite, a crystalline ferric oxide. The iron and, to a lesser extent, the manganese content of the samples varied as a function of their grains sizes: the largest metal concentrations were found in the samples with the smallest particles, which are characterized by a larger surface to volume ratio. This points to a surface dependent precipitation mechanism. The amount of the precipitated iron and manganese correlated well with values estimated from a mass balance.

Moreover, an even distribution of the Fe and Mn precipitates among the samples was observed. A rather homogeneous precipitation of Fe and Mn in the precipitation zone together with the formation of a dense crystalline Fe-Oxide indicate a low risk of clogging.

Since largest amount of goethite were found associated with carbonate minerals (calcite and dolomite), the influence of calcite on the formation of Fe(III)-oxides was tested in laboratory experiments. The interaction of Fe(II) with calcite was investigated in the absence and in the presence of oxygen. Extended equilibration times of Fe(II) with calcite lead to the formation of a mixed Fe(II)/Ca-carbonate, with a mole ratio Fe/Ca of 0.4 %. The oxygenation of Fe(II) adsorbed to calcite is accelerated compared to a homogeneous system. However, if Fe(II) is equilibrated for several hours with calcite before oxygenation (> 15 hours), an acceleration is not observed. Moreover, Fe(II) is not completely oxidized. This can be explained by an incorporation of Fe(II) into the calcite phase, which results in a protection of Fe(II) against oxidation. When small increments of Fe(II) are added to calcite and then are oxygenated, the suspension becomes a better catalyst of the Fe(II) oxygenation than either calcite alone or goethite alone. This is probably due to the formation of small clusters of ferric oxides (very high specific surface area). Unfortunately, these ferric oxides could not be identified by spectroscopic methods. Their dissolution behavior resembles amorphous ferric oxide.

The system Fe(II)-calcite-O_2 was compared to a similar system Fe(II) goethite-O_2. On a time scale of 24 hours, goethite has a larger adsorption capacity than calcite (3, versus 0.6 sites / nm^2). The rate of oxygenation of Fe(II) on goethite is faster than on calcite (factor 100 or 3 depending on whether the rates are normalized to the mass of the solid or to its surface site concentration).

As a result from our studies we propose that the removal of Fe(II) is due to a heterogeneous oxygenation precipitation mechanism. In a first step the dissolved Fe(II) from the reduced ground water is adsorbed at the natural surfaces of the aquifer matrix. In the consecutive oxygenation step it is locally precipitated as ferric oxides onto the surface. The freshly formed ferric oxides are characterized by a particularly large adsorption capacity, in addition they dramatically accelerate the oxygenation of Fe(II). In summary, the ferric oxide coatings, which have been produced during ongoing operation of the *in situ* treatment plant, transform the precipitation zone into a highly efficient filter zone. Rapid oxygenation kinetics is decisive in a system, where other competing reduced species rapidly consume the limited amount of oxygen.

Such a surface dependent precipitation of Fe(II) leads to a gradual growth of Fe-oxides at the aquifer surfaces. It contrasts to the bulky precipitates formed by homogeneous oxygenation of Fe(II). The controlled growth of Fe-oxides on the aquifer matrix together with a generous dimensioning of the volume of the precipitation zone in a homogeneous aquifer should prevent clogging of the aquifer. It could be shown that mass balance is a useful and simple tool to estimate the necessary volume of the precipitation zone.

TABLE OF CONTENT

1 INTRODUCTION 1

1.1 Iron and manganese removal from ground water 1
1.1.1 The "iron calamity" 1
1.1.2 Iron and manganese in ground water 2
1.1.3 Removal of iron and manganese 7
1.1.4 Open questions 19
1.1.5 Focus of this study 21

2 CHARACTERIZATION OF IRON AND MANGANESE PRECIPITATES FROM AN *IN SITU* GROUND WATER TREATMENT PLANT 23

2.1 Introduction 23
2.2 La Neuveville site 26
2.3 Materials and Methods 27
2.3.1 Aquifer sample selection 27
2.3.2 Analytical methods 28
2.4 Results and Discussion 31
2.4.1 Grain size distribution of the aquifer material 31
2.4.2 Extraction by 5M HCl (Fe_{tot}, Fe(II), Mn_{tot}) 32
2.4.3 Reductive dissolution experiments 34
2.4.4 Identification of Fe-oxides by XRD 37
2.4.5 Mössbauer Spectroscopy 41
2.4.6 Comparison of the results from the different analytical methods 42
2.4.7 Accumulation of iron and manganese in the aquifer 44
2.4.8 Risk of clogging 46
2.5 Conclusions 47

3 SORPTION AND OXYGENATION OF Fe (II) IN CALCITE SUSPENSIONS 49

3.1 Introduction 49
  3.1.1 Adsorption of cations on carbonate minerals 49
  3.1.2 Interaction of Fe(II) with $CaCO_3$ 50
  3.1.3 Mineralogy of Fe(II)/Ca carbonate 51
  3.1.4 Ferrous iron oxygenation: kinetics and product formation ... 52
  3.1.5 Deferrisation for drinking water production 53
3.2 Materials and Methods 54
  3.2.1 Chemicals 54
  3.2.2 Preparation of the calcite suspension 55
  3.2.3 Analytical methods 56
  3.2.4 Characterization of the solids 57
  3.2.5 Sorption experiments 58
  3.2.6 Desorption of Fe(II) with ligand 58
  3.2.7 Dissolution kinetics with CO_2 58
  3.2.8 Fe(II) oxygenation kinetics in calcite suspensions 59
  3.2.9 Products of oxygenation of Fe(II) in calcite suspensions 59
3.3 Results and discussion 60
  3.3.1 Adsorption kinetics 60
  3.3.2 Fe(II) sorption capacity on calcite 63
  3.3.3 Remobilization of Fe(II) adsorbed to calcite 68
  3.3.4 Homogeneous and heterogeneous oxygenation kinetics of Fe(II) in presence and in absence of calcite. 76
  3.3.5 Adsorption versus oxygenation kinetics of Fe(II) in presence of calcite 78
  3.3.6 Repeated adsorption and oxygenation of Fe(II) in calcite suspensions 82
  3.3.7 Analysis of the Fe oxides produced after repeated addition and oxidation of Fe(II) in calcite suspensions 84
  3.3.8 Heterogeneous oxygenation kinetics of Fe(II) 85
3.4 Summary 87

4 ADSORPTION AND OXYGENATION OF Fe (II) IN PRESENCE OF GOETHITE 91

4.1 Introduction 91
  4.1.1 Ion adsorption on goethite 92
  4.1.2 Adsorption and oxidation of Fe(II) on goethite 94
  4.1.3 Fe(II) adsorption kinetics 99
  4.1.4 Sorption reversibility 100
  4.1.5 Effect of the major ions HCO_3^-, Ca^{2+} and Mg^{2+} 101

4.2 Materials and methods 103
  4.2.1 Reagents 103
  4.2.2 Analytical and experimental methods 104

4.3 Results and Discussion 106
  4.3.1 Adsorption experiments 106
  4.3.2 Fe(II) oxygenation 113
  4.3.3 Heterogeneous oxidation of Fe(II): Comparison of the goethite with the calcite system 118

4.4 Conclusions 121

5 CONCLUSIONS AND OUTLOOK 123

5.1 Fe(II) removal from ground water by heterogeneous oxidation and precipitation 123

5.2 Manganese removal 125

5.3 In situ deferrisation and risk of clogging the aquifer.... 126

5.4 Outlook 127

APPENDIX 129

Binding constants 129

In situ treatment plants worldwide 129

REFERENCES 131

CURRICULUM VITAE 146

1

INTRODUCTION

1.1 Iron and manganese removal from ground water

1.1.1 The “iron calamity”

At the end of the 19th century growing population and waste water problems led to contamination of surface waters with, sometimes, dramatic consequences, when these were used for drinking water. In Zürich due to a contamination of fresh water by wastewater a typhus outbreak happened in 1884. The city council decided then to buy the springs of the Sihl and the Lorze valleys, situated in the neighboring canton Zug, and built the pipes to bring the clean water downtown. Today this water still supplies the city fountains.

In Germany, the cities of Halle, Leipzig, Frankfurt a. O., Potsdam, Charlottenburg, Berlin-Tegel were confronted with similar problems, but they did not have such a fresh water reservoir in their neighborhood. They also invested in new water sources, installed pumps, wells and reservoirs to supply ground water from the aquifer. After a few days in the reservoirs, the ground water, however, turned reddish to black and hosted an increasing number of microorganisms. The color of these waters was due to precipitation of iron(III) and manganese(III,IV) oxides. This is known since then as the “iron calamity”.

These events led to the development of iron and manganese removal technologies with the first operating installation in Germany

(Charlottenburg) in 1874. In the US, the first plant was built in 1883 at Atlantic Highlands (New Jersey). The first plant that removed manganese along with iron, was completed in 1889 in Zuphten, Holland (O'Connor, 1971). Development of *in situ* technologies date from the same time, the first *in situ* iron removal plant was built in Berlin, Germany in 1898/99 (Olthoff, 1986).

1.1.2 Iron and manganese in ground water

Iron and manganese are the most widespread metals found in the earth crust. Iron comes first with a concentration of 6.2 % (w/w), it is followed by titanium and manganese (0.106 %) (Greenwood and Earnshaw, 1990). At the earth surface, iron and manganese are found predominantly as oxides or oxy-hydroxides. In the oxidized form (oxidation state > II) they are hardly soluble: in surface waters, concentrations as small as 10^{-9} M were measured (Stumm and Morgan, 1996; Emmenegger, 1999). In aquatic systems, both iron and manganese take part in redox reactions and can be reduced to the more soluble bivalent forms, Fe(II) or Mn(II).

1.1.2.1 Iron oxides

In the following text Fe- (or Mn-) oxides is used for both “oxyhydroxide” and “oxide” for simplification, unless the distinction is emphasized.
The term “Fe-oxides” is mostly used for trivalent iron (Fe(III)), however mixed Fe(II)/Fe(III) phases exist as well. So far fifteen different Fe-oxyhydroxides have been identified, partly as oxide (Fe_2O_3) or as oxyhydroxides (FeOOH) (Schwertmann and Cornell, 2000). All these Fe-oxides consist of iron bound to oxygen (“-oxy”) and hydroxyl ions (“hydroxide”). The structural unit of the Fe-oxides is an octahedron. The Fe(III) forms the center of the octahedron, it is surrounded at the 6 corners by either O or OH. The most common Fe- oxyhydroxides found in our environment are ferrihydrite, goethite and lepidocrocite. Ferrihydrite, goethite (α-FeOOH) and lepidocrocite (γ-FeOOH) differ only in the way the octahedrons are arranged to each other and how well

they are ordered (crystallinity. See Table 1-1). Another distinctive mark of the Fe-oxides is the color, which varies from yellow over red to brown or black (Cornell and Schwertmann, 1996; Schwertmann and Cornell, 2000).

Ferrihydrite

Ferrihydrite is the least crystalline of the three Fe-oxides. Its structure is not fully understood, probably it is formed by hexagonally close-packed oxygen planes with Fe in octahedral interstices. The low crystallinity of ferrihydrite is due partly to vacant Fe sites and partly to the replacement of oxygen by H_2O or OH. Based on the number of X-ray peaks, the 2-line ferrihydrite can be distinguished from the better-ordered 6-line ferrihydrite. Ferrihydrite is formed by fast oxidation of Fe(II) followed by fast hydrolysis of Fe(III). It is ubiquitous as very reactive solid with a large specific surface area (>200 m^2/g). Ferrihydrite ages and transforms to the thermodynamically more stable goethite (α-FeOOH) or hematite (α-Fe_2O_3).

Table 1-1
Some properties and crystal structure of selected Fe-oxides (Schwertmann and Cornell, 2000).

	Ferrihydrite	**Goethite** **α-FeOOH**	**Lepidocrocite** **γ-FeOOH**
Color	brown	yellow	orange
Crystal structure	Low crystallinity	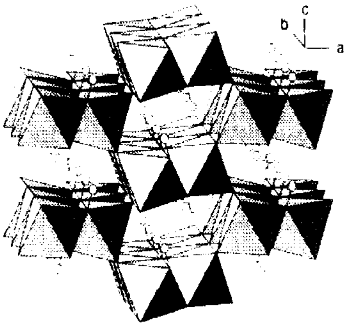	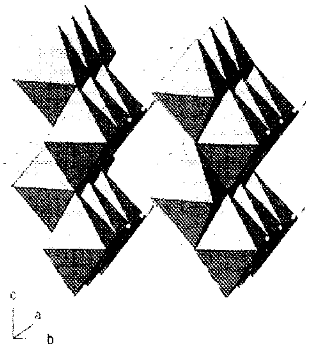
Solubility product (pK) $Fe(OH)_3$ (s) ⇔ Fe^{3+} + $3OH^-$	37-39.4	43.3-44	40.6-42.5

Goethite (α-FeOOH).

Goethite is thermodynamically the most stable of the three Fe-oxides. It is formed by slow oxidation of Fe(II) from solution at neutral pH, followed by the nucleation and crystal growth of the Fe(III) precipitate. The formation of goethite is favored in carbonate rich environments. Goethite is built by an edge-sharing double-band of octahedra, which alternate in orientation and are linked by corner sharing (seeTable 1-1). The tunnels are large enough for protons only. The O and OH form hexagonally close-packed layers.

Lepidocrocite (γ-FeOOH).

Lepidocrocite forms at lower pH (6 > pH > 7) by slow oxidation of Fe(II). It is also built by edge-sharing double band of octahedra, which form zigzag layers interconnected by OH-bound (cp. Table 1-1). The O and OH are arranged as cubic close-package.

1.1.2.2 Manganese oxides

There are several Mn- oxides and oxy-hydroxides (Burns and Burns, 1979; Graham et al., 1988; Friedl, 1995). Manganese occurs, in the di- and trivalent oxidation state, as well as in the quadrivalent oxidation state. Similarly to iron, Mn(II) is well soluble, whereas Mn(III) and Mn(IV) occur mostly as solids. Like for the Fe-oxides, the structural unit is a Mn octahedron surrounded by six oxygens (or hydroxyl ions). The initial product of the chemical Mn(II) oxygenation is either hausmannite ($Mn^{II,III}_3O_4$), feitknechite (β-$Mn^{III}OOH$) or manganite (γ-$Mn^{III}OOH$. Murray et al., 1985; Junta and Hochella, 1994). In natural systems, however, such as in lakes, seas and ground water, often quadrivalent manganese dioxides are found (Piper et al., 1984; Murray et al., 1984; Friedl et al., 1997). An explanation of this finding may be a disproportionation of the pseudo-stable Mn(III)- oxides to Mn(IV) and Mn(II). Alternatively, Mn(II) oxidation can be catalyzed by microorganisms, which produce Mn(IV) by a two-electron oxidation process (Mandernack et al., 1995b; Wehrli et al., 1995; Tebo et al., 1997; Bargar et al., 2000). The reaction product of the biologically mediated Mn(II) oxidation is a δ-MnO_2, which transforms into birnessite after 2-3 days (Bargar et al., 2000). Birnessite consists of layers of edge-sharing octahedra. Charge imbalance due to site vacancies is compensated by cations (Na^+, K^+, Mg^{2+}) (Friedl et al., 1997; Figure 1-1).

Figure 1-1
Birnessite (Friedl, 1995)

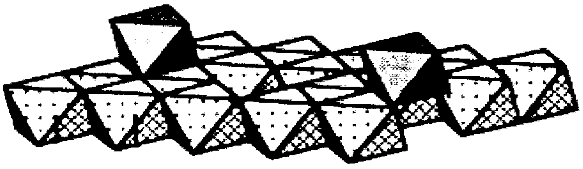

1.1.2.3 Dissolution of Fe- and Mn- oxides

In the natural aquatic systems microbially mediated reduction of the Fe and Mn -oxides can take place in the absence of oxygen and nitrate. This obeys the sequence of redox reactions for the oxidation of organic matter. The strongest locally available oxidant is exploited first, once depleted, the second strongest is reduced and so on. In environmental systems the sequence of the predominant oxidants is: $O_2 > NO_3 > MnO_2 > FeOOH > SO_4^{2-} > CH_4$ (Stumm and Morgan, 1996). Therefore, when the oxygen has been consumed, the dissolved organic matter (DOM, is measured as dissolved organic carbon, DOC) is oxidized by the next available oxidants, first nitrate, then Fe- and Mn- oxides. In the last case Fe- and Mn- oxides are reduced to Fe(II) and Mn(II). In the following equation the DOM is represented as "$\{CH_2O\}$", an oxidizable carbon species.

$$1\{CH_2O\} + 4FeOOH\ (s) + 8H^+ \Rightarrow 1CO_2 + 7H_2O + 4Fe(II) \qquad (1\text{-}1)$$

$$1\{CH_2O\} + 2MnO_2\ (s) + 4H^+ \Rightarrow 1CO_2 + 3H_2O + 2Mn(II) \qquad (1\text{-}2)$$

Such electron transfer processes are mediated by microorganisms (Lovley, 1987; Lovley and Phillips, 1988; von Gunten and Zobrist, 1993; Straub et al., 2001). In the bivalent form, Fe(II) and Mn(II) are well soluble, concentrations of several mg/L can be reached in reduced ground water (10^{-5}-10^{-3} M; see also Table 1-2). As bivalent ions their solubility is controlled by the solid carbonates siderite ($FeCO_3$) and rhodocrosite ($MnCO_3$) or by sulfides (FeS, FeS_2 and MnS). In reduced environment supersaturation of Fe(II) with respect to siderite is often found (Postma, 1981; Wajon et al., 1985; Wersin et al., 1991; Amirbahman et al., 1998) and indicates that precipitation of siderite is kinetically controlled. Wajon et al. (1985) proposed that not siderite, but that a mixed calcian siderite, $Ca/FeCO_3$, controls the solubility of Fe(II) in carbonate rich environment.

In Table 1-2., examples of water composition common to reduced environment are shown. They typically contain no or low oxygen (< 1 mg/L), elevated dissolved organic carbon (DOC) and hardness (1°F is equivalent to 10 mg/L dissolved $CaCO_3$). Moreover, they contain reduced species like Mn(II), Fe(II) and NH_4^+.

Considering each example separately, it appears that at Sursee, the ground water is not really reduced, since it still contains >1mg/L O_2 as well as a larger nitrate concentration. In Menznau, the pumping of the ground water possibly draws reduced ground water with larger Fe(II)

Table 1-2.
Chemical composition of reduced ground water, which are treated for iron and manganese removal.

Component	Unit	La Neuveville	Menznau	Root	Sursee
Conductivity	µS	400		447	660
Hardness	°F	25	34.3	31.1	39.5
pH		7.2	7.1	7	7.2
DOC	mg/l	1.5	0.9	3.5	0.4
O_2	mg/l	<0.1	0.2	0.1	1.5
NO_3^-	mg/l	0.5	23	0.3	9.7
NO_2^-	mg/l	0.005		0.002	0.03
NH_4^+	mg/l	0.8		0.035	0.31
Mn(II)	mg/l	0.1-0.2	0.6	0.4	0.15
Fe(II)	mg/l	0.3-1.0	5.9	0.9	0.03
SO_4^{2-}	mg/l	< 1	7.3	13.2	37

content as well as unreduced water with high NO_3^- concentrations. The very low sulfate concentration in La Neuveville could indicate that sulfate is being transformed to sulfide. At Root and La Neuveville reducing conditions prevail with large DOC and little nitrate.

1.1.3 Removal of iron and manganese

Both iron and manganese are necessary nutritional elements and are not toxic for human consumption. A daily intake of iron of 10-15 mg is recommended for adults. An adult body contains between 2.5 and 3.5 g Fe (Letterman, 1999). Large doses of Fe are needed to harm the human body: toxic symptoms are observed above doses of 20 mg/kg Fe. For acute poisoning, quantities >40-70 mg/kg Fe need to be ingested (Beers and Berkow, 1999).

Information about manganese toxicity is more controversial. The adult body contains about 20 mg Mn and a daily intake of 2-5 mg Mn is recommended. On the other side, a lowest adverse effect level of 0.2 mg/L was determined (Valezquez and Du, 1994; Letterman, 1999). Seemingly, there is a very small margin between potentially risky manganese concentrations and the daily exposition (EU, 2000). Manganese toxicity predominantly causes neurological damage. Manganism is a neurotic disease, known to affect miners by the inhalation of manganese oxide dusts (Griffith, 2002).

Therefore, treatment of Fe(II)- and Mn(II)-containing water is not necessary for toxicological reasons. Upon aeration these waters turn red-brown (Fe) or gray-black (Mn) due to the oxidation of the dissolved Fe(II) and Mn(II) to solid Fe- and Mn-oxides. In addition to the bad esthetics of these waters, nuisances, like taste, staining of the laundry, clogging of wells and corrosion of the pipes are associated with them. Moreover, iron and manganese containing waters can favor growth of microbial colonies and fouling of pipes. In consequence, World Health Organization recommends limiting the Fe and Mn concentrations to maximum concentration of 0.3 mg/L and 0.05 mg/L respectively (World

Table 1-3
Drinking water standards for dissolved iron and manganese.

	Fe [mg/L]	Mn [mg/L]
CH[1]	0.3	0.05
EU[2]	0.2	0.05
US[3]	0.3	0.05

[1] Fremd- und Inhaltstoffverordnung, 1995; [2] European Union, 1998; [3] USEPA, 2001

Health Organization, 1996). Similar standards are adopted as drinking water standards in most countries (see Table 1-3).

The standard technology for iron and manganese removal includes an oxidation-precipitation of the soluble Fe(II) and Mn(II) to the insoluble Fe- and Mn- oxides followed by filtration. This can be achieved in two ways: (i) the pumped ground water is treated chemically or biologically above ground. This process is referred to as conventional treatment, or (ii) by *in situ* ground water treatment, where Fe and Mn are precipitated in the underground.

For an efficient treatment most of the dissolved Fe(II) and Mn(II) have to be precipitated within detention time in the treatment plant, which means the time span between oxidant addition and filtration. Reaction conditions are different for Fe(II) and Mn(II) oxidation.

1.1.3.1 Oxidation of Fe(II)

The oxidation of Fe(II) by oxygen (oxygenation) occurs as follows:

$$Fe^{2+} + 0.25O_2 + 2.5H_2O \Leftrightarrow Fe(OH)_3\,(s) + 2H^+ \qquad \log K = 30.7 \qquad (1\text{-}3)$$

The kinetics of the Fe(II) oxygenation has been extensively studied. An empirical rate law has been determined by Stumm and Lee (1961) and verified by others for pH above 5 (Singer and Stumm, 1970; Sung and Morgan, 1980; Davison and Seed, 1983; Millero et al., 1987; Millero and Miguel, 1989; von Gunten and Schneider, 1991; King, 1998):

$$-d[Fe(II)] / dt = k_{hom}\,[Fe(II)]\,[O_2]\,[OH^-]^2, \qquad k_{hom} = 2 \times 10^{14}\ M^{-3}s^{-1} \qquad (1\text{-}4)$$

The half-live of Fe(II) at pH 7 and oxygen concentration in equilibrium with the atmosphere is 23 minutes. The strong pH dependence ($[OH]^2$) is due to fast reacting Fe(II) species, which become more important the higher the pH, these are $Fe(OH)^+$, $Fe(OH)_2$ (Figure 1-2). In carbonate containing waters the reactive species are $Fe(CO_3)_2^{2-}$ and $Fe(CO_3)(OH)^-$ (King, 1998). Also other dissolved inorganic ligands (H_4SiO_4, $H_2PO_4^-$, Cl^-, SO_4^-) potentially affect the rate of oxidation of Fe(II). However their effect is negligible at environmental concentrations (Davison and Seed, 1983; Faust and Aly, 1998).

In addition to dissolved ligands also surfaces can bind Fe(II) and accelerate the oxygenation of Fe(II). Tamura determined the following rate law in presence of Fe(III) oxyhydroxides (Tamura et al., 1976; Tamura et al., 1980):

$$-d[Fe(II)] / dt = [Fe(II)] [O_2] \{k_{hom} + k_{het} [Fe(III)]\} \qquad (1\text{-}5)$$

with $k_{het} = k^* K / [H^+]$, K being a binding constant for Fe(II) onto FeOOH. k_{het} varies according to the type of the FeOOH. The effect of Fe(III) is noticeable for higher concentrations of Fe-oxides ($[Fe(III)] \geq 5$ mg/L) and binding of Fe(II) to FeOOH is relevant for $pH > 4$ (Sung and Morgan, 1980; Tamura et al., 1980; Jeon et al., 2001).

In contradiction to the expected kinetics, Ghosh et al. (1966) noticed large unexplained discrepancies in the oxidative removal of Fe(II) from ground waters of different origins with half lives varying between 4 and 54 minutes ($7.4 < pH < 7.8$). These kinetics resulted in partly incomplete removal of the Fe(II). A low pH, as seen above, can slow down the kinetics. Moreover, reduced ground waters often contain larger concentrations of dissolved organic matter (DOM). DOM binds Fe(II) and Fe(III) prevents the precipitation to Fe-oxides (Stumm and Morgan, 1996; Faust and Aly, 1998; Emmenegger et al., 1998; Sivan et al., 1998). In such cases stronger oxidants, higher concentrations or longer contact times are required. Alternative oxidants can be chlorine, chlorine dioxide (ClO_2), ozone (O_3) or permanganate (MnO_4^-).

Figure 1-2
(a) Relative concentration of the predominant Fe(II) species (10 μM Fe(II), saturated $CaCO_3$, $6.5 < pH < 7.5$). At pH 7, Fe^{2+} and $FeCO_3$ are the predominant species. **(b)** Rate determining species for the oxygenation of Fe(II) under the same conditions as in (a). At pH 7, the species $Fe(CO)_2^{2-}$ reacts the fastest with O_2, even though its concentration is below 1/1000 of the total Fe(II).

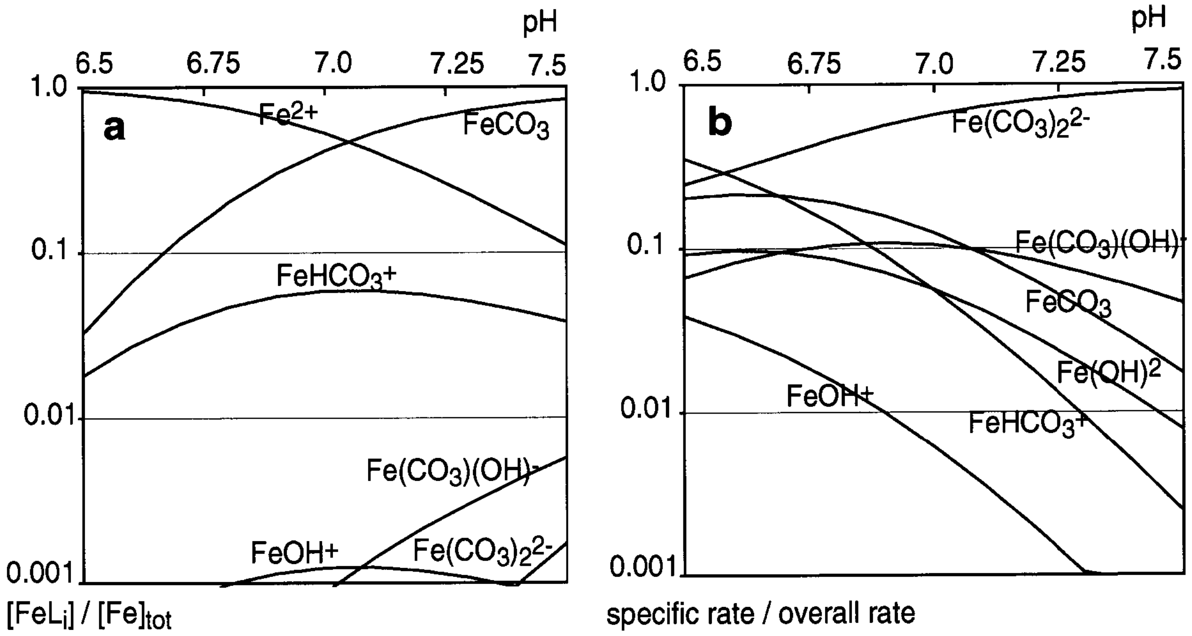

Without DOM half times of the Fe(II) oxidation with ClO_2, O_3 and MnO_4^- are below a second (Hoigné et al., 1985; Knocke et al., 1991a; Reckhow et al., 1991; Logager et al., 1992; Hoigné and Bader, 1994).

1.1.3.2 Oxidation of Mn(II)

The oxygenation of Mn(II) to the stable oxidized form, Mn(IV), consists of a two electron transfer reaction and is thermodynamically not as favorable as the oxygenation of Fe(II) to Fe(III) (cp. Eq 1.4):

$$Mn^{2+} + 0.5O_2 + H_2O \Leftrightarrow MnO_2\,(s) + 2H^+ \qquad \log K = 0.2 \qquad (1\text{-}6)$$

However, when Mn(II) is oxygenated abiotically, Mn(IV) is only produced after disproportionation of an intermediate low valent $Mn^{II,III}{}_3O_4$, or $Mn^{III}OOH$ (Hem and Lind, 1983; Murray et al., 1985; Junta and Hochella Jr., 1994; Mandernack et al., 1995a): Thus, Eq. 1.6 is the sum of the oxidation of Mn(II) to Mn(II,III) or Mn(III):

$$3Mn^{2+} + 0.5\,O_2 + 3\,H_2O \Leftrightarrow Mn_3O_4\,(s) + 6\,H^+ \qquad (1\text{-}7)$$

and the disproportionation to Mn(II) and Mn(IV):

$$Mn_3O_4 + 4\ H^+ \Leftrightarrow MnO_2\ (s) + 2\ Mn^{2+} + 2\ H_2O \qquad (1\text{-}8)$$

The oxygenation reaction of Mn(II) to Mn(III) takes place at large pH (pH >8.0). However, a large pH also stabilizes the Mn(III)oxyhydroxide and prevent its further transformation to MnO_2 (Hem and Lind, 1983; Murray et al., 1985). On the other side, microorganisms likely enable direct oxidation of Mn(II) to Mn(IV) (Mandernack et al., 1995b; Wehrli et al., 1995; Tebo et al., 1997; Bargar et al., 2000).

The chemical oxygenation of Mn(II) is kinetically inhibited. Larger pH (pH > 8.0) is needed to be able to measure it, the rate law is written according to (von Langen et al., 1997; Davies and Morgan, 1989; Sung and Morgan, 1981; Diem and Stumm, 1984; Morgan, 1967):

$$-d[Mn(II)] / dt = k_1\ [Mn(II)]\ [O_2]\ [OH^-]^2 + k_2\ [Mn(II)]\ [O_2]\ [OH^-]\ [MnO_2(s)] \qquad (1\text{-}9)$$

The rate constants are $k_1 = 2\text{-}4 \times 10^{12}\ M^{-3}\ s^{-1}$ and $k_2 = 1\text{-}2 \times 10^{13}\ M^{-4}\ s^{-1}$. As can be seen, the reaction is autocatalytic, the oxygenation of Mn(II) is accelerated by the formation of Mn- oxide. Other oxides like Fe-, Al-oxides and in a lesser extend Si- oxides also enhance the oxygenation kinetics (Davies and Morgan, 1989). It has been hypothesized that the species $Mn(OH)_2$ is rate determining in solution, whereas at the Fe-oxide surface it is an adsorbed binuclear Mn(II) species.

To efficiently oxidize Mn(II) stronger oxidants such as chlorine dioxide (ClO_2), ozone (O_3) and permanganate (MnO_4^-) are required (See Table 1-4; Knocke et al., 1991a; Knocke et al., 1988; Knocke et al., 1991b; Hao et al., 1991; Reckhow et al., 1991; van Benschoten et al., 1992). Ozonation in presence of Fe(II) potentially remobilizes manganese by formation of the soluble permanganate species, MnO_4^-, which must then be removed by a reducing filter of activated carbon (Reckhow et al., 1991; von Gunten, 2002). Chlorine (HOCl) does not react fast enough under homogeneous conditions (see Table 1-5). Therefore it is employed under conditions, where heterogeneous oxidation prevails, in combination with filter media. The same catalytic effect by the reaction

Table 1-4.

Mn(II) oxidation reaction and kinetics with different oxidants. Homogeneous rate constants and corresponding half times at pH 7 and 1 mg/L oxidant.

Oxidant	Reaction	k_1, $M^{-1} s^{-1}$	$t_{1/2}$ (pH7)
O_2	$Mn^{2+} + 0.5O_2 + H_2O \Leftrightarrow MnO_2(s) + 2H^+$	^{a}2-4 10^{12}	years
O_3	$Mn^{2+} + O_3 \Leftrightarrow MnO_2(s) + H_2O$	^{b}1.5 10^3	23 s
HOCl	$Mn^{2+} + HOCl + H_2O \Leftrightarrow MnO_2(s) + Cl^- + 3H^+$	^{c}9	1.5 hours
ClO_2	$Mn^{2+} + 2ClO_2 + 4OH^- \Leftrightarrow MnO_2(s) + 2ClO^- + 2H_20$	^{d}1.3 10^4	4 s
MnO_4^-	$3Mn^{2+} + 2MnO_4^- + 4OH^- \Leftrightarrow 5MnO_2 (s) + 2H_20$	^{e}2-14 10^4	< 1s

[a] Morgan, 1967

[b] Jacobsen et al., 1998; von Gunten, 2002

[c] Hao et al., 1991; Reckhow et al., 1991

[d] van Benschoten et al., 1992; Reckhow et al., 1991

[e] van Benschoten et al., 1992; Knocke et al., 1991a

product MnO_2 (s) is observed for the oxidation with MnO_4^- and ClO_2, at low pH (< pH 7). At neutral to basic pH, the homogeneous oxidation controls the kinetics. Oxidation of Mn(II) by permanganate and chlorine dioxide produces Mn(IV) dioxide directly (van Benschoten et al., 1992).

In drinking water treatment practice, the catalytic effect of MnO_2 is frequently applied. Mn(II) removal can be performed on a filter media coated with solid MnO_2 (Faust and Aly, 1998; Knocke et al., 1991b; Letterman, 1999; O'Connor, 1971). The coating is first produced by addition of potassium permanganate to the raw water, the MnO_2 particles then stick to the filter. The large exchange capacity of the precipitated MnO_2 allows the uptake of Mn(II) even if the oxidation capacity is insufficient. The adsorbed Mn(II) is subsequently oxidized by the next supply of permanganate.

Oxygenation of Fe(II) and Mn(II) can be catalyzed by microorganisms. They are of special interest in water treatment, when the chemical oxidation is impeded. Examples are low pH, large DOM for Fe(II) removal, or slow Mn(II) removal (Mouchet, 1992a; Mouchet, 1992b;

Søgaard et al., 2001). There are many species of Fe- and Mn-oxidizing microorganisms, which are not phylogenetically related, most common are Shewanella, Leptothrix, Geobacter, Gallionella. Often the same bacterium can oxidize both metals; others are able to oxidize only either Fe(II) (Gallionella) or Mn(II) (Pseudomonas manganoxidans; Mouchet, 1992b; Emerson and Moyer, 1997).

In a biological treatment plant separate treatment steps are required for the removal of both iron and manganese: first the iron, then the manganese is removed. Biological treatment is performed in sand filters, which are coated by the micro fauna. Each filtration step is preceded by aeration (see Figure 1-3).

1.1.3.3 Conventional removal of iron and manganese.

Conventional treatment is performed after pumping the ground water. It consists of the following steps: (1) Dosage of oxidant (air, ozone, chlorine, chlorine dioxide, permanganate) and eventually base (lime, sodium hydroxide). (2) Filtration (sand bed).

Conventional iron / manganese removal plants can be operated either chemically or biologically. In the case of the chemical process additional means may be required such as:

-Addition of lime or calcium hydroxide (CaO, CaOH) to control the alkalinity by elevation of the pH and precipitation of $CaCO_3$.
-Addition of a base to neutralize the pH (e.g. NaOH).
-Addition of coagulant to remove DOM.
-Pre-oxidation with ozone and/or pre-filtration to eliminate DOM
-Use of especially strong oxidants (chlorine dioxide, ozone or permanganate). Specially indicated for manganese, which is more difficult to oxidize.

Manganese removal is possible only, when ferrous iron has been completely taken out, which may require a separate treatment step. Figure 1-3 shows a treatment train for biological iron removal with distinct Fe(II) and Mn(II) removal steps. At first, the raw water (RW) is aerated and conducted through filters containing Fe-oxidizing

Figure 1-2

Biological iron removal plant (Hochfelden, France) with distinct Fe(II) and Mn(II) removal step (Mouchet, 1992b).

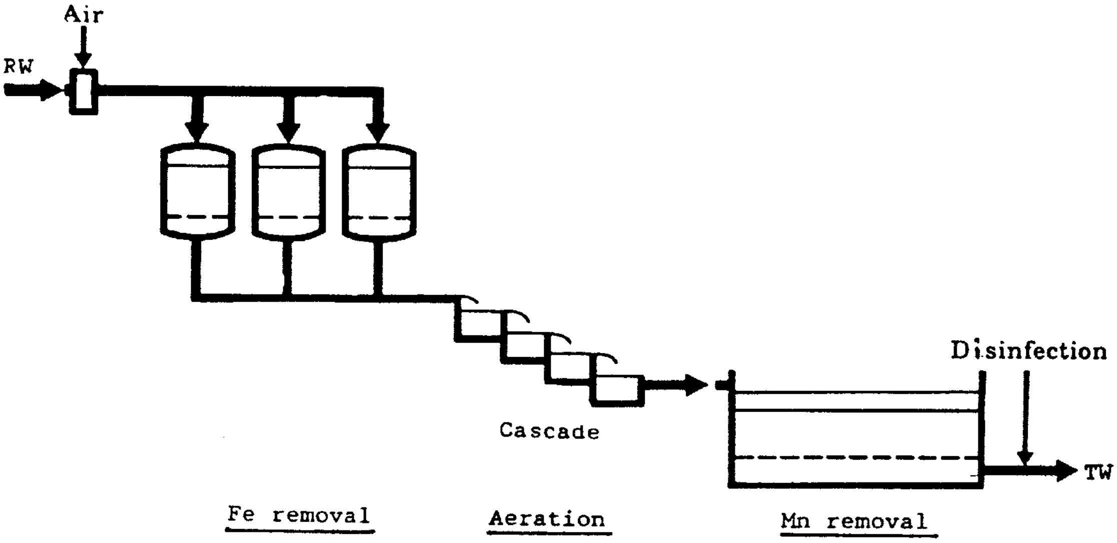

microorganisms for Fe-removal, afterwards it follows another aeration step (cascade). Besides aeration nitrification also, the biological transformation of NH_4^+ to NO_3^-, takes place in the cascades. Finally Mn(II) is oxidized in the large filter basin, with the help of Mn-oxidizing microorganisms. The addition of a disinfectant, mostly chlorine, prevents an eventual bacterial contamination of the pipes. In both chemical and biological treatment the filters need regular backwashing of the precipitated Fe- and Mn- oxides and the produced sludge has to be disposed of. According to (Mouchet, 1992b), the oxides precipitated biologically are denser and less voluminous, which needs fewer backwashing. Another advantage of biological removal is the decreased need of chemicals. However, there is a certain risk of poisoning of the micro-fauna by organic pollutants.

1.1.3.4 *In situ* removal of iron and manganese.

In situ ground water treatment for iron and manganese removal has been applied as long as conventional processes. However, due to poor acceptance it is not as widespread.

In the *in situ* process an oxidation/precipitation zone is created around the supply well by regular injection of aerated water in the aquifer (Figure 1-4a. Injection). The pumped ground water traverses the precipitation zone, which functions as a filter for Fe(II) and Mn(II). This hinders Fe(II) and Mn(II) to get into the supply well, which ultimately could lead to clogging (Figure 1-4b. Extraction). As the filter capacity is exhausted, increasing Fe(II) and Mn(II) concentrations are measured in the pumped water. When the level of the drinking water standard is reached, aerated water is injected to "regenerate" the precipitation zone. The oxygen transforms the Fe(II) and Mn(II) to Fe(III)- and Mn(III,IV)-oxides, capable to sorb more Fe(II) and Mn(II) from the reduced water. Along with each cycle of injection and extraction coating of Fe- and Mn-oxides builds up in the aquifer. In contrast to conventional removal the solid Fe- and Mn-precipitates are not disposed of, but remain in the underground.

The oldest systems consist of one borehole only, which functions alternatively as injection well and as supply well (Olthoff, 1986; Rott and Meyerhoff, 1993; Waldburger, 1994). Consequently, during the injection phase, no ground water is supplied. In such a system, moreover, the precipitation zone is closer to the extraction well, leading to a larger risk of clogging the well.

More recent installations (e.g. Vyredox$^{©}$, like in Figure 1-4) work with several wells: the supply well is surrounded by a circle of 5 to 23 injection wells (Hallberg and Martinell, 1976; Mengis, 1984; Zienkiewicz, 1984; Rey and Schindler, 1984; Bernard and Serieys, 1986; Braester and Martinell, 1988). Such systems allow continuous water supply. In this case the precipitation zone corresponds approximately to a cylinder built up by the circle of the injection wells and the depth of the aquifer. This design allows optimizing and dimensioning the precipitation zone.

Figure 1-3
Schematic representation of an *in situ* treatment plant consisting of several injection wells and one supply well. **(a)** Injection. **(b)** Extraction.

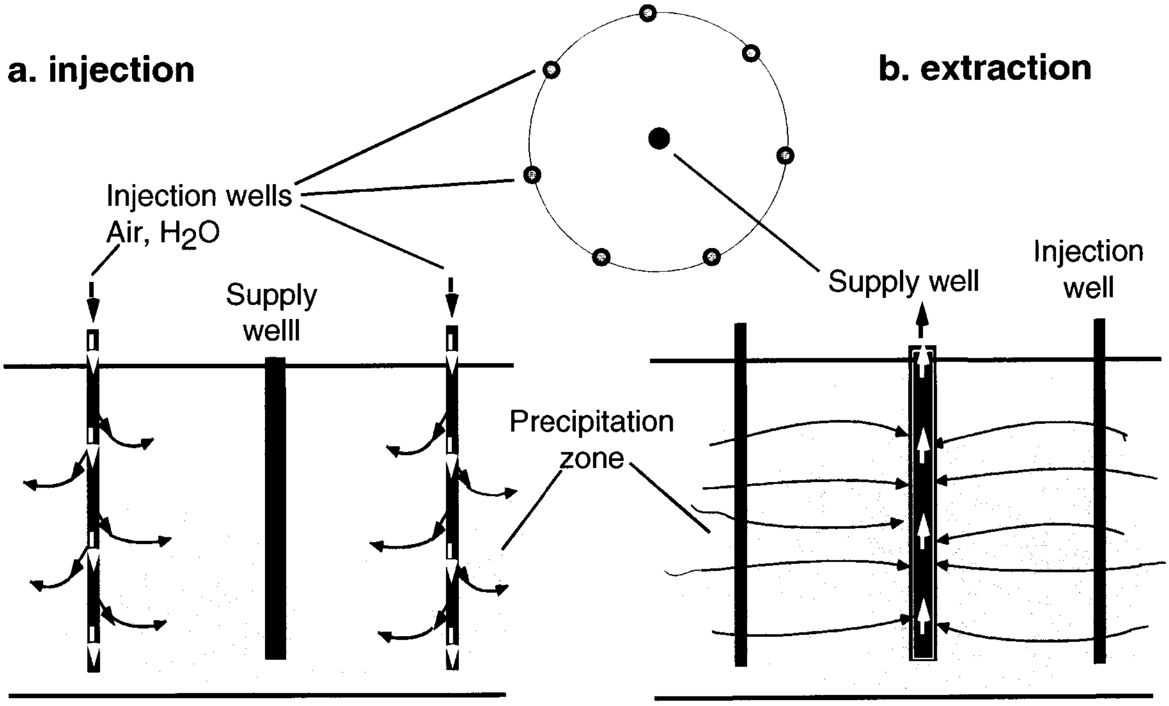

The size of the precipitation zone must be large enough to hold the produced volume of Fe- and Mn- precipitates for at least 100 years. The radius of the circle and the number of injection wells are set up, such that the precipitates take up at most 5 % of the pore volume of this cylinder (for examples, see 2.4.7 or Hallberg and Martinell, 1976; Rey and Schindler, 1984).

The output of the *in situ* treatment plant is described by the efficiency ratio, E_r, which is the ratio of the volume of clean ground water supplied, V_{out}, divided by the volume of injected water, V_{in} (Hallberg and Martinell, 1976):

$$E_r = V_{out} / V_{in} \tag{1-10}$$

An ideal efficiency ratio, $E_{r,ideal}$ can be calculated from the stoichiometry of the Fe(II) and Mn(II) oxygenation (see Equations 1.3 and 1.6), the oxygen concentration of the injected water (aerated water with 0.25 mM O_2) and the Fe(II) and Mn(II) concentrations of the reduced ground water. Thus each volume of aerated water can theoretically produce 40 equivalent volumes of a ground water that contains 25 μM Fe(II) (1.4 mg/L Fe(II)). The ideal efficiency ratio can be calculated after the formula (van Beek, 1985):

$$E_{r,ideal} = 1 + \{ 4\,(1\text{-}f\text{-}a)\,[O_2] \} / [Fe(II)] \qquad (1\text{-}11)$$

Where $[O_2]$ and [Fe(II)] are the concentration of oxygen of the injected water and the concentration of Fe(II) of the reduced ground water; f is the fraction of the oxygen concentration consumed by the oxidation of other reduced species and a, the fraction of the unused oxygen, which is pumped with the subsequent extraction. The factor (1-f-a) is a measure of the oxygen efficiency.

In reality the efficiency ratio ranges from 6 to 22 depending on the plant. The coefficient of oxygen use amounts to around 0.1 (10 %), with a maximum around 0.5 (50 %) (van Beek, 1985; *in situ* treatment plants in Switzerland). Most of the oxygen injected is thus consumed by reduced species other than Fe(II) and Mn(II) (50-90% of the O_2), which efficiently compete with the metallic cations for the dissolved oxygen. Most probably aerobic respiration, the microbial oxidation of DOM, is responsible for the oxygen consumption. *In situ* treatment is not recommended in strongly reduced ground water, which contains dissolved hydrogen sulfides (HS^-) or larger concentrations of ammonium (NH_4^+). These are high-oxygen consuming species, which prevent the oxidation of Fe(II) and Mn(II): each mole of either HS^- or NH_4^+ requires 2 moles of oxygen.

The operational optimum of the *in situ* treatment plant is preceded by a start-up phase. The start-up consists of several cycles (ca. 10) of injection of O_2-containing water followed by extraction of ground water. During this time an increase of the efficiency ratio is observed for each subsequent cycle, until the E_r finally stabilizes at a constant value. A start-up phase of a test installation in Root is shown in Figure 1-5. The numbers corresponds to the extraction cycle. For each additional cycle, the volume of extracted clean ground water (with Fe(II) < 0.3 mg/L) augments. It gives evidence that in the course of the first cycles changes

Figure 1-4

Iron concentration in function of the volume of extracted ground water in the start-up phase. The number of the curves corresponds to the number of consequent extraction/injection. The iron standard (0.3 mg/L, see Table 1-3) is indicated as a line in the graphic. The injection of 6 m^3 of aerated water with $[O_2]$ = 9 mg/L follows each extraction.

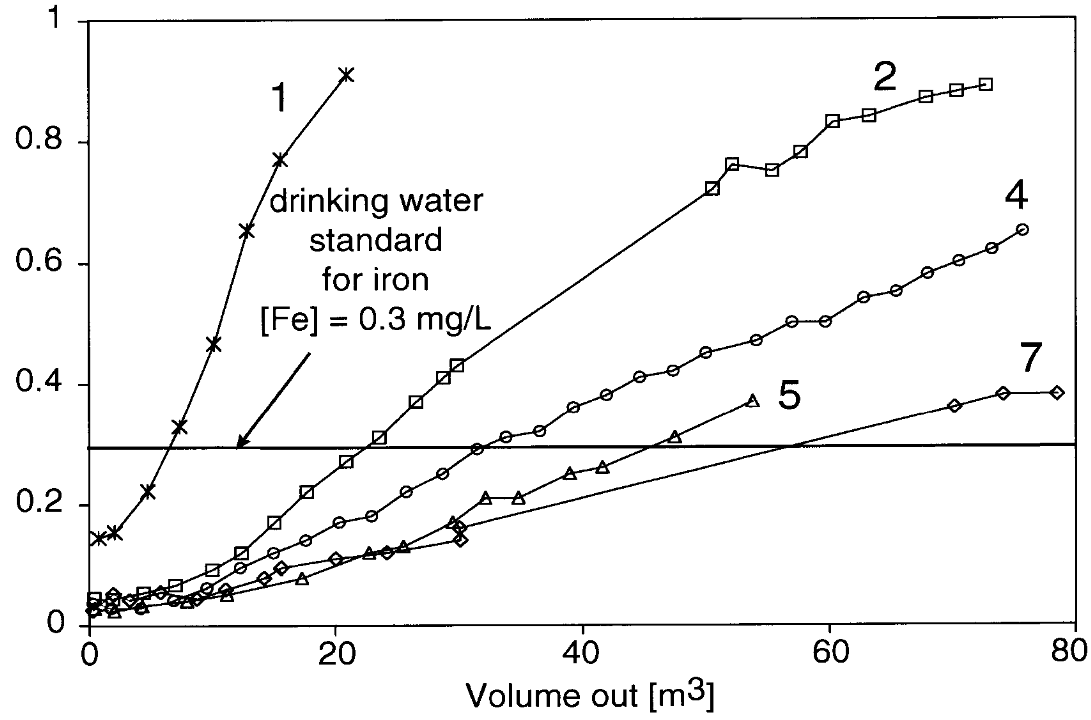

occur in the precipitation zone, which allow a better retention of the Fe(II) and Mn(II) in the subsequent cycles. The elimination of Mn(II) needs a longer start-up phase.

Oxygen is the only oxidant used in Figure 1-5. It has been shown that also nitrate (NO_3^-) contained in the injected water can oxidize Fe(II), but not Mn(II) (Kölle and Schneider, 1992; Meyerhoff, 1995). This reaction is mediated by microorganisms (Benz et al., 1998; Hauck et al., 2001).

Other strong oxidants like hydrogen peroxide (H_2O_2) and potassium permanganate ($KMnO_4$) have been tested as well. The efficiency ratio increased slightly, however the oxidant efficiency was lower than with oxygen. Moreover, a shortening of the start-up phase of the treatment plant has been observed. Permanganate led to a drop of the hydraulic permeability (Olthoff, 1986; Olthoff, 1987).

Varying alkalinities and major ion concentration possibly affect the efficiency of *in situ* removal of iron. Rundell and Randtke (1987) found a correlation of the efficiency ratio and the alkalinity of the treated ground water. Even though alkalinity may not directly interfere with the removal mechanism, it correlates with a good proton buffering capacity and larger Ca^{2+} and Mg^{2+} concentrations in solution.

1.1.4 Open questions

Over a hundred *in situ* treatment plants with pumping rates varying between 2 to 100 m^3/days are in operation worldwide; Switzerland counts ten (See Appendix). Due to operational advantages, *in situ* treatment should be more widely applied. However, there is still a lot of skepticism among engineers and politicians, which leads to a prefered application of conventional processes.

One of the main reasons for skepticism is the fear that the growing amount of precipitated Fe and Mn may clog the aquifer and dramatically reduce the lifetime of the well.

This reservation is further fortified because the mechanisms for iron and manganese removal are still largely unknown. So far *(i)* biotic as well as *(ii)* chemical pathways have been proposed.

- The biotic mechanism involves Fe(II)- and Mn(II)-oxidizing microorganisms. The elevated flow of Fe(II) and Mn(II) containing water in alternation with aeration makes the precipitation zone a welcome habitat for colonies of Fe(II)- and Mn(II)-oxidizing microorganisms (Benz et al., 1998; Emerson and Moyer, 1997; Straub et al., 2001). They settle during the start-up phase and allow optimum oxidation-precipitation of Fe(II) and Mn(II) during operation (Hallberg and Martinell, 1976; Bernard and Serieys, 1986; Rundell and Randtke, 1987; Rott and Meyerhoff, 1994).

-Chemical oxidation-precipitation takes place in two steps at the surface of the solid aquifer matrix (see Figure 1-6). The matrix consists of minerals like quartz, clays or calcite. These are oxides or carbonates,

Figure 1-5

Chemical mechanism responsible for the oxidation precipitation of Fe(II) or Mn(II): (**a**) Fe(II) binds to the aquifer surfaces. (**b**) The sorbed Fe(II) is oxidized and hydrolyzes to Fe(III)OOH; (**c**) A coating of reactive FeOOH is formed at the surface of the solid matrix.

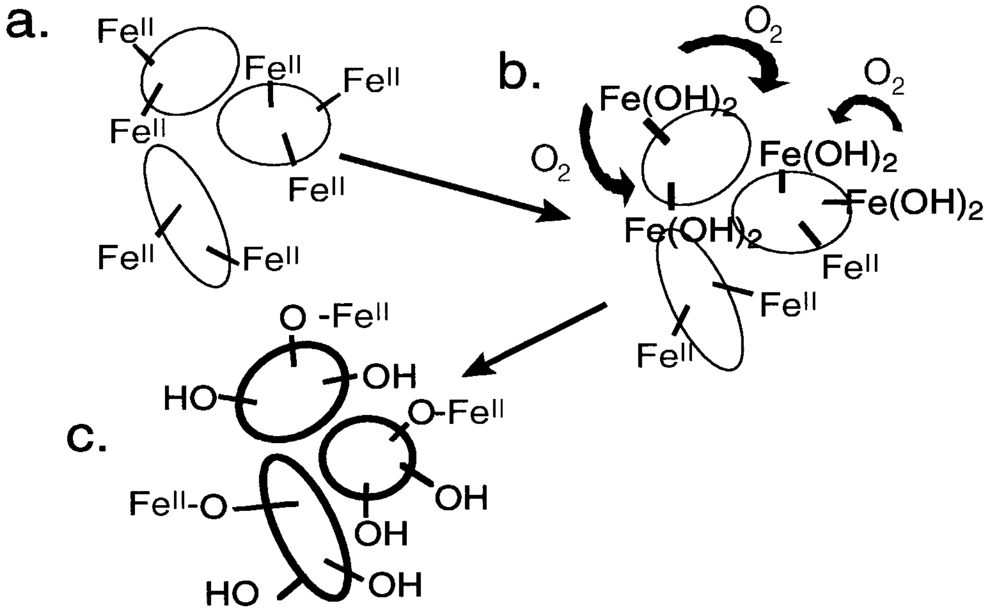

which in aqueous environments hydrolyze to surface hydroxyl ($>OH^-$) or carbonate ($>HCO_3^-$) groups capable of binding cations like Fe(II) and Mn(II) from the solution. In a first step, the Fe(II) and Mn(II) sorbs to the surface groups (**a**). Then, they are oxidized to Fe- and Mn- oxides when oxygen-containing water is injected (**b**). With time the aquifer matrix gets coated with Fe- and Mn-oxides (**c**). These surfaces have a high adsorption efficiency for Fe(II) and Mn(II), and facilitate the oxygenation of Fe(II) and Mn(II) (Rundell and Randtke, 1987; Olthoff, 1986; Olthoff, 1987; Appelo et al., 1999). The same biotic and chemical mechanisms described above for Fe(II) have generally been proposed for the removal of Mn(II). However the slow kinetics of Mn(II) oxidation makes the chemical process unlikely. Microorganisms probably play a decisive role in the removal of manganese from ground water. In contrast to iron, a longer start up phase of the treatment plant is generally observed before manganese can be efficiently removed (van Beek, 1985).

1.1.5 Focus of this study

The goal of the present study is to investigate the open questions concerning *in situ* removal of iron and manganese, with the emphasis on the mechanism of the Fe(II) removal and the fate of the precipitates.

Chapter two describes a field study carried out at a full-scale *in situ* treatment plant. The plant serving 3’400 inhabitants with drinking water after removal of iron and manganese has been operating for more than ten years. Aquifer samples taken from the precipitation zone were analyzed for precipitated iron and manganese and compared to local reference samples. The objective of this study was to investigate the chemical and structural form of iron and manganese precipitates and the preferred environment of precipitation. Conclusions about the risk of aquifer clogging will be drawn from the results.

In chapter three and four results of laboratory experiments are reported, which deal with the mechanisms leading to Fe(II) removal. Only chemical processes were investigated. Oxidation of manganese was not examined.

Chapter three covers a study on the interactions of Fe(II) with calcite. Calcite was chosen as a model surface based on the results of the field study, which showed a high affinity of iron precipitates for calcite. The experiments were performed in presence and in absence of oxygen, as well as with alternating oxic-anoxic conditions to mimic the conditions occurring during *in situ* deferrisation.

Chapter four reports data on Fe(II) and goethite interactions. Goethite was the most important Fe-oxide precipitation product found in the field site. These experiments, therefore, represent reference conditions for the reactions, which take place, once the available natural surfaces are coated with the precipitated Fe-oxide.

In chapter five, the most important results are summarized and related to practical implications for *in situ* deferrisation processes.

Seite Leer /
Blank leaf

2

CHARACTERIZATION OF IRON AND MANGANESE PRECIPITATES FROM AN *IN SITU* GROUND WATER TREATMENT PLANT*

2.1 Introduction

The concentrations of iron and manganese in natural waters are controlled by the solubility of the corresponding oxidic phases. This explains their low concentrations in most waters. In the absence of oxygen Fe-oxides and Mn-oxides can function as electron acceptors: mostly biotic processes reduce Fe(III) and Mn(III, IV) to the divalent ions that have a much higher solubility. These processes take place in lakes or in aquifer systems rich in organic matter where oxygen is depleted and a whole series of reduction processes can occur (Lovley, 1987; Lovley et al., 1988; von Gunten et al., 1993; Cornell et al., 1996).

If such reduced ground waters are used for drinking water production, iron and manganese have to be removed before distribution. Even if these metals are of no toxicological concern, iron and manganese have various undesired effects in drinking waters: corrosion, precipitation and clogging of pipes, staining of laundry and in some cases strong metallic taste. Therefore, the World Health Organization (WHO) recommends removal of Fe and Mn when concentrations are higher than 0.3 mg/L and 0.1 mg/L, respectively (World Health Organization, 1996). Similar standards are adopted in different countries: 0.3 mg/L and 0.05 mg/L in the USA (USEPA, 2001) 0.2 mg/L and 0.05 mg/L in the European Union (European Union, 1998).

---

* GROUND WATER, Vol 39, N° 6, November-December 2001 (921-930)

In general iron and manganese are removed after pumping the ground water by oxidation followed by filtration. The oxidation step is conducted either chemically by various oxidants (Cl_2, ClO_2, $KMnO_4$, O_2) or microbiologically, using iron or manganese oxidizing microorganisms (Mouchet, 1992). Frequently, separate treatment steps are need for chemical or biological deferrisation and demanganation because of the different reaction conditions for the oxidation step. This leads to high investment costs. In addition the filtration produces large volumes of Fe- and Mn-sludge, which have to be disposed. Alternatively, in situ treatment can be applied, where iron and manganese are precipitated directly in the aquifer after oxygenation. For this purpose air-saturated water is injected in the aquifer. Compared to conventional treatment, this requires only a relatively simple infrastructure. Other advantages of in situ removal of iron and manganese are no clogging of the supply well, no sludge disposal and no dosing of chemicals (Hallberg et al., 1976; Mengis, 1984; Rey et al., 1984; Groth et al., 1988; Meyerhoff, 1995;). Despite of these advantages, in situ treatment is applied with reservation: questions about reaction mechanisms, efficiency and consequences for the aquifer are not entirely resolved. Especially, the risk of clogging the aquifer by the reaction products raises questions about the lifetime of such installations.

In most previous studies about *in situ* deferrisation and demanganation, optimum operation conditions were investigated with little emphasis on precipitation products (Hallberg and Martinell, 1976; Boochs and Barovic, 1981; Mengis, 1984; Zienkiewicz, 1984; van Beek, 1985; Olthoff, 1986; Rundell and Randtke, 1987; Groth et al., 1988; Kölle and Schneider, 1992; Appelo et al., 1999). Usually, the size of the precipitation zone is designed to be large enough to ensure a lifetime of the treatment plant of at least one hundred years. This can be calculated, based on the dry bulk density and the porosity of the aquifer and the expected amount of precipitated iron- and manganese-oxides (Hallberg and Martinell, 1976; Mengis, 1984; Rott and Meyerhoff, 1993). No reports of aquifer clogging under these conditions were found in the literature. In a demonstration plant Olthoff (1986) found "hardly measurable changes of permeability". Jechlinger et al. (1985) could not observe any major precipitates exceeding a few percent of the pore volume. However, in both cases the systems were only operated for a short time (up to two years). In some cases aquifer material after *in situ* treatment was analyzed. Oxalate / dithionite extractions showed that half of the ferric oxides were poorly crystallized. Additional X-ray diffraction showed traces of lepidocrocite (Olthoff, 1986). Iron-enriched "hot spots" were found by microscopy in samples from a 10 years old *in situ* deferrisation plant, where up to 12% of the pore volume was filled with Fe- oxides. These spots were located at the interface of well (sand and gravel) and less permeable layers (Kleefeldt, 1988).

It is generally accepted that for an efficient and long lasting *in situ* treatment plant the precipitates should be crystalline, which requires a smaller precipitation zone (filter volume) than amorphous products (Seyfried and Olthoff, 1985; Olthoff, 1986; Braester and Martinell, 1988). It has been shown that, for the type of products formed by oxidation of Fe(II) and subsequent precipitation of ferric oxides, reaction conditions have a high impact on product formation (Cornell and Schwertmann, 1996).

In the present study we will focus on the precipitates formed in an *in situ* treatment plant in La Neuveville (Switzerland). The following main questions were addressed:

- Can iron or manganese phases, produced by *in situ* treatment, be identified?
- What kind of minerals are precipitated?
- Are there preferential precipitation zones, sites or surfaces?
- Based on these findings, what is the risk of clogging the aquifer?

2.2 La Neuveville site

The site of La Neuveville is located in western Switzerland. At this site an alluvial deltaic aquifer lies over limestone till (Rey and Schindler, 1984). The sediment material of the aquifer is highly heterogeneous, and the water table is at a depth of ca. 2 m. At a depth of 18-19 m, an impermeable layer of clay forms the bottom of the aquifer.

Ground water contains dissolved iron and manganese in concentrations of 0.3 to 1 mg/L and 0.1-0.2 mg/L respectively; the dissolved oxygen concentration is below 1 mg/L. The pH of the ground water varies between 7.0-7.3 and the temperature between 10 and 13 °C, it has a hardness of 25° fH (250 mg/L $CaCO_3$). The ground water contains NO_2^- (5 mg/L), NO_3^- (0.5 mg/L), NH_4^+ (0.8 mg/L), Cl^- (10 mg/L). The DOC concentration is 1.5 mg/L and the conductivity is around 400 μS.

Figure 2-1
Schematic representation of the iron and manganese *in situ* removal plant of La Neuveville.

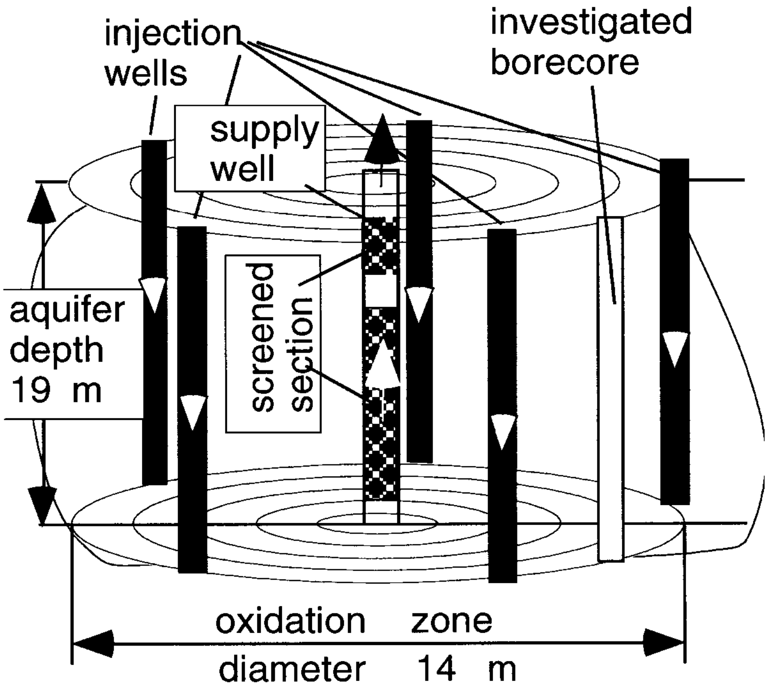
injection wells
investigated borecore
supply well
screened section
aquifer depth 19 m
oxidation zone diameter 14 m

An *in situ* plant for iron and manganese removal from ground water, which is depicted in Figure 2-1, was installed in La Neuveville in 1988. Ground water is pumped through two screened parts of a water supply well at depths of 4.8-6.8 m and 8.6-18.6 m with a pumping flow rate of 2400 L/min. At a distance of 7 m from the supply well, there are five injection wells (satellite wells), where air-saturated water is injected intermittently to regenerate the oxidation zone (oxygen = 8 mg/L; iron and manganese < 0.2 mg/L). Injection periods last for about one day (injection flow rate 480 L/min). To ensure a complete removal of iron and manganese the treatment plant is designed to have overlapping oxidation zones around the satellites. The precipitation zone comprises the entire volume of inflowing water. After the injection period iron and manganese free water can be pumped from the supply well until concentrations of the metal rise above drinking water standards (ca. 5-10 days). A continuous supply of drinking water is only possible because the site is operated with two identical well systems, which are alternatively exploited and regenerated.

2.3 Materials and Methods

All solutions were made with deionized water (Q-H_2O grade Barnstead nanopure). Chemicals were at least reagent grade (Fluka or Merck): Titanium chloride 15% in HCl and Ferrozine, Hydrochloric acid (32%), L-ascorbic acid, Ethylene-diamine-tetra-acetic acid disodium salt, MnO_2 (pyrolusite) and acetic acid.

2.3.1 Aquifer sample selection

All samples in this study were taken from a new bore hole (18.8 m deep) drilled in the precipitation zone between two injection wells (Figure 2-1). Samples from the depths of 4-5 m, 7.5-8 m, 11.3-11.8 m, 12.5-13 m and 17-17.5 m were analyzed. The sample from 4-5 m represents a reference above the precipitation zone, similar to the aquifer before the installation of the treatment plant. To normalize the concentrations to reproducible quantities of aquifer material, measurements were partly performed with sieved samples. The samples were dried for 1 hour at 100° C and then sieved dry with metallic sieves to separate the fractions of different grain size. This treatment does not transform amorphous Fe-oxides into more crystalline forms (Weidler, 1997). The grain size fractions <0.063 mm, 0.063-0.09 mm, 0.09-0.125 mm, 0.125-0.25 mm and 0.25-0.5 mm were investigated; they represent a large fraction of the specific surface area and are expected to be coated with fresh precipitates. Four other samples were analyzed without sieving: these are the stones P1 and P20, found at 16.1 and 17.1 m, as well as samples P22 and P24, consisting of gravelly material from the depths 6.4 m and 9.0 m. P1 is a calcite stone with a diameter of about 15 cm, coated with an orange-brown layer. P20 consists of several orange-brown stones (diameter ca. 3-5 cm), mostly agglomerated sand of quartz and calcite. P1 and P20 were first air dried, then material was scratched from the surface of the colored spots and ground with an agate mortar for measurements. Samples P22 and P24 were frozen under argon atmosphere and then freeze dried, with only the most colored material chosen for analysis.

2.3.2 Analytical methods

Metals were measured with flame atomic absorption spectroscopy (Perkin Elmer 5100 PC): Detection limits for Fe and Mn were 0.03 mg/L and 0.01 mg/L, respectively. Ferrous iron (Fe(II)) was measured separately with the Ferrozine method with a detection limit of approximately 3×10^{-7} M in a 1 cm cuvette (Stookey, 1970; Gibbs, 1976).

2.3.2.1 Chemical characterization of Fe- and Mn oxides

The following dissolution methods were used to characterize the iron and manganese minerals in the aquifer: acid dissolution with 5 M hydrochloric acid, reductive dissolution with ascorbic acid (0.114 M) at pH 8 and an EDTA complex of titanium III (0.008 M) at pH 7 (Ti-EDTA). The methods were described and applied previously (Heron et al., 1994;

Kostka and Luther III, 1994; Amirbahman et al., 1998). Reductive dissolution methods are widely used to characterize Fe-oxides; in the present study we used the same methods for the identification of Mn minerals. However, for the latter, additional test experiments on synthetic Mn-oxides had to be performed (see below). Because of the metal binding character of the buffers used in reductive extractions, dissolution experiments were also conducted without a reducing agent to correct the results for this blank. All of the concentrations given below are mean values of three measurements, the indicated error is the standard deviation of these measurements.

For all dissolution experiments, aliquots of a sample (0.2-1g) were equilibrated with the reagents for 24 hours, and suspensions were filtered through 0.45 mm filters (Sartorius, cellulose nitrate) and analyzed for the metal concentrations.

In the present study dissolution in 5M HCl is defined as yielding total manganese (Mn_{tot}) and iron (Fe_{tot}) contents of the aquifer material. Ti-EDTA extraction has been shown to dissolve most of the Fe- oxides except magnetite. Therefore, it corresponds to the total content of ferric oxides (FeIII(TiEDTA)). Ascorbic acid only dissolves the amorphous fraction of Fe-oxide (FeIII(AscA)). Thus the difference between the dissolved iron from TiEDTA and ascorbic acid yields the crystalline ferric oxides.

Additional test experiments on Mn-oxides dissolution allow the following conclusion: 5M HCl treatment dissolves MnO_2 almost entirely (> 87%). Reductive methods were not as selective for crystalline (pyrolusite, Merck) and synthesized amorphous manganese dioxide (Murray, 1974) as for the Fe-oxides. The reduction by ascorbic acid dissolved both the crystalline and the amorphous MnO_2. However, the citrate buffer already completely dissolved the amorphous MnO_2. It dissolves Mn(II)-containing carbonates as well, and thus does not differentiate between Mn(II) and Mn(III,IV)oxides. Ti-EDTA reduced all the amorphous and half of the crystalline MnO_2. Therefore, the Ti-EDTA method is more specific for Mn-oxides than the other treatment and is used here to quantify the fraction of Mn-oxides.

2.3.2.2 Concentration of aquifer samples

X-ray diffraction (XRD) measurements showed a high content of calcite in the aquifer material (≥30 %). To concentrate the samples with respect to Fe- and Mn-oxides, the calcite was selectively removed by shaking 1 g of the sample in 10 ml of a 20 % (v/v) solution of acetic acid during 24 hours (Mahapatra et al., 1996). The resulting suspensions were then centrifuged for 10 minutes at 8000 rpm and finally stabilized by freezing; for spectroscopic measurements they were freeze dried. The method was tested on synthetic ferrihydrite (prepared according to Schwertmann and Cornell, 1991) as well as with amorphous and crystalline manganese dioxide (same materials as above). Only the amorphous manganese dioxide was dissolved entirely. The other synthetic oxides were not affected by this treatment. To check the influence of the acetic acid pretreatment on chemical extractions, they were repeated after acetic acid pretreatment. For the chemical extraction methods, the resulting concentrations were the same for treated and untreated samples, because the analyzed iron or manganese fractions were always related to the initial dry weight of the sample before calcite was removed. Spectroscopic results, however, refer to the remaining sample mass free of calcite.

2.3.2.3 X-ray Diffraction (XRD)

X-ray diffraction allows the determination of crystalline minerals in natural samples as long as their concentration is larger than a few percent (w/w). XRD-measurements were performed with samples from the smallest grain size fraction of the sieved samples (<0.063 mm) and with specially collected samples P1, P20, P22, P24, which were hand ground in an agate mortar with ethanol (with acetone in the case of samples treated with acetic acid). The XRD measurements were performed on a Scintag XDS 2000, (Bragg-Brentano geometry) with a CuKα X-ray radiation wavelength (λ =0.15418 nm) and a solid state lithium-silicium detector. Some measurements were performed in continuous scan mode (0.5° and 1°/minute) over a 2Θ range of 2-70°. The samples, which were quantified by Rietveld refinement, as well as the sediments pretreated in dilute acetic acid were measured in the step scan mode between 10° < 2Θ < 70° with an interval of 0.025°/ 4 seconds. The diffractograms were interpreted by Rietveld refinement using the multiphase Rietveld package WYRIET (Schneider, 1989; Schneider and Dinnebier, 1991). This is a least square fit of variables combining a crystallographic database, the optics of the apparatus and the peak shape (Weidler et al., 1998).

2.3.2.4 Mössbauer spectroscopy

^{57}Fe Mössbauer spectroscopy is the most proficient method to characterize the iron species in solid phases. Mössbauer spectra can reveal the presence of minute amounts of Fe-oxides associated with phyllosilicates, but moreover, they enable an unequivocal identification of these minerals and their quantification down to 1% w/w ratio of mineral to total sediment mass (Murad and Wagner, 1994). The Mössbauer spectra were measured by means of a constant acceleration spectrometer with a 50 mCi source of ^{57}Co in Rh. The spectrometer was calibrated with a 25 µm foil of α-Fe at room temperature. The products were analyzed at low temperature (12 K) to distinguish goethite, ferrihydrite and phyllosilicates. The cryostat consisted of a closed Mössbauer cryogenic workstation with a vibration insulation stand manufactured by Cryo Industries of America®. Computer fittings were done using Lorentzian-shape lines with variable widths for taking into account spectral asymmetry.

2.4 Results and Discussion

2.4.1 Grain size distribution of the aquifer material

The grain size distribution of the sieved samples is shown in Figure 2-2. Two types of aquifer material can be distinguished: a sand type and a gravel type. The samples from a depth of 7.5-8.0 m and 11.3-11.8 m containing around 10% of clay and silt (fraction <0.063mm) as well as 50

Figure 2-2
Grain size distribution of the five sieved samples. Arrow depicts the range of the analyzed fractions.

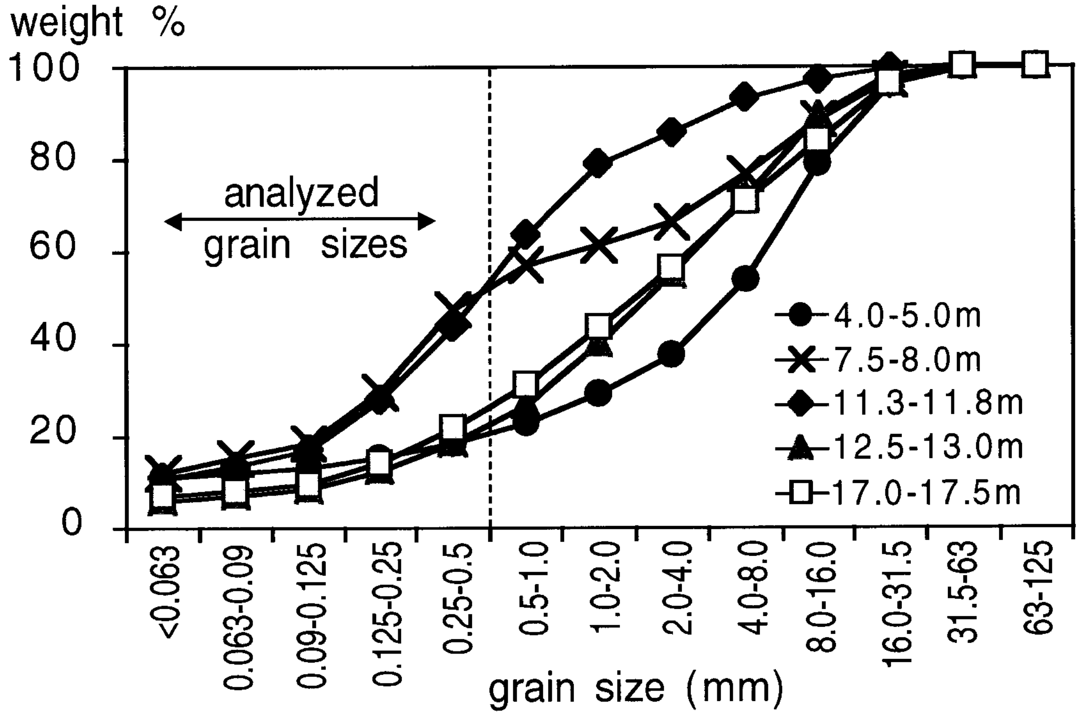

to 70% sand (fraction 0.063-2mm) are referred to as sand type. Samples from a depth of 4.0-5.0 m, 12.5-13.0 m and 17.0-17.5 m consist merely of gravelly material (fraction > 2mm is larger than 50%).

2.4.2 Extraction by 5M HCl (Fe_{tot}, Fe(II), Mn_{tot})

2.4.2.1 Iron

The results from the acid extractions are shown in Figure 2-3. Figure 2-3a shows the concentration of Fe_{tot} for each grain size fraction at various depths. Fe_{tot} is significantly higher in all four samples situated below the reference sample. The specific Fe_{tot} content increases with decreasing grain size and is usually twice as high in the smallest grain size compared to the largest. This difference in Fe_{tot} distribution among the grain size fractions is not seen in the reference sample (4–5 m), which

Figure 2-3
Specific concentrations in the fine fractions (<0.5mm) of the sieved samples at different depths of the aquifer: **(a)** Fe_{tot} (5M HCl), **(b)** ferric oxides (Fe(III)(TiEDTA)) and **(c)** non reducible Fe from the difference Fe_{tot} - Fe(III)(TiEDTA).

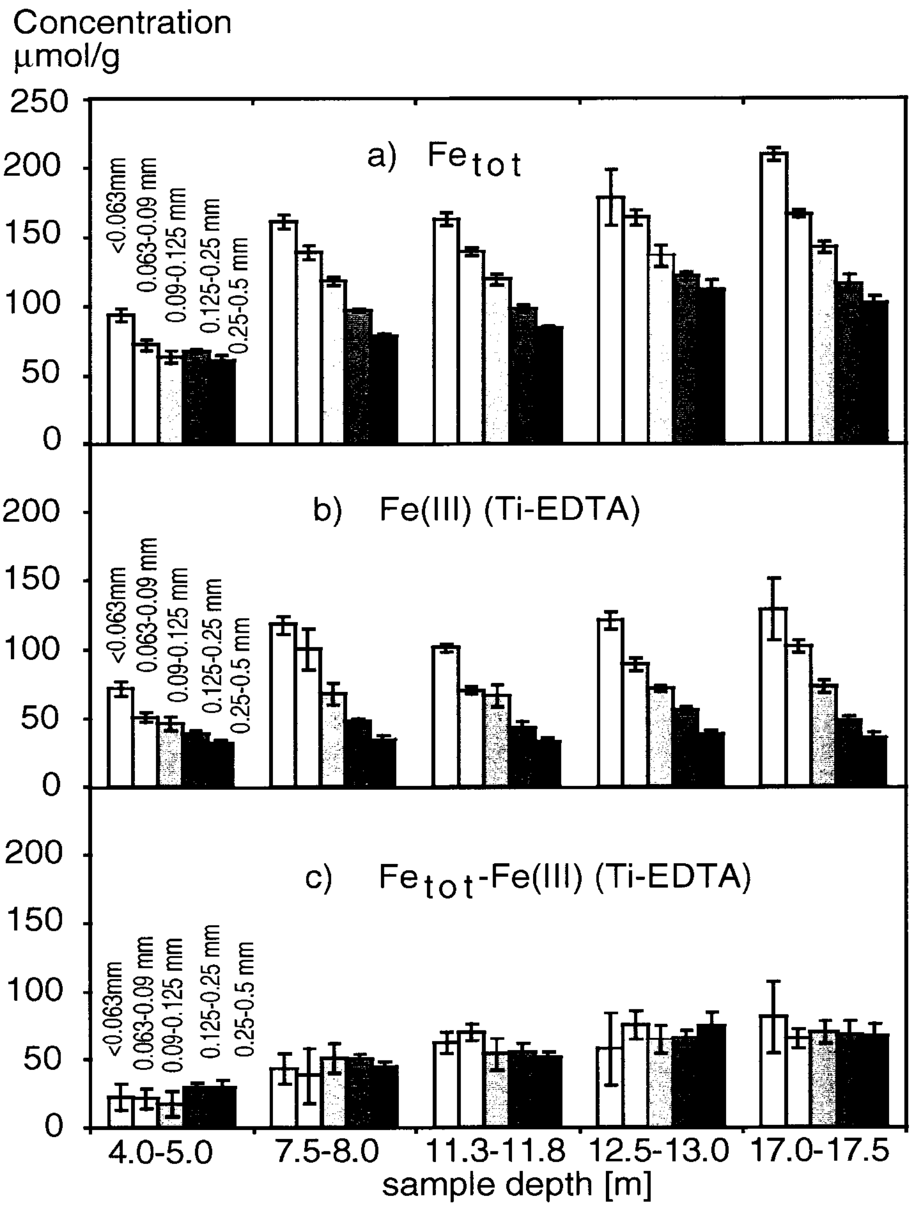

indicates that the deeper samples have been altered by the *in situ* treatment of ground water.

2.4.2.2 Manganese

The same representation is shown for Mn_{tot} in Figure 2-4. In a similar way there is more Mn_{tot} in the samples from the precipitation zone (> 5m,

Figure 2-4
Specific concentrations Mn_{tot} (5M HCl) in the smallest grain size fractions (<0.5mm) of the sieved samples at different depths of the aquifer.

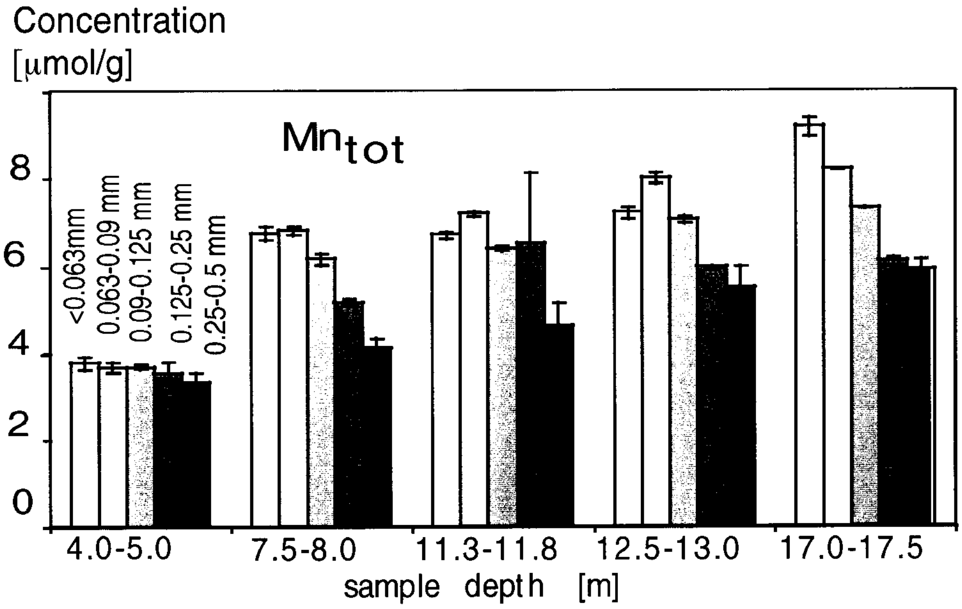

4-9 µmol/g) than in the reference sample (4-5 m, 3 to 4 µmol/g). In the sample from a depth of 4-5 m there is almost no grain size dependence, whereas the other samples show a higher content in the smaller grain sizes, but not as pronounced as for Fe_{tot}.

2.4.3 Reductive dissolution experiments

2.4.3.1 Iron

The total Fe-oxide concentrations (FeIII(TiEDTA)) determined by the Ti-EDTA extraction are shown in Figure 2-3b. A comparison with Figure 2-3a shows that ferric oxides account for the major fraction of iron (50-80% of Fe_{tot}) in the analyzed grain size fractions. There is again significantly more FeIII(TiEDTA) in the deeper samples than in the reference sample (4.0-5.0 m). The distribution of the ferric oxides is strongly grain size dependent. The largest difference between the background sample and the other samples is observed for the smallest grain size fractions, whereas in the 0.25-0.5 mm fraction, the Fe(III)-oxide contents are similar in the sample from 4-5 m and in the lower samples (30-35

Figure 2-5
Correlation between ferric oxide concentrations Fe(III)(TiEDTA) in the sieved samples and their respective specific surface area, which was calculated from the radius of the particles and a density $\rho = 2.6$ g/cm^3.

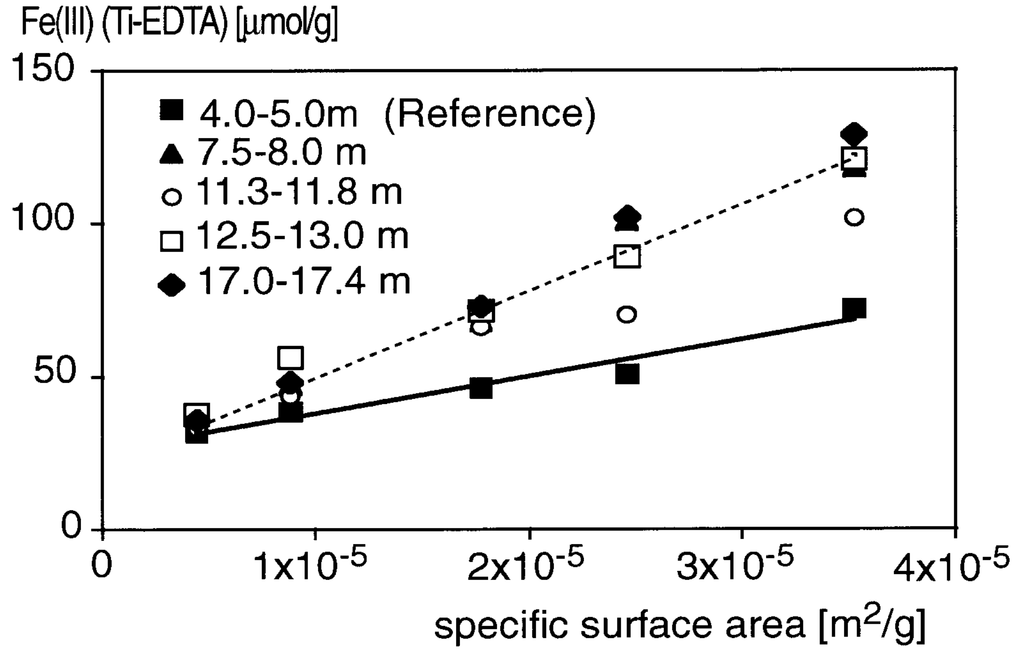

μmol/g). Amorphous ferric oxides, determined by dissolution with ascorbic acid, FeIII(AscA), make up a very small fraction of the ferric oxides, slightly higher in the reference sample (8-12%) than in the deeper samples (< 6%) (data not shown).Figure 2-3c shows the concentration distribution of the difference between Fe_{tot} and FeIII(TiEDTA). No large difference is found for the various grain size fractions, demonstrating that the pattern of Fe_{tot} dependence on the grain size in the samples below 5 m is due to the ferric oxides. This is an evidence that most of the FeIII(TiEDTA) fraction is produced by the *in situ* treatment. Ferrous iron, which was measured from the 5M HCl extract, does not account entirely for the non-reducible Fe fraction, additional forms of iron are present which are not reducible by Ti-EDTA. The striking pattern of the FeIII(TiEDTA) distribution among grain sizes suggests that precipitation of Fe-oxides is related to the available surface area. The specific surface area (SSA, m^2/g) is larger for small particles and can be calculated from their radius and the density of the aquifer sediment (2.6 g/cm^3). In Figure 2-5 FeIII(TiEDTA) concentrations are plotted versus the calculated specific surface area and show a good linear correlation. The straight line for the samples below the reference sample (< 5m) have a higher slope than the straight line for the reference. The origin is about the same for all samples including the reference and amounts to 21-28 µmol/g.

In addition to the sieved samples, the stones P1 and P20 as well as the samples P22 and P24 were measured for Fe_{tot}, FeIII(TiEDTA) and FeIII(AscA). The samples P1 and P20 are enriched in ferric oxides; they contain at least ten times more than the sieved samples. For P22 and P24, the Fe-concentrations are similar to the concentrations in the sieved samples, but the ferric oxide fraction is more important, 90-100% of the iron dissolved by 5 M HCl is reducible by Ti-EDTA. In samples P1, P20, P22 and P24, the Fe-oxides are crystalline to an extent of over 95%.Manganese

In the sieved samples reductive reagents extracted only small amounts of manganese, inferring that most of the manganese (Mn_{tot}, Figure 2-4) is present as Mn(II). The samples P1, P20, P22 and P24 contained two to three times more Mn_{tot} than the sieved samples and Mn was mostly reducible by Ti-EDTA (60 to 80% of Mn_{tot}). These are the only samples containing significant Mn-oxide concentrations, which occur together with the largest crystalline Fe-oxide fraction. The oxygenation of manganese(II) is much slower than the oxygenation of iron(II) (Stumm and Morgan, 1996). At pH 7 and in the absence of microorganisms the oxygenation of Mn(II) has a half-life time of in the order of years (Diem and Stumm, 1984), and ferric oxides are known to enhance its oxidation (Davies and Morgan, 1989). Therefore, the association of Mn-oxides with Fe-oxides is not surprising and suggests a Fe-oxide catalyzed mechanism.

Additional information can be gained from sieved samples by comparing extraction results for the Mn fractions, Mn_{tot} and Mn(III,IV)(TiEDTA), with and without pretreatment with acetic acid (for selective calcite removal), in Table 2-1. No significant manganese concentrations were found by reductive dissolution (Mn(III,IV)(TiEDTA). At least 50% of the total manganese of the sieved samples is soluble in acetic acid solutions

Table 2-1
Selective chemical extractions with (HAc) and without(Δ) pretreatment with dilute acetic acid.

	Manganese [μmol/g]			
	∅	HAc	∅	HAc
samples	Mn_{tot}		MnIII,IV(TiEDTA)	
P20	19.6 ±2	8.8 ±1	15.8 ±0.2	7.7 ±0.4
Sieved <0.063mm				
4.0-5.0	3.8 ±0.1	2.5 ±0.1	0.4 ±0.6	0.6 ±0.0
11.3-11.8	6.7 ±0.1	1.6 ±0.1	0.6 ±0.7	0.9 ±0.2
17.0-17.5	9.2 ±0.2	1.8 ±0.1	0.5 ±0.4	1.1 ±0.0

(HAc). Thus it is likely that the mostly bivalent manganese is incorporated in the calcite matrix or even present as manganous carbonate (rhodocrosite). Solubility calculations indicate that the system is saturated with respect to $MnCO_3$ ($K_{so} = 2.5x10^{-11}$, $I = 0.02$, $T = 15°C$) under the chemical conditions found in the ground water of La Neuveville with a hardness of 5mM HCO_3^-, a pH of 7.2 and 0.2 mg/L Mn(II). These ground water parameters indicate a CO_2 partial pressure, which is 50 times higher than the atmospheric partial pressure. The air-saturated ground water, which is injected back into the aquifer, has lost its excess of carbon dioxide, which leads to a higher pH (calculated pH = 8.8). Therefore it will be oversaturated with respect to the carbonate minerals $CaCO_3$, $MnCO_3$ and $FeCO_3$. Hence, from a thermodynamic point of view, rhodocrosite is likely to precipitate. Only in sample P20, the amount of Mn_{tot} remaining after pretreatment with acetic acid is equivalent to the reducible fraction (Mn(TiEDTA)), indicating the presence of crystalline Mn-oxides (Table 2-1).

2.4.4 Identification of Fe-oxides by XRD

The sieved samples studied by chemical extraction methods (above) as well as samples P1, P20, P22 and P24 were analyzed by XRD. The sieved samples as well as P22 and P24 did not show reliable signals of any iron or manganese containing minerals. The iron and manganese content of these samples was below the detection limit of this method (1-2 %, w/w FeOOH, resp. MnO_2). However, samples P1 and P20, which were found in the same bore core and contained brown-orange coatings, showed significant amounts of goethite. Also, in these samples, no manganese minerals could be detected by XRD. By selectively removing calcite with acetic acid we could concentrate the iron fraction of the samples. The aquifer samples P1, P20, P22 and P24 as well as the three sieved samples from a depth of 4.0-4.5 m, 11.3-11.8 m and 17.0-17.5 m corresponding to the smallest size fraction (<0.063mm) were pretreated with acetic acid and then measured by XRD.

To check the influence of the acetic acid treatment on the Fe-oxides, chemical extractions were repeated after this pretreatment. The corresponding results are shown in Table 2-2. The results for Fe_{tot} and FeIII(TiEDTA) before (∅) and after pretreatment (HAc) agree within 20% for almost all of the samples. The largest differences were observed for sample P20 with respect to the fraction Fe_{tot}, FeIII(TiEDTA) and FeIII(AscA). This may be due to the inhomogeneity of the samples taken from the surface of the stone. Among the sieved samples the largest differences relate to the fractions FeIII(AscA) and Fe(II). For FeIII(AscA), the difference can be related to the small absolute concentrations of this fraction which result in a large relative error. Fe(II) is partly incorporated in the calcite matrix which is dissolved by acetic acid explaining why there is less Fe_{tot} in the pretreated than in the untreated samples.

Figure 2-6 shows diffractograms of sample P22 with (lower) and without (upper) pretreatment with acetic acid. After pretreatment, calcite disappeared and dolomite remained. The dominant peaks of goethite located at 2Θ equal to 21.2° > 36.6° > 33.2° > 53.2° > 34.7° > 59.0° (decreasing intensities) become stronger as indicated by the assignments in the lower diffractogram. The presence of goethite becomes evident by the appearance of the peaks at 21.2° and 53.2°.

Table 2-2
Selective chemical extractions with (HAc) and without (Ø) pretreatment with dilute acetic acid.

		Iron [µmol/g]							
Samples		Fe_{tot}		Fe(II)		Fe(III) (Ti-EDTA)		Fe(III) (Asc. acid)	
	HAc	Ø	HAc	Ø	HAc	Ø	HAc	Ø	HAc
P20		3061±67	2096±67	25±1	21±4	1763±134	2196±48	29±4	22±3
4.0-5.0	< 0.063 mm	94±5	77±5	19±2	9±0	72±5	54±2	9±1	3±2
11.3-11.8	< 0.063 mm	163±5	156±5	15±4	10±2	101±3	81±21	3±2	3±1
17.0-17.5	< 0.063 mm	210±4	180±4	20±3	18±1	129±22	130±2	4±2	6±5

Figure 2-6
Diffractograms of sample P22. Upper curve: untreated sample, with peak positions of calcite ("c"). Lower curve: same sample after pretreatment with acetic acid, the peak positions of goethite are indicated as "gt" ("dol" = dolomite, "qz"=quartz).

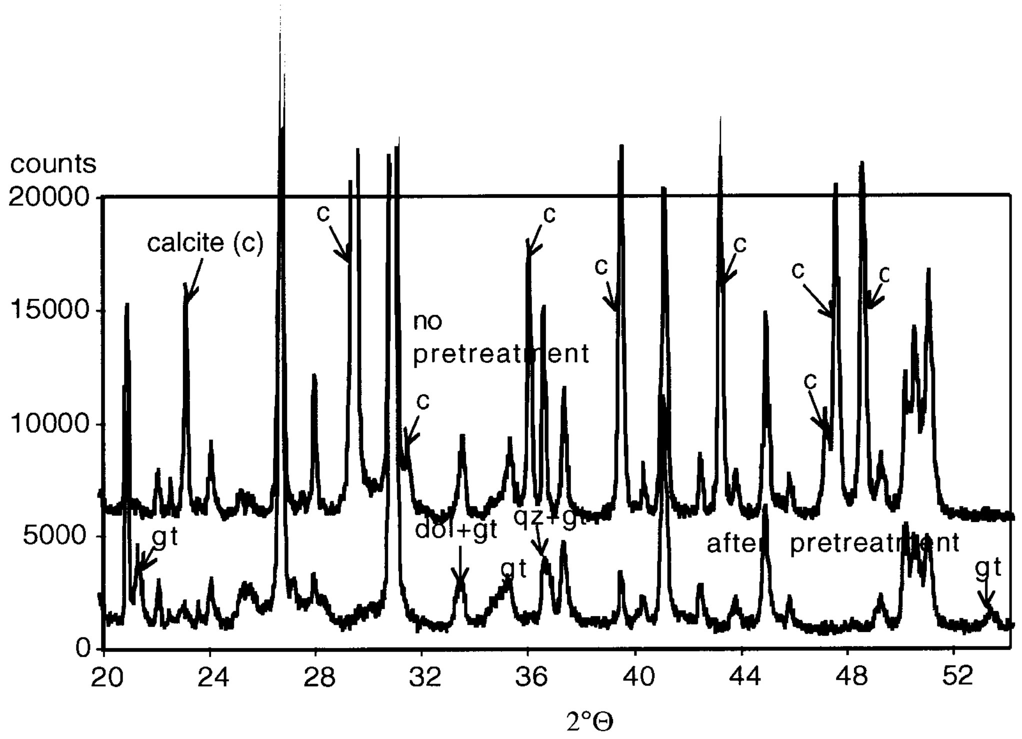

Table 2-3
Goethite content determined by Rietveld refinement (XRD) in the samples with (Hac) and without (Ø) treatment with dilute acetic acid. Numbers with asterisks (*) were calculated from concentration factor corresponding to calcite removal.

	Ø	**HAc**	**Ø**
	Goethite		**Calcite**
Samples	**% (w/w)**		**% (w/w)**
P1	18	80	72
P20	36	75	33
P22	3*	6	47
P24	3*	5	48
Sieved, <0.063 mm			
4.0-5.0 m	< 1	< 1	37
11.3-11.8 m	2*	3	34
17.0-17.5 m	1*	2	39

The diffractograms were quantified by the Rietveld refinement method. The results for samples P1 and P20 without (∅) and with acetic acid pretreatment (HAc) are shown in Table 2-3.

For the other samples goethite concentrations were too low to be detected and Rietveld refinements were performed with the pretreated samples only. The goethite concentration for the initial samples (without pretreatment) was then calculated by multiplication with a concentration factor (numbers with * in Table 2-3). This factor was derived from the calcite content, which was determined by XRD (P1 and P20) or by analyzing the calcium concentrations in the acetic acid extract. The fraction of calcite in the samples P1 and P20 was between 30 and 70 % (w/w), respectively. Thus a concentration factor of 4 and 1.6 is expected compared to the untreated sample. The Rietveld refinement method indicated 18% and 36 % (w/w) of goethite in the untreated samples P1 and P20, respectively. After pretreatment, goethite concentration amounts to 80 and 75%, respectively, corresponding to the expected concentrations for P1 (factor of 4) and P20 (factor of 2). In the pretreated samples P22 and P24, the goethite amounts to approximately 5 %. Witha calcite content of 50% in both samples, this yields an estimate of 2-3% goethite in the initial samples.

2.4.5 Mössbauer Spectroscopy

Mössbauer spectroscopy was applied to further characterize the Fe-oxide fractions in the samples. The results are given in Table 2-4 as fractions of the iron species relative to the total iron in the sample (in percent). Removing calcite should not affect the relative concentration, but improves the quality of the background. The samples with higher concentrations of iron, P1 and P20, were measured without pretreatment (Δ), whereas the others were pretreated with acetic acid (HAc). The sample 17-17.5 m (< 0.063mm) was measured before (Δ) and after acetic acid pretreatment (HAc). The results for both measurements agree within a few percent, which confirms the observation that the pretreatment does not affect the iron minerals in the samples.

Table 2-4
Relative fraction of solid iron determined by Mössbauer spectroscopy

Samples	Pretreated with acetic acid	Goethite	Ferrihydrite	Fe(II)	Fe(III)
			[% of total Fe]		
P1	no	100	0	0	0
P20	no	84	8	0	8
P22	yes	72	4	9	15
P24	yes	62	0	23	15
4.0-5.0 m <0.063mm	yes	41	5	26	28
11.3-11.8m <0.063mm	no	43	0	32	24
17.0-17.5m <0.063mm	no	46	3	28	23
17.0-17.5m <0.063mm	yes	50	1-2	27	23

The Fe-oxides goethite and ferrihydrite were identified. In addition, there were other Fe(II) and Fe(III) species. The Mössbauer data of these species correspond to iron in phyllosilicates (isomer shifts of 1.2-1.31 mm/s for Fe(II) and 0.48-0.52 mm/s for Fe(III) and quadrupole splitting of 2.81-2.84 mm/s and 0.54-0.6 mm/s, respectively). Goethite is the most abundant iron phase in all the samples, accounting for 40 to 100 % of the total iron. The highest fraction of goethite is found at the surface of the stones P1 and P20, accounting for 100 and 84% of the total iron, respectively. The unsieved samples P22 and P24, follow with 72 and 62% goethite. This is 150 to 200% of the goethite fraction found in the sieved samples (40-50% of the iron fraction). In all samples ferrihydrite represented only a minor fraction of ≤ 8 % of the total iron.

2.4.6 Comparison of the results from the different analytical methods

Generally a fairly good agreement between the different methods can be observed. Table 2-5 shows a comparison of the results from chemical extraction and XRD. The fraction Fe(III)(AscA) being negligible, the concentrations of Fe(III)(TiEDTA) were transformed from μmol/g Fe to weight percent FeOOH using the molecular weight of FeOOH, which

Table 2-5

Total crystalline FeOOH content measured from different methods

Samples		**Chemical extractions**	**XRD**
		FeIII(TiEDTA) w/w% FeOOH	**Goethite** w/w% FeOOH
P1		16	18
P20		16	36
P22		1	3*
P24		1	3*
4.0-5.0 m	<0.063mm	1	<1
11.3-11.8 m	<0.063mm	1	2*
17.0-17.5 m	<0.063mm	1	1*

Numbers with asterisks (*) were calculated from concentration factor corresponding to calcite removal

allows a comparison with the goethite concentrations from XRD. Similar results for samples P1 with concentrations of goethite between 16 and 18% were observed with chemical extractions and XRD, respectively. In sample P20, chemical extractions found only half the content measured by XRD, a result possibly due to inhomogeneous sampling. For the samples P22 and P24 the chemical extraction yielded 1%, whereas XRD indicated 3 % goethite. For the sieved samples from a depth of 11.3-11.8 and 17.0-17.5 m chemical extractions resulted in about 1% goethite, the same as was measured by XRD.

The relative concentrations of Fe-species calculated from the extraction results agree well with the results from Mössbauer spectroscopy in Table 2-4. 50 to 80% of Fe is found by chemical extraction to be ferric oxides (FeIII(TiEDTA); Figure 2-3), Mössbauer indicates 50 to 100%. The amorphous fraction (FeIII(AscA)) makes up ≤ 9% of the iron, Mössbauer showed ≤ 8%). Among the sieved samples it was found by chemical extraction that the reference sample contains slightly more FeIII(AscA) than the lower samples. This could not be verified with Mössbauer spectroscopy.

2.4.7 Accumulation of iron and manganese in the aquifer

After 10 years, 9 to 31 μmol/g of iron and 3 to 6 μmol/g of manganese are expected in the precipitation zone. These concentrations are based on an estimate for the last 10 years of operation of the treatment plant and are shown in Table 2-6. The estimates were calculated from the operational parameters of the plant assuming a homogeneous precipitation of the metals in a cylindrical precipitation zone defined by the injection wells (radius 7 m, depth 15 m; see Figure 2-1). The estimate was made with a range of iron and manganese concentrations in the ground water, since these varied over time.

The estimates can now be compared with the measured concentrations from the chemical dissolution of the sieved samples: iron was mostly precipitated as Fe-oxide, and thus Fe(III)(TiEDTA) is used, whereas for manganese Mn_{tot} is used. From these, net or "accumulated" concentrations are calculated, which are the differences between concentrations of the lower samples and the reference sample for each grain size (i.e. correction for the background iron and manganese). The

Table 2-6
Calculated Fe and Mn precipitated in the aquifer in 10 years operation time.

	Unit	Fe	Mn
[Me] in ground water	mg/L	0.3 - 1	0.1 - 0.2
Amount precipitated	kg	2519 -8395	840 - 1679
[Me] in the oxidation zone	kg/m^3	1.4 – 4.6	0.5 - 0.9
	mg/g	0.5 – 1.8	0.2 - 0.4
	μmol/g	**9 – 31**	**3 - 6**

The values were calculated assuming:

Average pumping rate over the last decade: 2300 m^3/d

Porosity n = 0.2

Filter volume V = 2300 m^3

Density of aquifer material ρ = 2.6 g/cm^3

"accumulated" concentrations are then multiplied by the fraction of the corresponding grain size (see grain size distribution, Figure 2-2) and added up. The results are shown in Table 2-7 and represent accumulated Fe-oxide and manganese concentrations for the sample fraction < 0.5 mm; these can be considered as minimum "accumulated" concentrations.

For the other fractions > 0.5 mm of the samples, it can be assumed from the results (Figs 2-3 and 2-4) that they contain less, or at most equal, iron and manganese. Thus the maximum precipitated concentrations will be twice to five times these values, since the fraction < 0.5mm makes up 18 to 50% of the sample. Our calculations yield a minimum range of 5 to 9 μmol/g and a maximum range of 11 to 27 μmol/g (Table 2-7). These numbers can be compared to the estimated 9 to 31 μmol/g. For manganese, a minimum of 1 μmol/g (Mn_{tot}) and a maximum of 2 to 4 μmol/g were found, which can be compared to the estimated 3-6 μmol/g manganese. The comparison of the calculated (Table 2-6) and measured (Table 2-7) concentrations, thus, shows good agreement.

The maximum concentrations shown in Table 2-7 indicate up to more than twice the iron and manganese in the two lower (12.5 m and 17 m deep) than in the upper samples (7.5 m and 11.3 m). This trend can also be seen in Figures 2-3 and 2-4, and these observations can be related

Table 2-7
Measured and extrapolated Fe and Mn concentrations accumulated in the aquifer in 10 years operation time.

Samples	**< 0.5 mm % (w/w) of the sample**	**FeIII(TiEDTA) < 0.5 μmol/g**	**FeIII(TiEDTA) Maximum μmol/g**	**Mn_{tot} < 0.5 μmol/g**	**Mn_{tot} Maximum μmol/g**
7.5-8.0 m	47.6	9	19	0.9	1.9
11.3-11.8 m	43.5	5	11	1.0	2.3
12.5-13.0 m	18.6	5	27	0.5	2.7
17.0-17.5 m	21.9	6	27	0.8	3.7
Reference (4-5 m)	18.5	11	59	0.7	3.8

to the hydraulic conductivities of the samples. The two lower samples, which were characterized based on their grain size distribution as gravel type, allow a larger flow rate than the upper sandy samples (see grain size distribution in Figure 2-2).

Most of the goethite was found in samples with very high calcite or mixed calcite and dolomite content: P1 contains 70% calcite, P20, 36% calcite and 33% dolomite. The question is whether these carbonate minerals favor Fe-oxide precipitation and the formation of goethite. Ongoing laboratory studies about adsorption and heterogeneous oxidation on calcite will help to develop an understanding of the formation of these coatings.

2.4.8 Risk of clogging

The dimensions of the treatment plant were calculated to be large enough to accommodate the iron and manganese removed from the ground water over hundred years. It is assumed that iron is precipitated homogeneously in the precipitation zone as crystalline Fe-oxide (like goethite). An adequate volume for the precipitation is foreseen. This approach was verified in the present study. A good agreement between measured and expected iron concentrations shows that the assumption of a homogeneous precipitation all over the precipitation zone is correct. Also Fe-oxides were mainly found to be goethite. Manganese could not be identified as Mn-oxide or another predominant mineral (e.g. $MnCO_3$). Thus, it is more difficult to estimate a volume of precipitated manganese (no density), but at least its mass can be estimated.

The solubility of carbonates can be affected through pH variations caused by the aeration of the ground water.

From this study the highest amount of precipitated iron and manganese is expected on the smallest particles of a coarse aquifer layer.

2.5 Conclusions

The study of aquifer samples from the *in situ* deferrisation and demanganation plant in La Neuveville allows the following conclusions:

- There is a net increase of solid iron and manganese in the precipitation zone. For a 10 years operation time of the plant, the increase of the metals doubles the background concentration of the aquifer. In some hot spots associated with carbonate minerals, a high enrichment in Fe- and Mn-oxides was found.
- The iron was mainly deposited as ferric oxide with a large crystalline fraction, which consists of 50-100% of goethite. This was confirmed by XRD and Mössbauer spectroscopy.
- Manganese was found essentially as Mn(II), probably in association with calcite or as $MnCO_3$. Exceptions are the samples with the highest Fe-oxide content (P1, P20), where Mn-oxides were found by chemical extraction.
- Chemical extraction, XRD and Mössbauer spectroscopy yielded similar concentrations of Fe-oxides. This shows that chemical extraction methods are useful tools for the characterization of small contents of Fe- and Mn-oxides.
- The largest accumulations of Fe and Mn are found in the samples of coarser material, which permit a better flow rate. In the same sample the smallest grain size fractions were always more concentrated, with ferric oxides essentially retained in the small fractions (< 0.09 mm).
- The amount of precipitation calculated from the treatment plant parameters (dimensions, pumping rate, iron and manganese concentration) and the measured concentrations (chemical extraction) in the precipitation zone are of the same order of magnitude. Therefore, this calculation is a useful tool to dimension the precipitation zone.

- If the heterogeneity of the aquifer in La Neuveville is taken into account, the spots highly concentrated in iron or manganese are far smaller than the volume of some impermeable layers.

Acknowledgement

I thank Gebr. Mengis AG for financial and technical support. Arnold Stahel kindly provided the XRD facilities. Jürg Zobrist and J.-M. Génin are acknowledged for fruitful discussions and Gary Amy for revision of the English of the manuscript. Elisabeth Salhi is thanked for assistance in the laboratory and in the field.

3 SORPTION AND OXYGENATION OF Fe (II) IN CALCITE SUSPENSIONS*

3.1 Introduction

3.1.1 Adsorption of cations on carbonate minerals

In the Swiss Central Valley ("Mittelland") ground waters are well buffered by carbonate minerals (calcite, dolomite) with resulting pH values in the range of pH 7.0-7.5. Besides the pH stabilization by fast dissolution and precipitation processes, carbonate minerals can act as sorbents and immobilize heavy metals.

Adsorption of metals on calcite has been investigated for numerous divalent cations: Mn^{2+}, Cd^{2+}, Zn^{2+}, Co^{2+}, Ni^{2+}, Pb^{2+}, Sr^{2+}, Ba^{2+} (Lorens, 1981; Franklin and Morse, 1983; Davis et al., 1987; Comans and Middelburg, 1987; Zachara et al., 1993; Xu et al., 1996; Temmam et al., 2000). Adsorption experiments were conducted in suspensions saturated with $CaCO_3$. Despite of the larger concentration of Ca^{2+}, metal cations are able to outcompete it for binding to carbonate surfaces. Adsorption is often not reversible and followed by an incorporation of the bivalent cation into the calcite. Incorporation produces a solid solution type of precipitation at the calcite surface. Depending on the predominant calcite faces and the available active surface sites, preferred adsorption of a cation can lead to zonal differences in composition (Paquette and Reeder, 1995; Reeder, 1996; Temmam et al., 2000; Astilleros et al., 2002). Moreover, Stipp et al. (1992, 1998) and Hoffmann and Stipp (2001) observed solid state diffusion of Cd^{2+}, Zn^{2+} and Ni^{2+} through the calcite lattice. Both affinity to the calcite surface and sorption reversibility differ as a function of the cation. The parameters affecting the sorption behavior are: (i) size of the substituting ion and (ii) hydration enthalpy. Cations, which are smaller than Ca^{2+} (e. g. < 1.0 Å) are more easily taken up by replacement of Ca^{2+} in the $CaCO_3$ lattice than the larger ones such as Sr^{2+} and Ba^{2+} (1.18 Å). A strong hydration shell hinders the incorporation of the ion into the solid phase, which facilitates desorption (Zachara et al., 1991). Moreover, replacement of Ca^{2+} by cations with distorted octaedral coordination geometry (e.g. Cu^{2+}) leads to a destabilization of the calcite lattice. Therefore Cu^{2+} is expected to favor sites with missing carbonate or close to the surface, which allows adjustment of the coordinative environment (Schosseler et al., 1999).

---

* *Submitted to* GEOCHIMICA ET COSMOCHIMICA ACTA

3.1.2 Interaction of Fe(II) with $CaCO_3$

Although considerable research has been performed on the interaction of metalic cations with calcite, only limited information is available for Fe(II). The only studies related to Fe(II) and calcite concern co-precipitation of Fe(II) in supersaturated $CaCO_3$ solutions. Dromgoole and Walter (1990) determined the homogeneous distribution coefficient between solid and solution for Fe(II) relative to Ca^{2+} in co-precipitation experiments. Fe(II)-co-precipitation increased with increasing precipitation rate and temperature (10°< T < 75°C). The final Fe concentration in the calcite was < 0.4 mol %. Rimstidt et al. (1998) determined a correlation function for the distribution coefficient, K_d, of a trace metal in solid carbonate (calcite or siderite). He considered several cations in binary $MeCO_3$-$CaCO_3$ systems near the precipitation equilibrium with the host carbonate. The predicted K_d for Fe(II) is ca. 7 times higher than the experimental value determined by Dromgoole and Walter (1990).

3.1.3 Mineralogy of Fe(II)/Ca carbonate

Thermodynamic of the aqueous Fe(II) carbonate system in a natural reduced environment were investigated by Bruno and coworkers (Wersin, 1990; Bruno et al., 1992a; Bruno et al., 1992b,) and reviewed by King (1998). The concentration of ferrous iron is limited by the precipitation of the ferrous carbonate (siderite), which has the same mineralogical structure as calcite (rhombohedral carbonate; Reeder, 1983). Regardless of this similarity, mixed calcite-siderite forms are unstable. The solid solution continuum between ferroan calcite and calcian siderite is interrupted by a large miscibility gap, where both phases coexist. Information relevant to natural environmental conditions was reported by Wajon et al. (1985). In this study Fe(II) (0.114 M) was precipitated in supersaturated $CaCO_3$-solutions with calcite and other natural calcareous sediments. The main products formed were a calcian siderite with 10% mol Ca^{2+} as well as pure siderite. They proposed that Fe(II) concentrations are controlled by a calcian siderite rather than siderite, which is slow to precipitate. This high substitution for the calcian siderite contradicts the results obtained by Rosenberg (1963), who could synthesize calcian siderite with 5.8 and 7 mol % of Ca^{2+} in siderite at elevated temperatures and pressures (400 °C < T < 550°C and 3.65 x 10^3 bar < p < 4.13 x 10^3 bar). Other information was found in a compilation about the average content of impurities in natural carbonates. There, Veizer (1983) indicates an average of 6.8 mole per mil Fe(II) in marine calcite, which is similar in composition to the synthetic Fe/$CaCO_3$ precipitates produced by Dromgoole and Walter (1990) in laboratory experiments (3.5-4 per mil).

Furthermore, in the field of steal pipe clogging by calcareous deposits, studies addressed growth inhibition of calcite by Fe(II). It appears that

Fe(II) is a very efficient cationic inhibitor of calcite crystallization (Meyer, 1984; Katz et al., 1993; Müller, 1998). Meyer (1984) found that already 1 x 10^{-8} M Fe(II) causes a 20% reduction of the calcite growth rate. Katz et al. (1993) observed reduced growth rates, and for high Fe(II) concentrations, supersaturation with respect to calcite. They found that Fe(III) is an even better inhibitor than Fe(II). Moreover, the best growth inhibition of calcite was reached by addition of Fe(II) in presence of oxygen. Thus, according to Katz et al. (1993), it is not Fe(II), but its oxygenation product, Fe(III), that causes a reduced calcite growth rate in Meyer‘s experiment at pH > 8. Fe(III) formed from oxygenation of Fe(II) leads to homogeneously distributed Fe(III) species, which efficiently hinder calcite formation. In contrast, direct Fe(III) addition leads to discrete areas with polynuclear Fe(III) hydroxides, which have a smaller impact on calcite growth rate.

3.1.4 Ferrous iron oxygenation: kinetics and product formation

Oxygenation of Fe(II) in aqueous solutions has been investigated in many studies (Stumm and Lee, 1961; Davison and Seed, 1983; Millero et al., 1987; von Gunten ans Schneider, 1991; Emmenegger et al., 1998). The reaction strongly depends on Fe(II) speciation, which is affected by the pH: ligands that raise the electron density around the Fe(II) atom facilitate its oxidation (Luther III, 1990). The most common ligand (OH^-) increases the second-order rate constant of the oxygenation of Fe(II) in the order $Fe^{2+} < Fe(OH)^+ < Fe(OH)_2$ (Wehrli, 1990). Also the Fe(II)-carbonato-complexes are oxidized more rapidly (King, 1998). Similarly, ferric oxide surfaces enhance the rate of Fe(II) oxygenation (Tamura et al., 1976; Tamura et al., 1980). The question arises, whether carbonate surfaces, like calcite, can accelerate the oxygenation of Fe(II) as well. The oxygenation of Fe(II) in calcite systems has been studied by Loeppert, who found that the rate increases with the surface concentration (Loeppert et al., 1984; Loeppert and Hossner, 1984; Clarke et al., 1985). However, in this work the oxidation of the 0.01M initial Fe(II) concentration produced so much protons that pH varied between 3.5 and 7.5 and that calcite was readily dissolved. Hence it is difficult to assess an effect of surface catalysis for these experiments.

Loeppert and coworkers also characterized the Fe oxides formed by the oxygenation of Fe(II) in presence of calcite; they identified mainly lepidocrocite. Goethite was formed as well at higher CO_2 concentrations. However, as stated above, the experimental conditions were not well defined.

3.1.5 Deferrisation for drinking water production

In reduced aquatic systems, microorganisms can use iron oxides as terminal electron acceptors, thereby releasing Fe(II) which is highly soluble and mobile (Lovley, 1987; Lovley and Phillips, 1988; von Gunten and Zobrist, 1993). Such reduced, Fe(II)-containing ground waters can not be used directly for drinking water purposes. Mostly because of esthetic consideration water treatment is recommended when the Fe(II) concentration exceeds 0.3 mg/L (World Health Organization, 1996). The removal of iron is typically carried out by oxidation followed by precipitation of iron oxides. One possibility is an in situ process, where oxygen-containing water is injected into the underground. As a result an iron oxide containing oxic zone is created around the supply well, which functions as a filter for the pumped ground water (Hallberg and Martinell, 1976; Zienkiewicz, 1984; Bernard and Serieys, 1986; Rundell and Randtke, 1987; Braester and Martinell, 1988; Appelo et al., 1999).

So far, there is no evidence for the precipitation mechanisms, which could be biotic, with the help of iron oxidizing microorganisms (Mouchet, 1992a; Søgaard et al., 2001) or abiotic, by chemical sorption on the aquifer surfaces followed by oxidation (Appelo et al., 1999). Recently, a field study was completed at an in situ ground water treatment site, which is located in a calcareous aquifer in La Neuveville, Switzerland (Mettler et al., 2001). The largest Fe oxide concentrations were found in the smallest grain size fraction (< 0,063 and 0.063-0.125 mm). Most of the Fe oxides were identified as the crystalline ferric oxide goethite.

Mettler et al. (2001) hypothesized the formation of these coatings by a chemical oxygenation of Fe(II), which is adsorbed to calcite.

The objectives of the present study are to investigate the Fe(II)-calcite interactions in the absence and in the presence of oxygen. This includes the following questions:
-Can Fe(II) be immobilized by calcite? How important is this process and how fast does it take place?
-Is the redox reactivity of Fe(II) changed in presence of calcite? Can the oxidation of Fe(II) be accelerated in presence of calcite as do other surfaces, especially Fe(III)-oxides?
-How does the redox reactivity of Fe(II) change under alternating anoxic-oxic conditions and with a growing amount of Fe(III) in the calcite suspension? Do Fe-oxide coatings form in the calcite suspension? Can the produced Fe-oxide be identified?

The first question will be addressed by sorption experiments on time scales varying between hours to one week. The sorption data will be compared with results from desorption and dissolution experiments. The redox reactivity of Fe(II) will be assessed by measurement of the oxidation kinetics of Fe(II) in presence and in absence of calcite, as well as after longer equilibration times of Fe(II) with calcite. Finally, changes of the oxidation kinetics upon repeated adsorption and oxygenation of Fe(II) will be measured. Only very little Fe(III)-oxides were produced under these experimental conditions, which could not be identified.

3.2 Materials and Methods

3.2.1 Chemicals

Chemicals used were at least reagent grade. Solutions were prepared with deionized water (Q-H_2O, Barnstead nanopure). At first $CaCO_3$-saturated water was synthesized with nanopure water and the calculated amount of Ca^{2+} ($CaCl_2$) and HCO_3^- ($NaHCO_3$), required for CaCO3 saturation at pH 7. These concentrations cannot be calculated precisely enough. To avoid any precipitation, $CaCO_3$-saturated water of the desired pH (7.0 ± 0.1) was then prepared by equilibrating calcite powder (Merck, Suprapur) at the requested CO_2 partial pressure for 4 days. Afterwards it was filtered and kept at higher pCO_2 (4.5-4.9 %) until use.

Glassware for the experiments was first cleaned with detergent, then soaked in 10% HNO_3 for at least 12 hours (Stipp and Hochella Jr., 1991) and rinsed with nanopure water.

All experiments performed with Fe(II) were performed in an anoxic glove box containing a palladium catalyst to remove oxygen (Coy Laboratory Products Inc., Michigan). Fe(II) was added as solution (0.01M) of the $FeSO_4.7H_2O$ salt (sealed, Riedel de Haehn).

For milling of calcite and for the calcite stock solutions, saturated water at atmospheric pCO_2 (pH 8.3) was prepared according to the same procedure. Gas flows of the desired volume percentage of CO_2 were mixed with flow meters (Brooks Instruments) from pure gases (N_2, CO_2) or gas mixtures (20 % CO_2 in N_2, 8 % O_2 in N_2 as well as compressed air).

3.2.2 Preparation of the calcite suspension

Calcite (Merck, suprapur; mean particle size ca. 80 μm) was milled in suspension in a zircon oxide ball mill to small particles of 1.5-1.8 μm diameter. A specific surface area of 2.4 m^2/g was determined by BET / nitrogen adsorption for the dried suspension. The milled product was then diluted to a concentrated calcite suspension (100.7 g/L), which served as stock suspension and was kept under atmospheric CO_2 partial pressure. Measurements of particle size distribution did not show noticeable changes of the particle sizes during the 8 months of the experiments.

Calcite suspensions were prepared by adding the adequate volume of calcite stock suspension to the $CaCO_3$-saturated water (pH 7) leading to the desired final $CaCO_3$ concentration (1, 2, 10 and 25 g/L). These

Figure 3-1

Particle size distribution of the calcite suspension (series A) before (initial) and after the experiment (here 25 cycles of Fe(II) addition and oxidation. See 3.3.9).

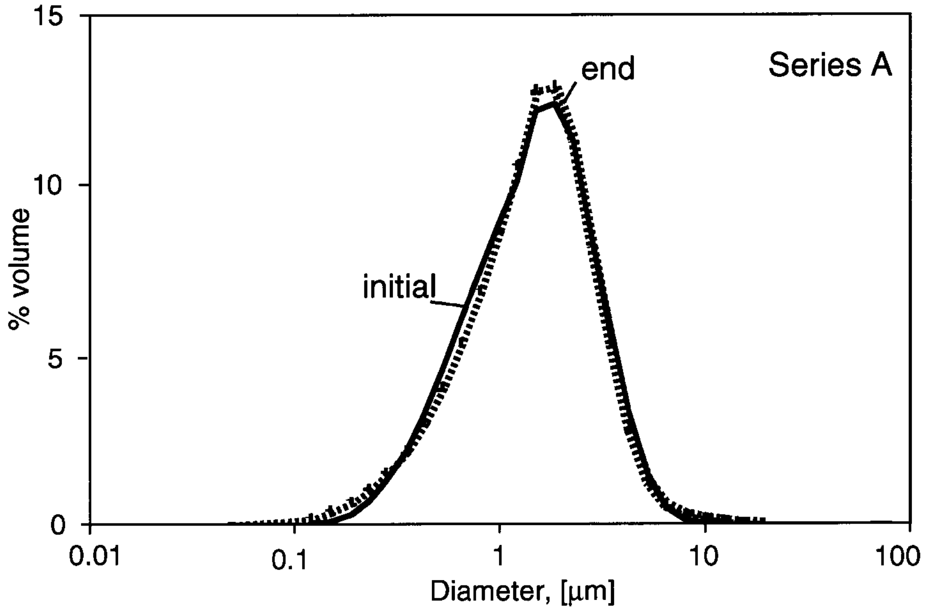

suspensions were prepared at least 4 days before the start of the experiments in sealed glassware, to avoid undesired precipitation in the course of the experiment. Measurements with X-ray diffraction revealed no traces of $CaCO_3$ polymorphs (aragonite, vaterite) other than calcite, even in the suspension that contained iron. No noticeable differences of grain size distribution were found between the fresh stock calcite suspension (10 days old), the stock suspension after 2 months and at the end of the experiments. Even in the presence of Fe(II/III), particle size distribution of the calcite suspensions was not altered (Figure 3-1).

3.2.3 Analytical methods

Fe(II) was measured with the Ferrozine method with a detection limit of 3 x 10^{-7} M in a 1 cm cell (Gibbs, 1976; Stookey, 1970; spectrophotometer Uvikon, Bio-Tek Kontron Instruments). The total Fe concentration was measured photometrically after reduction of Fe(III) with ascorbic acid.

Calcium concentrations of acidified samples (HNO_3, pH 1-2) were determined with inductively coupled plasma atomic emission spectroscopy (Spectro; detection limit < 0.02 mg/L).

Proton concentration was controlled with a pH glass electrode (Orion) calibrated with buffer solutions (Merck, Titrisol; pH 7 and pH 9).

3.2.4 Characterization of the solids

3.2.4.1 Chemical methods

The following methods were used to characterize the iron precipitates: reductive dissolution with titanium(III)-EDTA (0.008M/0.05M) and ascorbic acid (0.114 M) at pH 8 for the total Fe(III)-oxide (Fe(III)) and the amorphous fraction ($Fe(III)_{am}$). In addition total iron (Fe_{tot}) and Fe(II) were determined by acid dissolution in 5 M HCl (Heron et al., 1994; Kostka and Luther III, 1994). For all dissolution experiments, aliquots of a sample (0.05-0.1g) were equilibrated with the reagents for 24 hours. After filtration through 0.2 μm filters (nylon or teflon) the samples were analyzed for iron. All of the concentrations given below are mean values of three measurements, the indicated error corresponds to one standard deviation of these measurements.

For spectroscopic analysis, the calcite was first selectively removed, which was achieved best by acetic acid (20% vol. or pure). Afterwards, solid/liquid separation was performed with centrifugation (8000 rpm, 30 minutes) or filtration (0.1 μm, cellulose nitrate).

3.2.4.2 Spectroscopies

The solids ($CaCO_3$ and produced Fe oxides) were characterized by X-ray diffraction measurements (XRD; Scintag XDS 2000, CuKα) as well as ATR infrared spectroscopy (Spectrometer FTS 575C, Bio Rad). Fe oxides show characteristic infrared absorption bands, which allow their identification (Cornell and Schwertmann, 1996).

3.2.4.3 Laser diffraction

Grain size distribution was measured with laser diffraction (Malvern Master Sizer X). The diffraction pattern was calculated assuming spherical particles.

3.2.5 Sorption experiments

Various volumes of a $FeSO_4$ stock solution were added to 100 ml calcite suspension (1 and 2 g/L) and equilibrated for 24 hours, 72 hours and 1 week under constant stirring. After the equilibration time, samples were filtered through 0.2 μm nylon filters and measured for Fe(II). The recovery of the total Fe(II) in the suspension was also tested: calcite samples were dissolved in acetic acid and analyzed for Fe(II).

Adsorption kinetics were measured in the same way: to a 250 ml batch containing 1 or 10 g/L calcite, $FeSO_4$ was added to an end concentration of 1×10^{-5} M. Samples were taken as function of time and measured for Fe(II) after filtration.

3.2.6 Desorption of Fe(II) with ligand

To 50 ml of a calcite suspension (1 g/L), which was equilibrated with Fe(II) for 1h, 5h, 24h, 72h and 1 week, 1 ml ferrozine (0.02M) was added. Samples were taken after 1 hour and 15 hours, filtered (0.2 μm, nylon) and measured for aqueous Fe(II).

3.2.7 Dissolution kinetics with CO_2

A volume of 300 ml of a calcite suspension (1 g/L) was equilibrated with Fe(II) for 24 h, 72 h and 1 week. After these times, 80 ml were separated from the initial solution; aqueous and total Fe(II) were measured. Then, the suspension was sparged with a 20% CO_2/N_2 gas mixture and sampled in regular time intervals. The samples were filtered (0.2 μm) and measured for Fe(II) and calcium; pH was registered as well.

3.2.8 Fe(II) oxygenation kinetics in calcite suspensions

These experiments were conducted in a sealed batch under controlled $O_2/CO_2/N_2$ gas flow. The O_2 concentration was either 3.8 % or 15.3 % (v/v; equivalent to 2.4 and 6.2 mg/L O_2, respectively). Upon addition of Fe(II) to the equilibrated suspension, 3-4 ml of sample were taken after certain reaction times, quenched in acetic acid/sodium acetate buffer (2M, pH 4.5), filtered and measured for remaining Fe(II).

3.2.9 Products of oxygenation of Fe(II) in calcite suspensions

To a concentrated (25 g/L) calcite suspension sparged with CO_2/N_2, increments of Fe(II) were successively added in intervals of 24 hours (series B, “oxic”) or 15 hours (series A “anoxic”). Whereas in series B, Fe(II) was added in presence of oxygen (3.8 %); in series A, the suspensions were first deaerated (CO_2/N_2) and allowed to equilibrate with Fe(II) before oxygen addition. Suspensions (series A and B) were then oxygenated with a gas flow of $O_2/CO_2/N_2$ (15.3 % O_2). Because of the high calcite concentration, most of the Fe(II) (> 95% in serie A) is expected to be adsorbed at the calcite surface, thus the Fe(II) is principally oxidized as the adsorbed species. After the 5., 13., 16., 24., 44. Fe(II)-addition step, a sample of the Fe(III) containing calcite suspension was diluted to 1g/L, and Fe(II) oxygenation kinetics were measured as described above.

After the last addition and oxidation step, the suspensions were filtered (0.2 μm; Nylon), dried and kept in a dessicator to analyze the Fe oxides. For spectroscopic analysis (X-ray diffraction and IR) they were concentrated with acetic acid (see 2.3.2.1. *selective chemical dissolution*). Selective chemical dissolutions were done with the dried calcite suspensions.

3.3 Results and discussion

3.3.1 Adsorption kinetics

Adsorption kinetics with 1, 10 and 25 g/L calcite are shown in Figure 3-2a. Adsorption kinetics can be divided into 2 distinct steps. A fraction of Fe(II) is adsorbed very fast upon its addition to the calcite suspension (≤ 1800 s). This "instantaneous " Fe(II) adsorption is followed by a slower reaction.

In Figure 3-2b first order representation of the adsorption kinetics is shown. The first instantaneous adsorption step is hardly measurable. Therefore, no kinetics information can be extracted. The second phase obeys pseudo first order kinetics with a slope proportional to the surface concentration:

$$-d[Fe(II)]/dt = k'_{ads} \bullet [Fe(II)] = k_{ads} \bullet [Fe(II)] \bullet [CaCO_3] \,, \qquad (3\text{-}1)$$

Pseudo first order rate constants k'_{ads} of $3.0 \times 10^{-6}\ s^{-1}$, $2.8 \times 10^{-5}\ s^{-1}$ and $7.4 \times 10^{-5}\ s^{-1}$ were determined for 1, 10 and 25 g/L calcite, which results in a rate constant k_{ads} of $2.9 \times 10^{-6}\ L\ g^{-1}s^{-1}$.

For the first rapid adsorption step, Davis et al. (1987) proposed a diffusion-limited process. To normalize this process for various experimental conditions, they introduced the fraction F of sorbed Fe(II), ($[Fe(II)]_{ads}$), divided by the sorbed Fe(II) at the inflexion point ($[Fe(II)]_{ads,\mathbf{ip}}$. The inflexion point is the first point, which can be linearized in Figure 3-2b.

$$F = [Fe(II)]_{ads} / [Fe(II)ads]_{ads,ip} \qquad (3\text{-}2)$$

Drawing F against the square root of time resulted in a straight line (Figure 3-3). If we plot our data accordingly, a straight line with the three data sets can be obtained (1 g/L, 10 g/L and 25 g/L). The slopes are the same for all three experiments (b = 0.0049).

In agreement with our findings, adsorption of transition metals on calcite has been reported to occur in two kinetically distinct stages: one or two fast initial steps (10 to 30 minutes), which are followed by a slower

Figure 3-2

Adsorption kinetics of Fe(II) onto calcite with varying solid concentrations (Saturated solution of $CaCO_3$ at pH 7, 10 μM Fe(II)). **(a)** Fe(II) concentration versus time. **(b)** Logarithmic plot of data in (a). Inset shows more points measured up to 7 days.

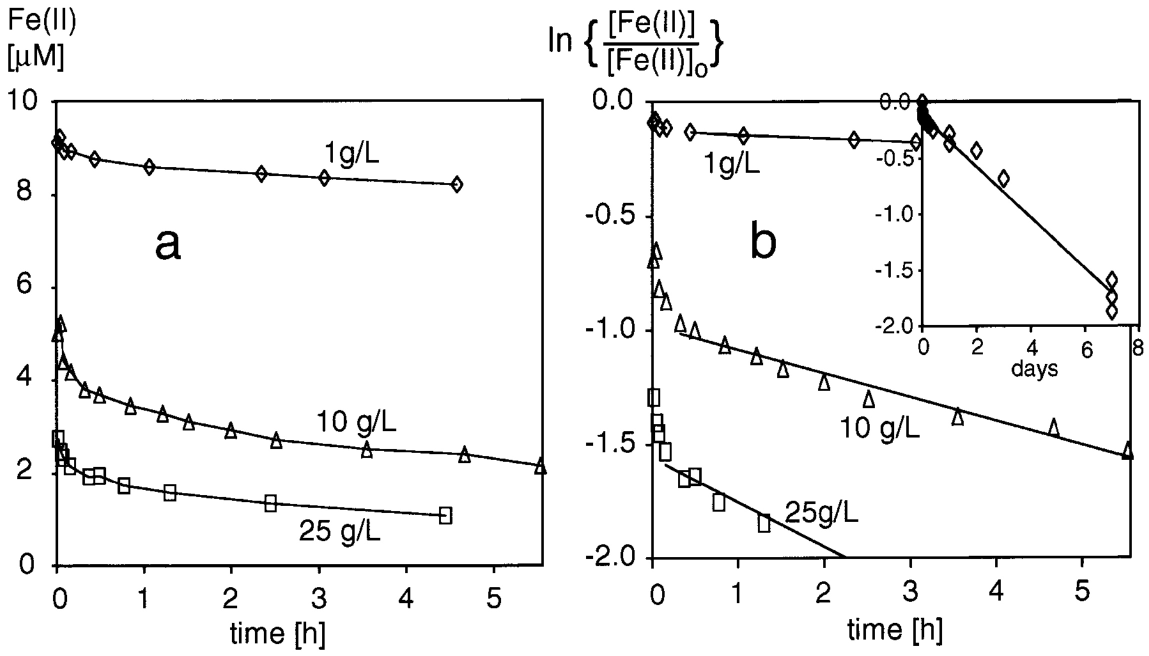

adsorption of several days (Lorens, 1981; Mn^{2+}:Franklin and Morse, 1983; Cd^{2+}: Davis, 1987; Zn^{2+}: Zachara et al., 1988).

There is no agreement regarding the kinetics of the first step: Davis could fit it with a diffusion model. The second slower step has been described by first order kinetics (Eq. 3-1), where the decrease of the ion concentration is proportional to the calcite concentration (Mozeto, 1984; Franklin and Morse, 1983; Zachara et al., 1988; Davis et al., 1987). The adsorption of Fe(II) on calcite can be formulated as follows:

1) fast: $Fe(II) + {>}CaCO_3 \Leftrightarrow {>}CaCO_3\text{-}Fe(II)$ (3-3.a)

2) slow: ${>}CaCO_3\text{-}Fe(II) \Rightarrow {>}CaFe(CO_3)_2$ (3-3.b)

The first step (3.a) is a fast, reversible adsorption, whereas the second slower step (3.b) can be interpreted as re-crystallization or co-precipitation. Fast dissolution and precipitation reactions characteristic for the calcite surface can incorporate components from the solution.

Figure 3-3
The first points of Figure 3-2 are drawn after the formula: F = $[Fe(II)]_{ads}$ / $[Fe(II)ads]_{ads,ip}$.

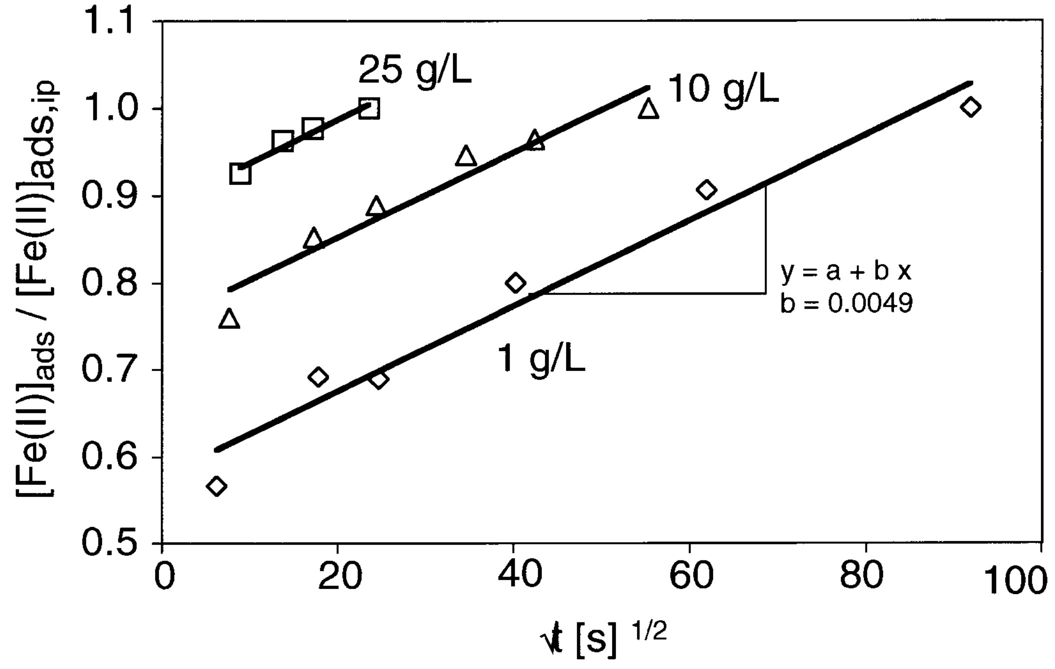

This re-crystallization transforms the solid from the surface; Stipp et al. (1998) showed that it reached depth of nm to μm after 9 months at ambient air. In water, Dove and Hochella Jr. (1993) showed that surface rearranges in near saturation conditions towards calcite. Small units dissolve and are precipitated leading to the growth of larger ones, without changing the total mass of the solid. Both adsorption and re-crystallization are more important in fresh calcite suspensions, whereas aged calcite is less reactive (Mozeto et al., 1984). During re-crystallization, adsorbed metal ions can be incorporated into the crystal structure (Zachara et al., 1988; Davis et al., 1987; Lorens, 1981). This is comparable with observations made for Cd^{2+} (Davis et al. 1987; Comans and Middelburg, 1987), Zn^{2+} (Zachara et al., 1989; Zachara et al., 1988), Mn^{2+} (Franklin and Morse, 1983) and Co^{2+} (Xu et al., 1996).

3.3.2 Fe(II) sorption capacity on calcite

The sorption capacity of Fe(II) on calcite was determined with Langmuir isotherms:

$$\Gamma = \Gamma_{max} \cdot K_{ads} \cdot [Fe(II)]_{aq} / \{1 + K_{ads} \cdot [Fe(II)]_{aq}\} \qquad (3\text{-}4)$$

Γ and Γ_{max} are the adsorption capacity and the maximum adsorption capacity expressed in mol/g, K_{ads} is the adsorption coefficient. Equilibrium concentrations of adsorbed Fe(II) (Γ, mol/g) are drawn against Fe(II) concentration in solution ($[Fe(II)]_{aq}$, mol/L). The equilibrium aqueous Fe(II) concentrations are measured from the filtered suspensions. The adsorbed concentrations of Fe(II), ($[Fe(II)]_{ads}$, mol/g) are calculated by subtracting the aqueous, from the initially added Fe(II) concentrations, ($[Fe(II)]_{tot}$):

$$[Fe(II)]_{ads} = [Fe(II)]_{tot} - [Fe(II)]_{aq}. \qquad (3\text{-}5)$$

Linearization of equation (3.4) to:

$$1 / \Gamma = 1 / \{\Gamma_{max} \cdot K_{ads} \cdot [Fe(II)]_{aq}\} + 1 / \Gamma_{max} \qquad (3\text{-}6)$$

allows to determine Γ_{max} from the intercept and K_{ads} from the slope of the line. Figure 3-4 shows the results of the adsorption experiments after 24 hours, 72 hours and 1 week (168 hours) equilibration time (calcite concentration 2 g/L).

The initially added $[Fe(II)]_{tot}$ concentrations were verified simultaneously with the measurement of $[Fe(II)]_{ads}$ by averaging the Fe(II) concentration determined after dissolving a small volume of the suspension in acetic acid. The fraction Fe(III) at the end of the experiments was usually in the range of the analytical error, typically < 12%. Adsorption capacities were difficult to measure because experimental parameters such as stirring intensity and saturation conditions impact the calcite surfaces. This is reflected in the scatter of the data and in the large error of the parameters (calculated for a 95 % confidence interval).

The figure shows that Fe(II) is continuously taken up by calcite during the whole week of the experiment, which looks like an increasing sorption capacity of the solid for Fe(II). On the other hand, we know from

Figure 3-4
Sorption capacity of calcite for Fe(II) in dependence of varying Fe(II) concentrations and equilibration times (24 hours, 72 hours and 1 week). A Langmuir isotherm was fitted for the data points measured after 24 hours. The dashed lines above and below the fit represent the 95 % confidence interval of the Langmuir parameters (2 g/L calcite, pH 7.0; $pCO_2 = 10^{-1.49}$).

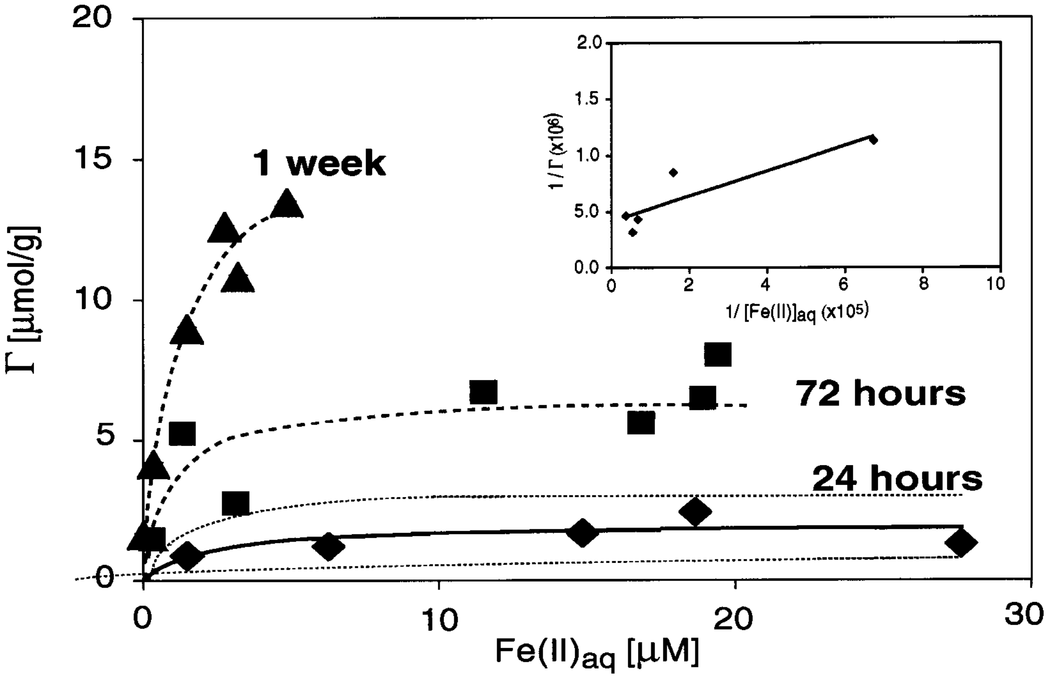

the kinetic experiments that sorption of metal ions on calcite surfaces occurs in two steps. During the second step the cations are incorporated proportionally to their solution concentration due to steady recrystallisation of the calcite surface. Indeed, the increasing sorption capacity of calcite after 24 hours, 72 hours and 1 week equilibration times of the suspension with Fe(II) is compatible with this kinetics. The first rapid adsorption step of the kinetics experiments is compatible with an adsorption process, which involves only the interface of the solid and the liquid phases and for which a maximum adsorption capacity (Γ_{max}) can be defined. For this reaction a Langmuir isotherm was calculated from the sorption data measured after 24 hours; they are closest to the reaction equilibrium achieved after ca. 30 minutes. The Fe(II) taken up within 24 hours by recrystallisation is negligible compared to the adsorbed Fe(II) in the first adsorption step. A maximum adsorption capacity, Γ_{max}, of 2.4±1.3 μmol/g and an adsorption coefficient K_{ads} of

$4.7 \pm 1.8 \times 10^{+5}$ (n = 5; 95% confidence intervall) is thus determined. The langmuir model fit is drawn in Figure 3-4 as solid line; the light lines above and below represent the 95 % confidence interval. Transformed with respect to the specific surface area of the calcite (2.4 m^2/g), the maximum adsorption capacity is equivalent to 0.6 adsorption sites per nm^2, which is equal to one Fe(II) every 170 $Å^2$. It corresponds to 10 % of the exchangeable Ca-sites on calcite, considering the [1014] face with 5 sites/nm^2 (Möller and Sastri, 1974; Stipp et al., 1992; Fenter et al., 2000).

3.3.2.1 Comparison with other bivalent metals

Adsorption properties of Fe(II) on calcite cannot be directly compared to other cations, because no parallel experiments with other cations were investigated in this study. However, a similar system, was used by Zachara et al. (1991) with a calcite concentration of 5 m^2/L (25 g/L; specific surface concentration 0.20 m^2/g, BET krypton adsorption). The mean particle size of the calcite was 9.0 μm. Metal concentrations ranged between 10^{-4} to 10^{-8} mol/L. These conditions can be compared to ours: calcite concentrations of the sorption experiments ranged between 1 or 2 g/L corresponding to 2.4, and 4.8 m^2/L, respectively. The ferrous iron concentration was 10^{-5} to 10^{-6} M. Zachara et al. (1991) found that the affinity of the cations toward calcite decreased in the order: Cd > Zn > Mn > Co > Ni. The adsorption edge was modeled using an exchange reaction of Ca^{2+} with the cation according to the equations:

$$\text{X-Me} + Ca^{2+} \Leftrightarrow \text{X-Ca} + \text{Me(II)} \qquad (3\text{-}7)$$

$$K_{ex} = [Me^{2+}]_{aq} / [Ca^{2+}]_{aq} \bullet \{(\text{X-Ca}) / (\text{X-Me})\} \qquad (3\text{-}8a)$$

Equation 8a in logarithmic form yields:

$$\log \{[Me^{2+}]_{aq}/[Ca^{2+}]_{aq}\} = i + s \log \{(\text{X-Me}) / (\text{X-Ca})\} \qquad (3\text{-}8b)$$

The surface site concentration, [X], was based on Ca^{2+} isotopic exchange measurements on the calcite surface. (X-Ca) and (X-Me), the fractions of [X] occupied with the corresponding cation are calculated from the corresponding adsorbed concentration: (X-Me) = $\{[\text{Me(II)}]_{ads}$ (mol/g) / [X] (mol/g) } and (X-Ca) = 1 – (X-Me). $[Me^{2+}]$ or $[Ca^{2+}]$, the concentrations of the aqueous ions, were determined by measurement after 24 hours and corrected according to a speciation program. Our experiments were performed at pH 7 only, which corresponds to one dissolved Ca^{2+} concentration, whereas Zachara et al. (1991) worked with a larger range of pH (6.5 - 9.5), with different range of Ca^{2+} and metal concentration for which they determined the parameters. The parameters s (slope) and i (intercept) from the fit of Equation 8 are listed in Table 1 together with the value determined for Fe(II). Except Zn and Fe(II) all cations have a slope close to unity. Zn has the lowest pK among the cations (pK 9.0, see Table 1). Zachara et al. (1988) hypothesized that both Zn^{2+} and $ZnOH^+$ may be sorbing species. Fe(II) with a slope of 1.4 has the next lowest pK (pK 9.5). In analogy, the species $FeOH^+$ could in addition to Fe^{2+} play a role in the sorption to the calcite surface.

With a more detailed fit Zachara et al. (1991) determined the exchange coefficients K_{ex}. They are listed in Table 3-1 as well.

The equation 8 is also the equation, which results from the law of mass action for the formation of mixed solid solution $MeCO_3$-$CaCO_3$ from two solid carbonates (Stumm and Morgan, 1996):

$$CaCO_3(s) + Me^{2+} \Leftrightarrow MeCO_3(s) + Ca^{2+} \qquad (3\text{-}8.c)$$

With a corresponding $\log K = \log K_{so}(CaCO_3) - \log K_{so}(MeCO_3) = \Delta \log K_{so}$

In the Table 1 the distribution coefficient after Rimstidt et al. (1998), K_d, which is a function of $\Delta \log K_{so}$, as well as the $\Delta \log K_{so}$ are shown. Both values predict the affinity of metal to the calcite surface. The trend of the exchange constants K_{ex} corresponds to the trend foreseen by the solubility constants, $\Delta \log K_{so}$.

In Figure 3-5 our results (24 h) are shown together with the data of Zachara et al. (1991): the logarithm of the dissolved metal concentration (mol/L) is drawn against the logarithm of the adsorbed concentration (mol/g). It appears that Fe(II) at pH 7.0 sorbs as strongly as Cd (pH 7.4), the divalent metal with the largest affinity for calcite. This shows that Fe(II) has a specially good affinity for $CaCO_3$ compared to the other cations. This is in accordance to the trend foreseen with $\Delta \log K_{so}$:

$\Delta \log K_{so}(Cd) > \Delta \log K_{so}(Fe) > \Delta \log K_{so}(Mn)$.

Table 3-1

Slope s and intercept of the Equation 8b determined by Zachara et al. (1991) for the listed cations and Fe(II) (this work). K_{ex} determined by Zachara et al. (1991) compared to the theoretical distribution coefficient K_d calculated after Rimstidt et al. (1998), $\log(\Delta K_{so})^1$ of the solid carbonate and hydration enthalpy ΔH_{hydr} for several bivalent metals (Marcus, 1994). Constants valid for I = 0.0 M , 298.15 °C, 1 bar.

Metal	**i**	**s**	**pK**	**log K_{ex}**	**log K'_d**	**$\log(\Delta K_{so})^1$**	**ΔH_{hydr} [kJ/mol]**
Ca^{2+}							-1600
Cd^{2+}	-2.77	1.07	10.1	3.02	2.3	5.4	-1830
Mn^{2+}	-0.76	1.15	10.6	1.31	1.3	2.1	-1870
Zn^{2+}	-0.04	1.86	9.0	2.43	1.3	1.7	-2070
Co^{2+}	-0.37	1.09	9.7	0.56	1.0	1.7	-2035
Ni^{2+}	-0.28	1.0	9.9	0.51	-0.6	-1.5	-2115
Fe^{2+}	-1.32	1.44	9.5		1.4	2.5	-1970

$\log(\Delta K_{so})^1 = \log (K_{so(CaCO3)}-K_{so(MeCO3)})\ K_{so(MeCO3)}$ from Stumm and Morgan (1996) except $K_{so(FeCO3)}$ from Wersin (1990).

Figure 3-5

Adsorbed and dissolved Fe(II) after 24 hours at pH 7.0, $pCO_2 = 10^{-1.49}$, with 4.8 m^2/L calcite (2 g/L). The dashed lines signalize the points obtained by Zachara et al. (1991) with Cd^{2+} and Zn^{2+} at pH 7.4 with 5 m^2/L calcite (25 g/L).

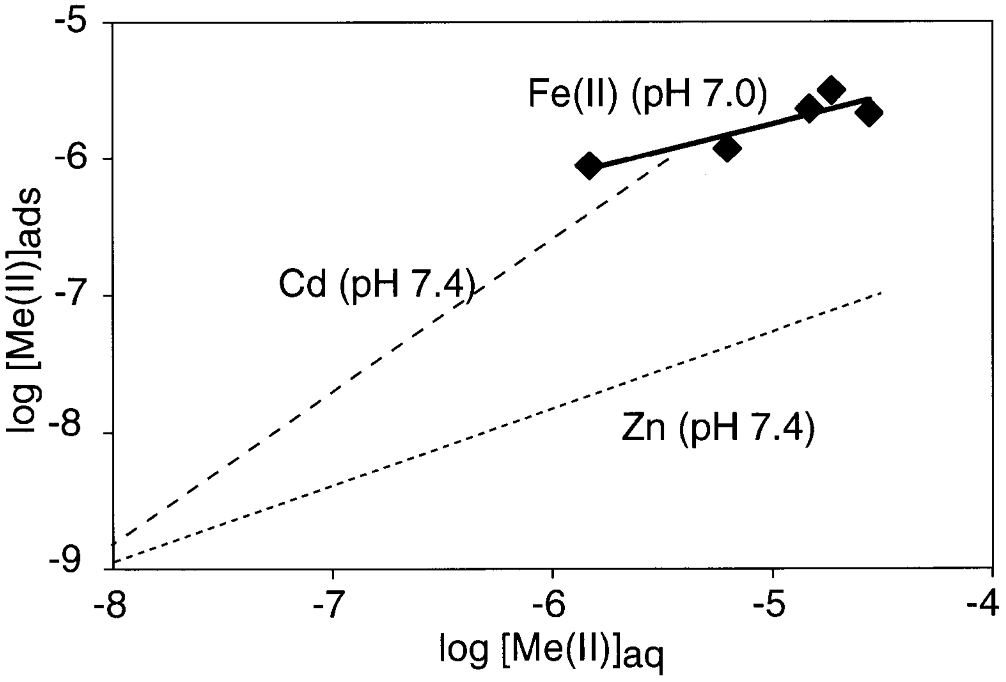

3.3.3 Remobilization of Fe(II) adsorbed to calcite

3.3.3.1 Ligand promoted remobilization

To understand the kinetics of the sorption process over several days, desorption experiments where performed with ferrozine for batch experiments that were equilibrated during one week ($CaCO_3$ = 2 g/L). As a function of the initial conditions, between 86% to 94% of the total Fe(II), were sorbed to the calcite after 1 week (Table 3-2). Despite a strong complexation of Fe(II), the fraction of sorbed Fe(II) remaining after 1 hour of the addition of ferrozine were 81 to 91 %. Consequently, it has to be hypothesized that after 1 week of equilibration of Fe(II) with calcite, Fe(II) is mostly incorporated into calcite and therefore not available for complexation with ferrozine anymore. In another experiment ($CaCO_3$ = 1 g/L), desorption of Fe(II) with phenanthroline was followed as a function of the equilibration times of Fe(II) with calcite (Table 3-3).

It was found that the irreversibly bound fraction of Fe(II) increased with longer equilibration time. After 1 hour of equilibration, close to all adsorbed Fe(II) was recovered with phenanthroline. After longer equilibration times, the irreversibly bound fraction reached a few percent of the Fe(II) after 1 hour, 9% after 5 hours to 11 % after 24 hours and 21 % after 72 hours. The total sorbed Fe(II) was 12%, 16 % and 29 % after 5 hours, 24 hours and 72 hours, respectively.

Table 3-2
Adsorbed Fe(II) fraction after 1 week equilibrium time and corresponding adsorbed fraction after addition of ferrozine to mobilize the adsorbed Fe(II).
2 g/L calcite, pH 7.

$Fe(II)_{tot}$	Adsorption (1 week)	With ferrozine (1 hour)
[μM]	% Fe(II) adsorbed	% Fe(II) adsorbed
20	94	91
24	88	84
28	91	87
32	86	81

Table 3-3
Adsorbed Fe(II) fraction in function of the equilibration time and corresponding adsorbed fraction after addition of phenanthroline.
10 μM Fe(II), 1 g/L calcite, pH 7.

time	Adsorption	With phenanthroline (1 hour)
[hours]	% Fe(II) adsorbed	% Fe(II) adsorbed
1	4	3
5	12	9
24	16	11
72	29	21

3.3.3.2 Partial dissolution of the calcite particles

The fate of the immobilized Fe(II) was further investigated in experiments in which calcite and Fe(II) were first equilibrated during a desired time span (24 h, 72 h and 1 week or 48h and 1 week). After equilibration the suspension was sparged with a gas mixture containing excess CO_2, which dissolved the outer layers of the calcite particles. In the first series, the gas mixture was composed of 20 % CO_2 (80% N_2 v/v), in the second 100% CO_2. A larger CO_2 concentration leads to faster dissolution kinetics and to a larger dissolved Ca^{2+} end concentration: 23 % of the solid $CaCO_3$ (1 g/L) are dissolved with 100 % CO_2, versus 9% with 20% CO_2.

Figure 3-6 shows the release of aqueous Fe(II) during the dissolution of calcite with 20 % CO_2: At time 0, the Fe(II) concentration corresponds to the fraction still in solution after 24h, 72h or 1 week equilibration time, which is 76%, 54% and 19% of the total Fe(II), respectively. In the course of the experiment the incorporated, as well as the adsorbed Fe(II) is released simultaneously with calcite dissolution. At the end, 97%, 86% and 62% of the initial Fe(II) concentrations are recovered.

Figure 3-6

Release of Fe(II) as function of time during dissolution of 1 g/L calcite with 20% CO_2 after prior equilibration of Fe(II) (1 x 10^{-5} M, at pH 7.0; $pCO_2 = 10^{-1.49}$) for 24h (◊), 72h (□) and 1 week (Δ,).

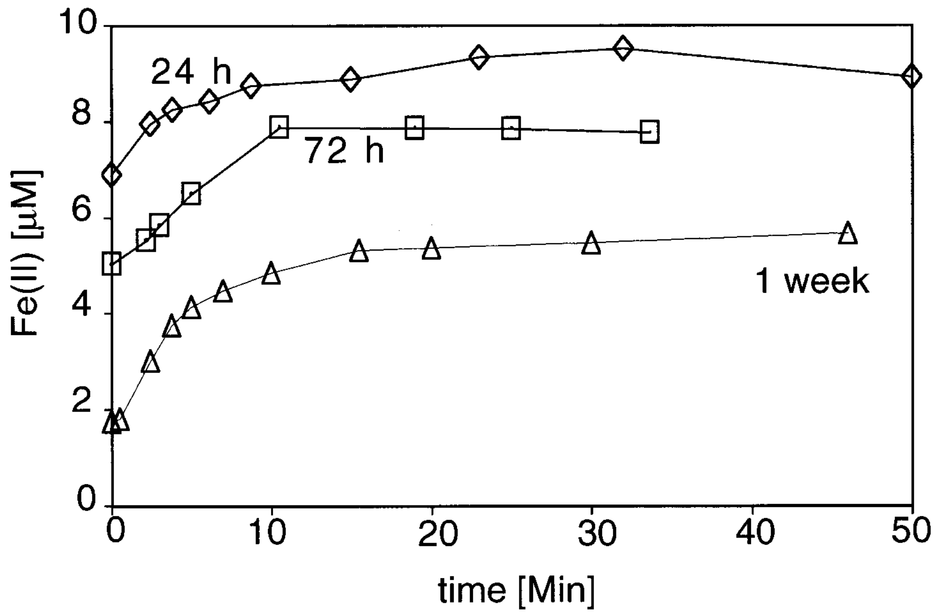

It can be concluded that the fraction of Fe(II) recovered by dissolution experiments decreases with increasing equilibration time: After 24 hours equilibration time, dissolution with 20% CO_2 mixtures led to an almost 100% recovery of Fe(II), whereas after longer equilibration times, a fraction of ≤ 40 % of the total Fe(II) still remains associated with the calcite. Re-adsorption of Fe(II) on the fresh surface can still happen even at lower pH (pH 6.5). However it must be small considering the case (24 h), where almost the total Fe(II) was recovered (97%).

Here, similar to above the ligand promoted desorption, the fraction Fe(II), which remains associated to the calcite increases with equilibration time. It can be hypothesized that this is a consequence of Fe(II) incorporation into deeper calcite layers, which are not dissolved under our experimental conditions.

In Figure 3-7 the net released Fe(II) and Ca^{2+} concentrations are drawn as fraction $\{[Fe(II)]_{diss} / [Ca^{2+}]_{diss}\}$ in dependence of the dissolution time; dissolution was performed with 100 % CO_2 after 1 week equilibration. A first abrupt drop follows into a gradual decrease, which goes until close to 20 minutes, then the Fe(II)/Ca ratio slowly diminishes. These indicate a large Fe(II)/Ca ratio at the surface, which then steadies and finally diminishes the more calcite is dissolved. An inset in Figure 3-7 shows an idealized spherical particle with radius r, Δr is the dissolved layer of the particle, the darker the line the more Fe(II). The three portions of the curves can be related to the distribution of Fe(II) in the particle: There is a concentrated layer of sorbed Fe(II) at the surface, which evolves into a region of constant ratio Fe/Ca, finally the Fe(II) becomes more diluted with increasing dissolved layer.

Assuming spherical particles, the width of the dissolved layer can be estimated from the dissolved calcium and a mean grain size of the particles (1.8 μm). In Figure 3-8 the released Fe(II) ($[Fe(II)]_{diss}$) concentrations are drawn against the released calcium concentration ($[Ca^{2+}]_{diss}$), which have been converted to a layer width of a spherical particle (nm, secondary X-Axis). All the dissolution data are shown (24h, 48h and 1 week equilibration, 100% CO_2). With 20 % CO_2 a depth of the dissolved layer can be calculated as ca. 20 nm, with 100% CO_2 it

Figure 3-7
Dissolved Fe(II) relative to the dissolved Ca^{2+} after 1 week equilibration of Fe(II) with calcite dissolution with 100 % CO_2 (▲). Inset: model particles of radius r and dissolved layer Δr.

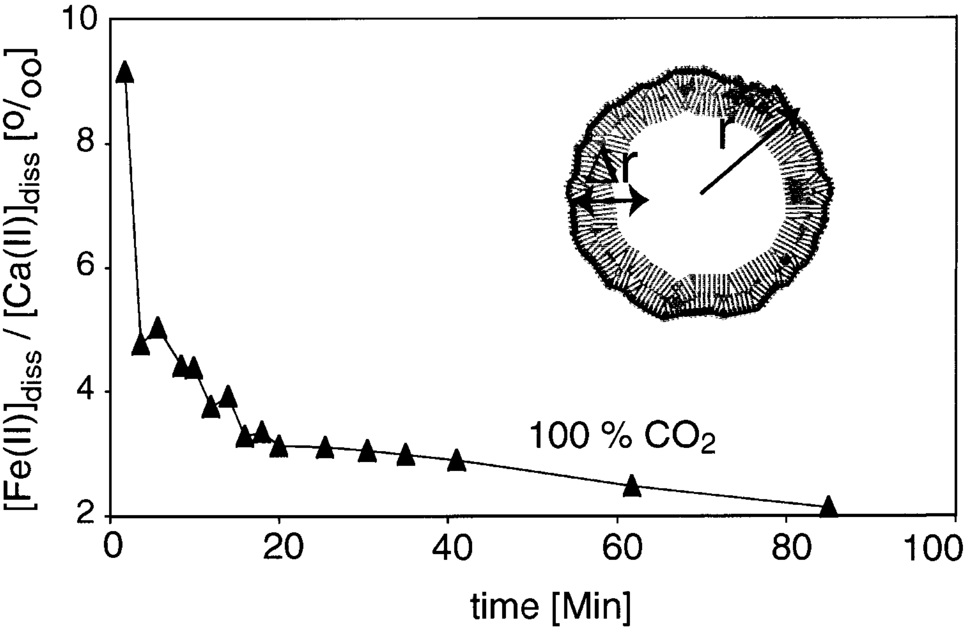

corresponds to a depth of ca. 70 nm. The longer the equilibration time the larger the Fe(II) dissolved relative to the Ca^{2+} dissolved.

For the longest equilibration time (1 week), the released Fe(II) is proportional to the Ca^{2+}, with a slope of ca. 4 $\times 10^{-3}$ for both CO_2 concentrations when dissolved calcium concentration 0.1 mM < Ca^{2+} <1 mM. At larger $[Ca^{2+}]_{diss}$ concentrations (> 1 mM) the quotient of [Fe(II)] / $[Ca^{2+}]$ decreases gradually until the end point of the dissolution at 2.2 mM $[Ca^{2+}]$ and 5.5 μM [Fe(II)]. The same slope after 1 week equilibration time for both series can be interpreted as the formation of a mixed $FeCO_3$-$CaCO_3$ phase at the upper layers of the calcite particles. The Fe/Ca ratio of this phase corresponds to 0.4 % mol $FeCO_3$ in $CaCO_3$, which represents 1 Fe(II) for every 250 Ca^{2+}. In deeper layers a smaller mole fraction (Fe(II)/Ca^{2+}) indicating that Fe(II) has not reached these layers.

Figure 3-8

Dissolved Fe(II) versus dissolved Ca^{2+} after different equilibration times: 24h (◊), 48h (O), 1 week (Δ, ▲). The secondary X-axis, Δr, represents the depth of the layer dissolved calculated form the amount calcium measured in solution. A straight line (dashed) between 2 nm < Δ r < 23 nm indicates the constant Fe(II)/Ca mole fraction measured in dissolution experiments that were equilibrated for 1 week.

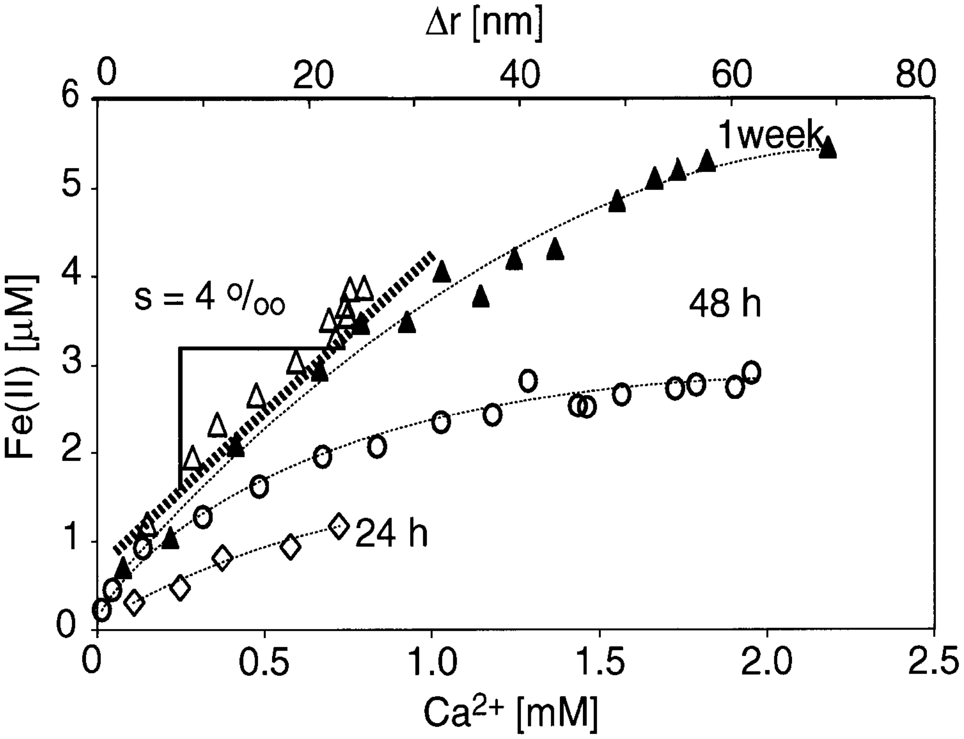

The observations from desorption and dissolution experiments can be summarized as follows:

- Complexation: Fe(II) is partly adsorbed, partly irreversibly bound to the calcite surface. The fraction Fe(II), which is not released anymore augments the longer Fe(II) and calcite were equilibrated.
- Dissolution with CO_2: An increased incorporation of Fe(II) into the calcite occurs with increasing equilibration times. After 1 week equilibration Fe(II) shows following enrichment pattern in the outer particle layers. There is close to 1 % Fe(II) relative to calcium at the surface, this ratio decreases to a constant ≤ 0.4 % in the next layers and slowly diminishes. It seems that a mixed $FeCO_3$-$CaCO_3$ phase with a maximum mole fraction of 0.4 mol % is formed in the intermediary layers.

For the reversibility of adsorption, Zachara et al. (1991) distinguished between cations that are well and others that are barely desorbed based on adsorption experiments of 24 hours. Co, Ni and Zn, are nearly totally desorbed, whereas Mn and Cd remain sorbed to calcite. They showed that reversibility of sorption is correlated with the Gibbs free energy of hydration of the aqueous ion. Hydration enthalpies are determining, since enthropies do not differ more than 0.3 kJ mol^{-1} K^{-1} among these cations (Marcus, 1994). From a thermodynamic point of view binding to surface carbonate sites by cations with a strong hydration is unfavorable. Hydration enthalpies of the best sorbing cations Cd^{2+}, and Mn^{2+} are –1830 kJ/mol and –1870 kJ/mol, these are the lowest from the series. Fe(II) comes next with –1970 kJ/mol. The other cations follow with hydration enthalpies larger than –2000 kJ/mol (see Table 1). Consequently Fe(II) is expected to be incorporated in calcite less easily than Mn^{2+} and Cd^{2+}, but better than Co^{2+}, Ni^{2+} and Zn^{2+}. Our results show that sorption of Fe(II) on calcite is reversible for equilibration times below 1 hour. After longer times (> 5hours), some of the Fe(II) can not be recovered by complexation anymore. Indeed Fe(II) is incorporated in deeper layers as a consequence of the second sorption reaction that goes on for several days (see sorption kinetics, Figure 3-2).

3.3.3.3 Incorporation of Fe(II) into calcite

In coprecipitation experiments of Fe(II) and calcium in seeded supersaturated calcium carbonate solution Dromgoole and Walter (1990) produced mixed Fe/$CaCO_3$ phases with a molar ratio of 0.35-0.4 % Fe(II). This mol fraction is very close to the Fe(II) mol fraction we find in calcite, which has been equilibrated for several days with Fe(II) (10 μM). This leads to the conclusion that after longer equilibration times of Fe(II) with calcite a mixed Fe/$CaCO_3$ phase forms with a molar ratio of 0.35-0.4 %.

There are two mechanisms for explaining the incorporation of cations into calcite:

(i) Re-crystallization has been put forward (see adsorption kinetics). It is identical to the slow sorption reaction with a pseudo first order rate constant of disappearance of Fe(II) from the solution $k'_{ads} = 3 \times 10^{-6}\ s^{-1}$ (Eq. 3-1). From this rate of re-crystallization it is possible to calculate a flow rate F of Fe(II) through the surface (in mol $m^{-2}\ s^{-1}$). For this purpose the rate equation has to be divided by the surface to volume ratio of the calcite suspension ($S = 2400\ m^2/m^3$) and multiplied by the volume of the solution ($V = 10^{-4}\ m^3$; $[Fe(II)] = 0.01\ mol/m^3$) :

$$F = (V / S) \bullet dFe(II)/dt = k'_{ads} \bullet [Fe(II)] \bullet (V / S) \qquad (3\text{-}9)$$

This results in a flow rate of $1.2 \times 10^{-15}\ mol^{-2}s^{-1}$ through the overall calcite surface present in solution. (ii) The second mechanism is solid state diffusion, it was proposed by Hoffman and Stipp as possible mechanism for the incorporation of cations in deeper calcite layers (Ni, Hoffmann and Stipp, 2001; Cd, Stipp et al., 1992; Zn, Stipp et al., 1998). They observed transport of these cations from the calcite surface by XPS measurements beyond the depth affected by recrystallization. The transport into the lattice was in the order of tens of Å per week to tens of nm per week, which corresponds to diffusion coefficients D of 10^{-17} and $10^{-21}\ cm^2/s$. This values are similar to $D = 8 \times 10^{-20}\ cm^2/s$ determined by Lahav and Bolt (1964) with ^{45}Ca-exchange experiment, who applied a diffusion function to explain the disappearance of the label concentration from the solution.

From our CO_2 dissolution experiments a diffusion coefficient can be estimated for the experiment, in which almost the total Fe(II) was recovered by dissolution (100% CO_2; after 48 hours equilibration):

$$D = \Delta r^2 / 2 \bullet \Delta t \qquad (3\text{-}10)$$

With a diffusion distance Δr =20-30 nm, and the equilibration time, Δt (48 hours) an average diffusion coefficient of $5 \times 10^{-17}\ cm^2/s$ can be estimated. This is comparable to the values above estimated from the data of Stipp et al. (1998). Moreover a flow rate can be estimated based on the dissolution experiments of the solid calcite with CO_2. This flow rate is calculated according to the transport equation:

$$F = D \cdot dC / \Delta r \qquad (3\text{-}11)$$

The concentration gradient dC / Δr is taken from Figure 3-8. The experiments with 1 week equilibration time were considered, because a better fit of Δr close to zero was feasible. Δr equal to zero corresponds to the calcite surface, where Fe(II) in solution is incorporated by re-crystallization. At this point the flow rate estimated from the sorption data should be identical to the flow rate estimated from the dissolution data. The flow rate estimated with Eq. 3-11 from dissolution data amounts to 8 $\times 10^{-16}$ mol $m^2 s^{-1}$. This value is within a factor of 1.5 equivalent to the flow rate of 1.2 $\times 10^{-15}$ mol $m^2 s^{-1}$ derived above from the precipitation rate (Eq. 3-9).

In a recent study by Fisler and Cygan (1999) the diffusion of Ca^{2+} and Mg^{2+} in calcite was determined at elevated temperature (400-800 °C). If extrapolated to ambient temperature, it results in a Mg^{2+} diffusion coefficient which amounts to 10^{-57} cm^2/s. Here the concentration profile of the cation as a function of the sample depth was determined with ion microprobe analysis. The diffusion coefficient was deduced from the concentration profile of the solid. In this geological process the movement of the Ca^{2+} and Mg^{2+} is believed to involve Ca^{2+} site vacancies. The diffusion coefficient estimated from Stipp et al. (1998) and the one calculated in our study are orders of magnitude higher. Consequently, the same diffusion mechanism is impossible at ambient temperature.

Moreover, we could show that the transport rate of Fe(II) from solution onto the calcite surface is compatible with the transport rate of Fe(II) inside of the calcite, based on the estimation of the flow rate at the interface. For transport through the calcite solid a diffusion coefficient compatible with the values predicted by Stipp, and Lahav and Bolt was used. In consequence, re-crystallization could well be the mechanism for the incorporation of cations even in deeper layers.

3.3.4 Homogeneous and heterogeneous oxygenation kinetics of Fe(II) in presence and in absence of calcite.

The Fe(II) oxygenation was investigated in saturated $CaCO_3$ suspensions. Fe(II) was either added to the aerated suspension or it was first equilibrated with $CaCO_3(s)$ before aeration (15h, 72h, 1 week). Same experiments in saturated $CaCO_3$ solution without solid were done for comparison. The decrease of Fe(II) from solution due to oxygenation is shown in Figure 3-9. One curve represents an experiment with direct aeration of the Fe(II) containing calcite suspension, the other, an experiment, where the Fe(II)-calcite suspension was aerated after 1 week of equilibration. The reaction corresponding to the second curve is slower than the first reaction, moreover it stops when 80 % of the Fe(II) has been oxidized (O_2 concentration 7 mg/L). An adsorbed concentration of $[Fe(II)]_{ads} = 2.0 \times 10^{-6}$ M was determined after 1 week of equilibration time prior to oxygenation. This value is comparable to the

Figure 3-9
Decrease of Fe(II) (initial concentration 1×10^{-5} M) as function of time after addition of oxygen (7 mg/L) to the calcite suspension (1 g/L), which was equilibrated during 1 week before with Fe(II) (O). For comparison the kinetics of Fe(II) oxygenation in presence of 1 g/L calcite without pre-equilibration are drawn as ☐.

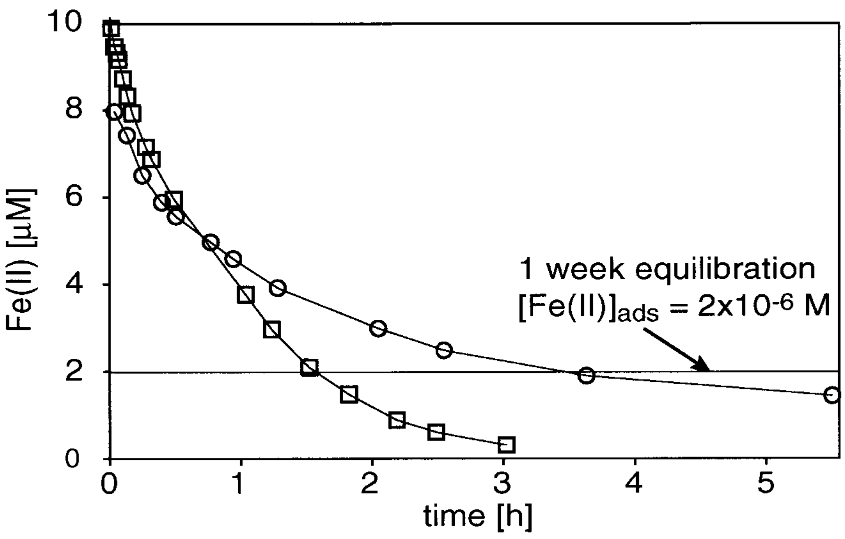

Figure 3-10

Pseudo first order oxygenation kinetics of $1 \cdot 10^{+5}$ M of Fe(II) with 2.5 mg/L oxygen at pH 7.0 ($pCO_2 = 10^{-1.49}$). (Δ) Without solid; (□ and ◊) with 1 g/L calcite. In the series represented by (+, ×, ✱), Fe(II) was first equilibrated over 15h (+, ×) and 72h (✱) with the calcite.

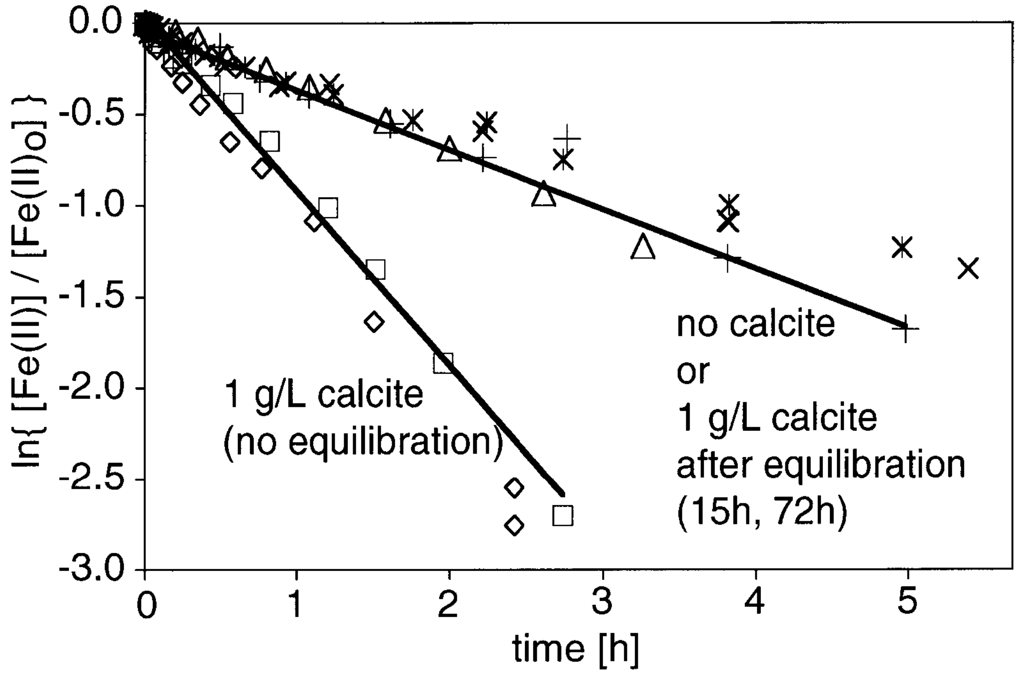

Fe(II) concentration left at the end of the oxygenation experiment (1.3 x 10^{-6} M). The incomplete oxidation of the Fe(II) is another indication that with time, Fe(II) is incorporated into deeper layers, where it is unaffected by aqueous phase reactions. The calcite used here had been dried and re-suspended for this experiment, which explains the lower fraction of adsorbed concentration compared with previous experiments.

Figure 3-10 shows a first-order representation of Fe(II) oxygenation kinetics in presence and in absence of calcite, with and without pre-equilibration time (pH 7, 1 g/L $CaCO_3$). The slopes of the lines equal the first order rate constants. Without pre-equilibration, the presence of 1 g/L calcite increased the rate constant by about a factor of two compared to the homogeneous oxygenation kinetics (3.7 versus 1.5 $M^{-1}s^{-1}$, see Table 3-4). In contrast, after longer equilibration (15h, 72h) the second order rate constants are comparable to the homogeneous rate constant (1 $M^{-1}s^{-1}$).

Table 3-4
Homogeneous, k_{hom}, and the heterogeneous rate constants, k_C and $k_{c,Eq}$ of the oxidation kinetics of 1 x10^{-5} M Fe(II) with 1 g/L calcite; the rate $k_{C,Eq}$ was obtained after prior equilibration of Fe(II) with calcite (≥ 15h). The rate constants correspond to the slopes of Figure 3-10. Experiments with 2.6 mg/L O_2 at pH 7.0.

Rate constant k	**M^{-1} s^{-1}**
k_{hom}	1.5± 0.3
k_C	3.7± 0.4
$K_{C,eq}$	1.0± 0.2

3.3.5 Adsorption versus oxygenation kinetics of Fe(II) in presence of calcite

In Figure 3-11 the adsorption kinetics of Fe(II) are compared to its oxygenation kinetics for two different $CaCO_3$ concentrations (1 and 10 g/L). Adsorption kinetics consists of a rapid step followed by an adsorption that obeys first order kinetics. A minimum rate constant for the rapid adsorption can be estimated with the first points measured: Fe(II) 0.91 x10^{-5} M at 40 s (1 g/L) and 0.5 x10^{-5} M at 60 s (10 g/L), which gives 2 x10^{-3} s^{-1} and 1 x10^{-2} s^{-1}, respectively.

In contrast to adsorption, the kinetics of the oxygenation of Fe(II) in presence of calcite follow one straight line over more than 95 % of the oxidation (Figure 3-11; open symbols). The decrease of Fe(II) can be formulated by pseudo-first order kinetics:

$$-d[Fe(II)]/dt = k''_C \bullet [Fe(II)] = k_C [O_2] \bullet [Fe(II)] \bullet [CaCO_3] \qquad (3\text{-}12)$$

$$k''_C = k_C [O_2] \bullet [CaCO_3] \text{ and } \quad [O_2], [CaCO_3] = \text{constant}$$

In our case the pseudo first order rate constant with calcite, k''_C, was determined as $3\bullet10^{-4}$ s^{-1} and $2\bullet10^{-3}$ s^{-1} for calcite concentrations of 1 and 10 g/L. It is 10 times faster at 10 g/L than at 1 g/L, which is another evidence for the enhancement of the oxygenation by calcite.

The acceleration of the oxygenation of Fe(II) in presence of calcite can only be explained by the very fast adsorption step of Fe(II) onto calcite, because the kinetics of the second adsorption step is significantly slower

Figure 3-11

Comparison of adsorption kinetics (filled symbols) and oxidation kinetics (open symbols). with Fe(II) $=1 \cdot 10^{+5}$ M at pH 7.0, adsorption under controlled N_2/CO_2 atmosphere; oxidation with 6.2 mg/L oxygen in solution. (O) 1 g/L and (◊) 10 g/L calcite.

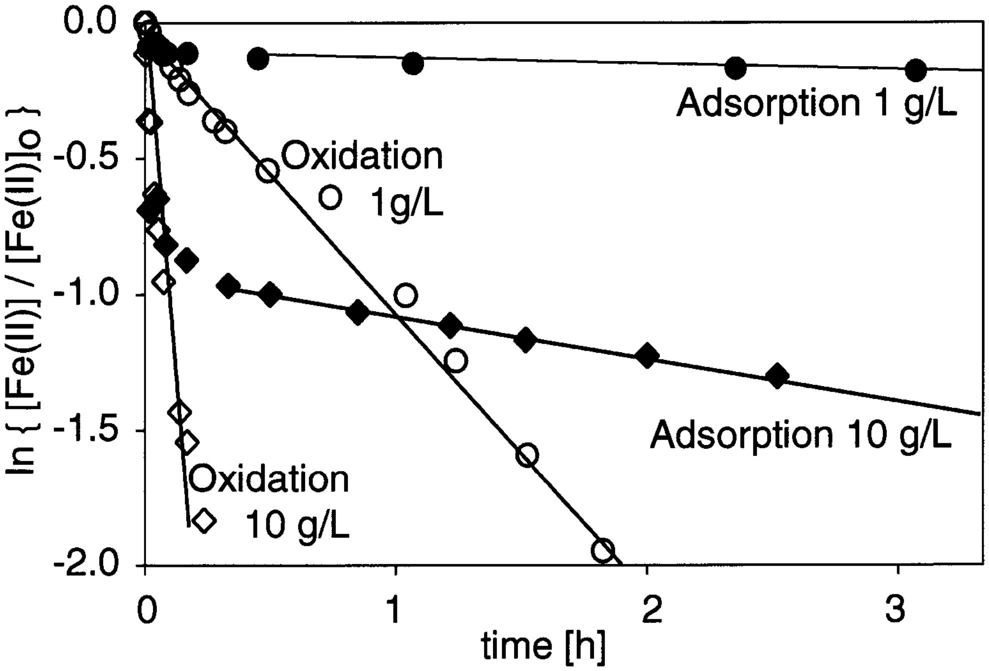

than the oxygenation. A comparison of the estimated rate constant of the first adsorption step with the rate constant of the oxidation shows that the fast adsorption is ca. 10 times faster than the oxidation, thus the oxidation is the rate-limiting step.

It can be summarized that relative to the homogeneous system the presence of calcite affects the oxygenation kinetics in various ways:

- Calcite enhances the oxygenation, when Fe(II) is added to an aerated calcite suspension. First order kinetics with respect to the solid calcite were measured with 1 and 10 g/L calcite.
- No difference of the kinetics with and without calcite is observed, when an equilibration time (> 3 hours) precedes the oxygenation step.
- After a longer equilibration time (>15 hours), no difference is observed, but the reaction is incomplete, not all the Fe(II) is oxidized.

Enhancement of the oxygenation kinetics in the presence of calcite can be explained by the formation of a more reactive adsorbed Fe(II) species at the solid surface. After a certain level of adsorption, the adsorption kinetics decrease, whereas oxidation kinetics remain the same. Thus, the species, which readily oxidizes initially must be constantly regenerated. This is only possible if the produced Fe(III) liberates a surface site for another Fe(II) adsorption and consecutive oxygenation.

Possibly a new reactive site is produced in the neighborhood of the hydrolyzing Fe(III). Fe(III) produced after oxidation of Fe(II) hydrolyzes in water under simultaneous liberation of protons:

$Fe^{3+} + H_2O = Fe(OH)^{2+} + H^+$ $pK_1 = 3.1$ (3-13.a)#

$Fe(OH)^{2+} + H_2O = Fe(OH)_2^+ + H^+$ $pK_2 = 3.3$ (3-13.b)

$Fe(OH)_2^+ + H_2O = Fe(OH)_{3\,(aq)} + H^+$ $pK_3 = 7.5$ (3-13.c)

$Fe(OH)_{3(aq)} + H_2O = Fe(OH)_4^- + H^+$ $pK_4 = 8.9$ (3-13.d)

$Fe(OH)_{3(aq)} + H^+ = Fe(OH)_3\,(s) + H^+$ $K_{prec} = 10^{9.9}$ (3-13.e)

At near neutral pH, $Fe(OH)_2^+$ and $Fe(OH)_{3\,(aq)}$ predominate and lead to amorphous $Fe(OH)_3(s)$ precipitates. The reactions can be summarized with the liberation of 3 H^+ for each Fe(III) produced from the oxygenation of Fe(II). The protons are then buffered by a localized reaction with $CaCO_3$, which through dissolution may be responsible for the creation of a new reactive site. The three reaction steps, adsorption, oxidation and formation of a new surface site by hydrolysis of Fe(III) are shown in Figure 3-12.

If calcite and Fe(II) are equilibrated for 12 hours or more before oxygenation of Fe(II), no acceleration of the kinetics were observed compared to the homogeneous reaction. This can be explained again with the adsorption and oxygenation kinetics: It has been shown in Figure 3-11 that the fast Fe(II) adsorbing species coincide with the easily oxidizable Fe(II) species. After several hours equilibration time with

---

# After Stumm W. and Morgan J. J. (1996) *Aquatic Chemistry*. John Wiley & Sons, Inc. New York. p. 267-269. Equilibrium constants for I = 3M; T = 25°C.

Figure 3-12
Schematic representation explaining the continuous formation of reactive surface sites at the calcite surface: **a**. and **c**: adsorption $>CaCO_3 + Fe^{2+} = >CaCO_3\text{-} Fe^{2+}$. **b** and **d**: oxidation: $>CaCO_3\text{-} Fe^{2+} + 0.25\ O_2 + 2.5\ H_2O = >CaCO_3\text{-} Fe(OH)_3 + 2\ H^+$. And hydrolysis: $>CaCO_3 + 2\ H^+ = Ca^{2+} + HCO_3^- + H^+$.

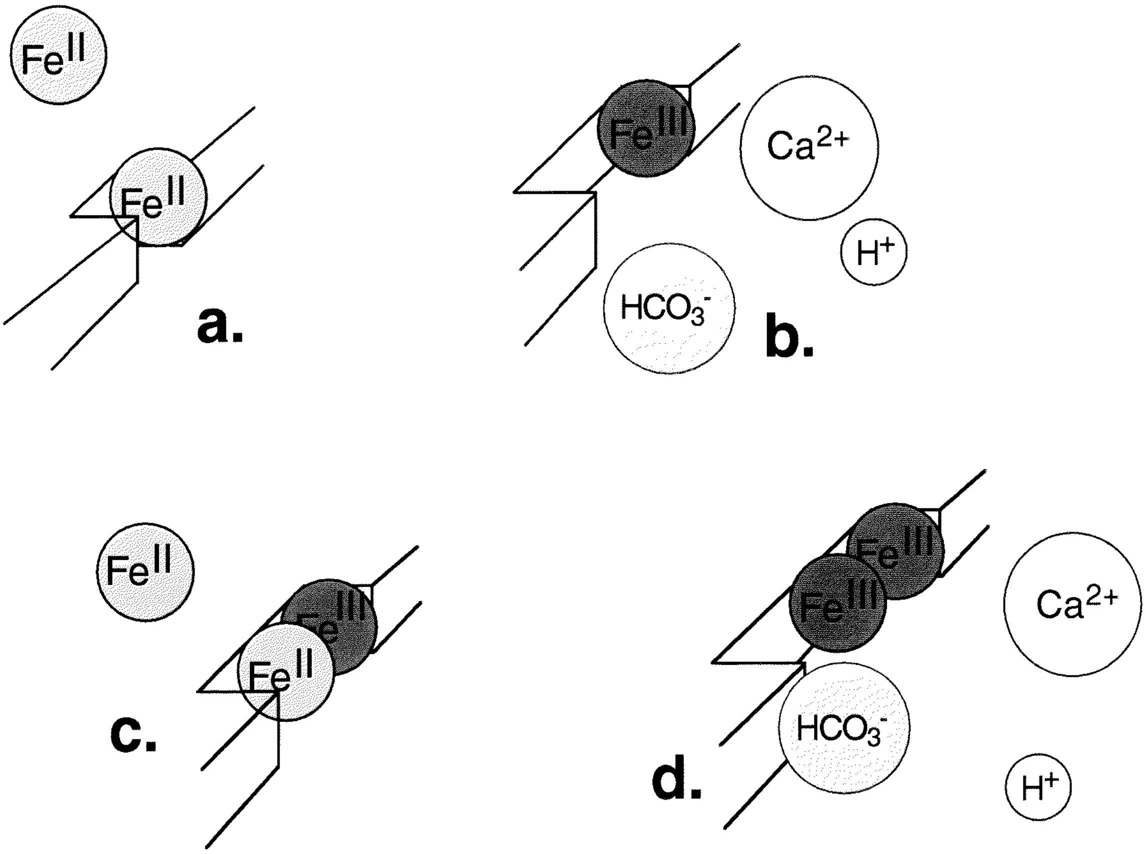

Fe(II), the reactive sites are transformed by re-crystallization, which leads to the formation of new mixed Fe/$CaCO_3$ phases. The fast adsorption sites are then not available anymore. It has to be considered that after 15 hours of equilibration time still ca. 90% of the initial 10 μM Fe(II) are in solution, so that any potentially formed reactive sites will be continously occupied and transformed. Consequently, when more Fe(II) is added to be oxidized, there are no reactive sites available anymore.

In the ultimate case, the oxygenation reaction stops before completion if Fe(II) has been equilibrated for several days with calcite. During this time span re-crystallization allowed a fraction of Fe(II) to be incorporated into the bulk calcite, where it can no longer be oxidized. Therefore, only a partial oxidation of Fe(II) is possible under these conditions.

3.3.6 Repeated adsorption and oxygenation of Fe(II) in calcite suspensions

The last question addresses the reactivity of a Fe-calcite system with respect to Fe(II) oxygenation, which goes through cycles of alternating anoxic and oxic conditions. It should simulate the reactions taking place in a reduced aquifer, which is intermittently aerated. In the anoxic state, the system is freed of the oxygen by purging nitrogen through it and then Fe(II) is added. A vigorous aeration follows, where the Fe(II) is oxidized.

The kinetics of Fe(II) oxygenation were followed as a function of cycles Fe(II)-addition–oxygenation. During Fe(II) addition, oxygen was either excluded (series A) or low (O_2 = 2.5 mg/L, series B). With increasing numbers of cycles, the total iron concentration of the calcite suspension augmented (2-12 μmol/g in series A and 2-20 μmol/g in series B). Note that the range of the Fe(II) concentrations corresponds to the saturation capacity of $CaCO_3$ for Fe(II) (Γ_{max} = 2.4 μmol/g). Surface concentration was high (25 g/L), to ensure that a large fraction of Fe(II) was sorbed before it was oxidized. Figure 3-13 shows oxidation kinetics for the 5th, 13th, 16th and 25th Fe(II) oxygenation cycle of series A under conditions similar to the results above (1 g/L, pH 7). The corresponding first order rate constants are listed in Table 3-5.

A comparison of the second-order rate constant as a function of the cycles shows the following behavior: The kinetics of the fifth oxidation with a rate constant of 1.6 $M^{-1}s^{-1}$ is comparable to the homogeneous kinetics. No acceleration is observed (1.5 $M^{-1}s^{-1}$: Figure 3-13 and Table 3-5). After the 13th oxidation cycle the rate constant increases to 11.5 $M^{-1}s^{-1}$, approximately 7 times the initial rate constant. Similar kinetics are observed for the 17th and 25th cycle with 9 $M^{-1}s^{-1}$.

In series B, the same kinetics is found for the 5th cycle (1.6 $M^{-1}s^{-1}$). With the following 12th and 25th cycles, there is a progressive increase of the

Figure 3-13

(a) Changing Fe(II) oxygenation kinetics in presence of calcite after several cycles of Fe(II) addition and oxygenation (pH 7.0; 1 g/L calcite; 2.5 mg/L O_2). The numbers indicate the cycle: (●) 5th, (▲) 13th, (◆) 16th and (■) 25th cycle. Homogeneous oxygenation kinetics are drawn as ✻. **(b)** Pseudo first order plot of the data in (a).

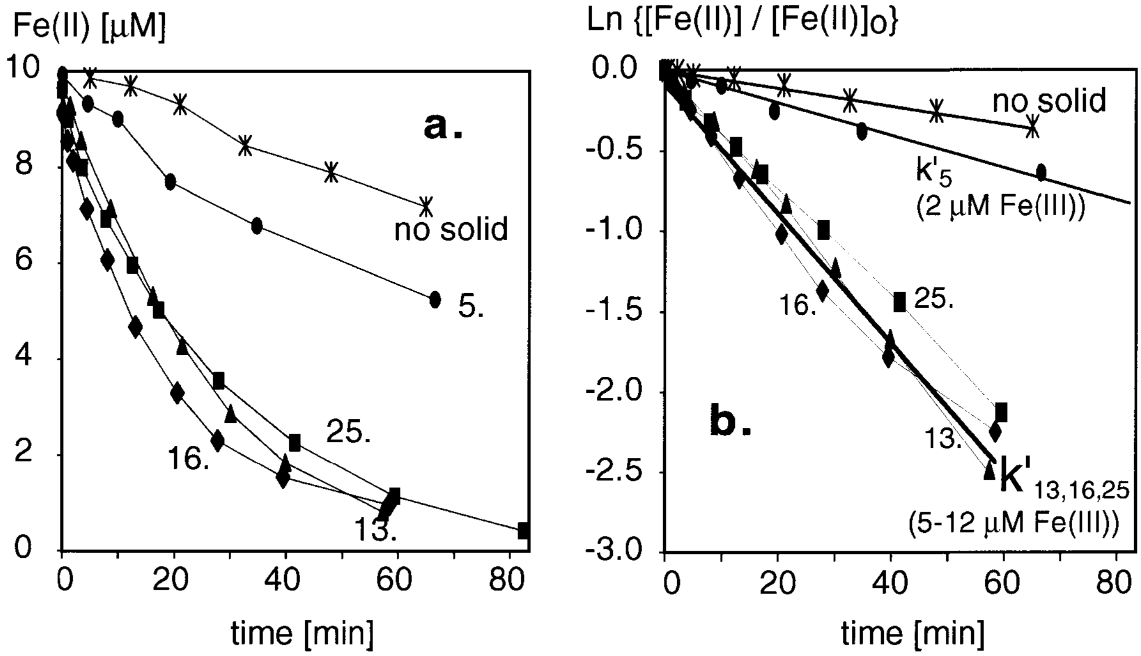

Table 3-5

Cycle number, Fe(III) content of the suspension, and second-order rate constants of the oxygenation kinetics after repeated cycles of Fe(II) addition and oxygenation (1×10^{-5} M Fe(II), 1 g/L calcite suspension, 2.6 mg/L O_2 at pH 7.0). The rate constants correspond to the slopes of Figure 3-13.

N° of Fe(II) addition	**Series A**		**Series B**	
	[Fe(III)] µmol / g	**k $M^{-1} s^{-1}$**	**[Fe(III)] µmol / g**	**k $M^{-1} s^{-1}$**
4./ 5.	2	1.6 ± 0.3	2	1.6 ± 0.1
13.	5	11.5 ± 3.0	5	4.0 ± 0.1
16.	7	9.3 ± 1.3		
25.	12	9.1 ± 2.3	11	3.8 ± 0.1
44.			20	7.8 ± 0.4

rate constants (4 $M^{-1}s^{-1}$), which finally reach 8 $M^{-1}s^{-1}$ at the 44th cycle. Even though the actual numbers are different, the same general trend can be observed in both type of experiments (series A and B).

These results can be summarized as follows: After the first Fe(II) addition cycles (5th), no pronounced changes are observed compared to the homogeneous reaction. There is no catalyzing effect of calcite either: probably the calcite re-crystallized partly with the Fe(II) in the time interval before oxygen addition, as described previously. In the consequent addition and oxidation steps, increasing iron content of the calcite suspension increased the oxygenation kinetics of Fe(II), which finally reached rate constants of 6 to 7 times the initial rate.

3.3.7 Analysis of the Fe oxides produced after repeated addition and oxidation of Fe(II) in calcite suspensions

Only semi-quantitative results were obtained by selective chemical dissolution experiments. These methods allow to distinguish between ferrous, ferric iron and reactive amorphous Fe-oxide, Fe(II), Fe(III), $Fe(III)_{am}$, respectively. The corresponding results are shown in Table 3-6. The amount of iron added to the calcite (2nd column, “calculated”) was well recovered (Fe_{tot}). Most of the precipitated Fe-oxides were characterized as reactive ferric oxide, ($Fe(III)_{am}$), it consisted of ca. 70 % of the total iron for both sample series A and B. Thus, a fraction of 30 % has a more crystalline character, but there is no structural information on these Fe(III)-oxides.

Table 3-6

Concentrations of the iron species determined by reductive and acid dissolution of the Fe-oxide products. The numbers represent the mean value and one standard deviation of three measurements (n=3; 95%).

Sample	**Calculated** µmol/g	**Fe_{tot}(5M HCl)** µmol/g	**Fe(III)** µmol/g	**$Fe(III)_{am}$** µmol/g	**$Fe(III)_{am}$** %
Series A	12	12 ± 5	13 ± 7	8 ± 1	68
Series B	20	22 ± 8	23 ± 6	14 ± 5	71

3.3.8 Heterogeneous oxygenation kinetics of Fe(II)

Oxygenation kinetics of Fe(II) depends strongly on its speciation. Solids can act like ligands and form "reactive" Fe(II) species, which are oxygenated faster. When a homogeneous reaction is conducted with an initial Fe(II) concentration > 3 mg/L at pH 7 auto-catalysis by the produced Fe oxides is observed (Tamura et al., 1976). The catalytic effect is due to the formation of adsorbed Fe(II) species at the freshly formed Fe-oxide surface. Kinetics is then linearly dependent on the solid concentration, according to Equation 3-14 (pH = constant):

$$\begin{aligned}
&-dFe(II)/dt \\
&= \{k_{hom} + k_{FeO} \bullet [Fe(III)]\} \bullet [Fe(II)] \bullet [O_2] \\
&= k_{app} \bullet [Fe(II)] \bullet [O_2] \qquad (3\text{-}14),
\end{aligned}$$

where k_{hom} represents the homogeneous and k_{FeO} the heterogeneous rate constant. Tamura et al. (1980) found that k_{FeO} varies as a function of the type of the Fe(III) oxide. He determined the following sequence for different Fe oxides: $Fe(OH)_3$ amorphous > α-FeOOH > γ-FeOOH > β-FeOOH, with the corresponding rate constants k_{FeO} at pH 7 of 0.156 > 0.033 > 0.023 > 0.011 L $mg^{-1}M^{-1}s^{-1}$ (with respect to Fe(III) concentration, in mg/L).

We also measured the oxygenation rate of Fe(II) in presence of 1 g/L goethite in $CaCO_3$ saturated solution as well as in bicarbonate buffered Ca^{2+}-free aqueous solutions at pH 7 (1 g/L α-FeOOH equivalent to 0.64 g/L Fe(III)). The resulting rate constants were k_{FeO} 0.3 to 0.5 L/mg Fe(III) $M^{-1}s^{-1}$ for the saturated $CaCO_3$ and Ca^{2+}-free solution respectively, which is twice the fastest values found by Tamura.

In presence of calcite, Loeppert et al. (1984) and Clarke et al. (1985) observed also an enhancement of the Fe(II)-oxygenation kinetics, which is proportional to the solid concentration. Similar observations are made for our conditions. However, acceleration of the oxygenation kinetics is not found when Fe(II) was first equilibrated with $CaCO_3$ several hours before oxygenation (15 hours). The equilibration took place in conditions where the added Fe(II) concentrations corresponded to the saturation capacity towards Fe(II) adsorption (10^{-5} M Fe(II), 2 x10^{-6} M >$CaCO_3$-site). In this case, upon addition of O_2, the oxygenation kinetics were comparable to homogeneous kinetics. No other oxygenation experiments were performed with equilibration times below 15 hours, though it could give more insight into the mechanism. Related to the sorption behavior of Fe(II) with calcite, we know that several hours of equilibration lead to a transformation of the calcite surface and incorporation of Fe(II).

3.3.8.1 Repeated addition and oxygenation of Fe(II) in calcite suspensions

After repeated addition and oxidation of Fe(II), the increasing Fe-oxide concentrations in the calcite suspension are expected to accelerate the oxygenation rate according to equation (3-14). To assess the effect of the produced Fe-oxides in the calcite suspension on the oxygenation kinetics, the rate constants were extrapolated to the final Fe(III) concentration. Final Fe(III) concentrations amounted to 0.6 and 1.05 mg/L in series A and B respectively, which results in rate constants k'_{FeO} of 0.6 and 0.9 $M^{-1}s^{-1}$ for series A and B with our experimental values. Addition of k_{hom} and k'_{FeO}, according to equation (3-14) gives an overall rate constant of $k_{app} \approx 2\ M^{-1}s^{-1}$.

The final rate constants we measured in the suspensions A and B, containing 0.6 and 1.05 mg/L Fe(III), were larger then the expected 2 $M^{-1}s^{-1}$: they were 9 and 8 $M^{-1}s^{-1}$. If Fe(III) is responsible for it, the produced Fe oxides were more reactive than the goethite utilized (17.5 m^2/g). A better reactivity could be related to larger available surfaces. It can be hypothesized that the Fe(III)-oxides produced in consequence of Fe(II) adsorption on calcite would form minuscule clusters widespread over the calcite surface (cp. Figure 3-12). These very small clusters offer more surface than the same amount precipitated in larger units. The specific surface area of the precipitated Fe(III) on calcite is certainly larger than that of the goethite we used (17.5 m^2/g). The very small sizes render the produced Fe-oxides very soluble to selective dissolution techniques and, therefore, the fraction of the reactive Fe-oxides may be overestimated.

Other effects, which could affect the calcite surface, cannot be excluded, especially considering the unsteadiness of the $CaCO_3$ surface. At the scale of the particle size (μm), no changes or even a shift to lower sizes was observed (see Figure 3-1).

3.4 Summary

The effective adsorption of Fe(II) onto calcite is difficult to quantify, since at this dynamic surface, adsorption is hardly distinguishable from the following co-precipitation reaction. Co-precipitation leads to a mixed $Fe/CaCO_3$ phase, for which a constant molar ratio Fe/Ca of 0.4 % can be determined over a certain depth. As a result the whole solid is expected to transform to the new phase over equilibration times longer than applied in this study (1 week). But it still has to be demonstrated though, whether the whole bulk of calcite or a layer only will be transformed by the incorporation of Fe(II).

The transport rate of the Fe(II) into the calcite at the surface of the particle is compatible with the rate of incorporation of Fe(II) measured in solution. Transport into the solid was estimated with a diffusion coefficient similar to the values, which correspond to solid state diffusion observed by Stipp (1998, 1992) and Hoffman (2001). Most probably transport of Fe(II) into the calcite happens by re-crystallization.

The incorporation of a redox active metal like Fe(II) into calcite makes it partly inaccessible for oxidation reactions. This is valid only for the case, when Fe(II) was allowed to interact with the calcite for several hours in absence of oxygen. Such conditions are frequent in anoxic ground water systems. In these systems calcite is expected to contain Fe(II), which is inert to oxygenation as long as the calcite is not dissolved.

When Fe(II) is added to an aerated suspension of calcite, acceleration of the oxygenation is observed, which depends on the surface concentration. The reactive Fe(II) species is formed very rapidly at the calcite surface. Later (> 15 hours), the reaction, which leads to the incorporation of Fe(II), transforms the surface in such a way that no acceleration of the Fe(II) oxygenation is observed anymore.

Under conditions of heterogeneous Fe(II) oxygenation on calcite products are expected to be very small clusters spread on the surface. The scarce Fe(III) produced in our study could not be identified. Other experimental set-ups, which would allow a better yield of Fe(III), like column experiments, may give more informations.

The chemical removal mechanism of in situ deferrisation involves natural surfaces like calcite as sorbent. In this process, Fe(II) is precipitated to Fe(III) in the aquifer. Surface adsorption allows the reactants Fe(II) and oxygen to interact in a system, where reduced and oxic waters do not overlap and mixing is not possible. By this mechanism Fe(II) is retained at the natural surfaces, which function like a filter and are oxygenated when oxygen containing water passes by. Calcite is a widespread mineral, which efficiently sorbs cations. Its sorption capacity for Fe(II) amounts to ca. 10% of the cationic sites at pH 7, which corresponds to 0.5 sites/nm^2. A site density of 3 sites/nm^2 was determined in similar experiments for the Fe-oxide goethite.

Several Fe(II)-adsorption-oxidation cycles (>13) in the presence of calcite led to a more reactive surface towards Fe(II) oxygenation: an acceleration of the oxygenation kinetics by a factor ≥5 compared to the initially measured kinetics was measured. This change could go along with the formation of small Fe(III)-oxide coatings at the calcite surface, which are specially reactive because of their small size. A similar process is believed to take place in the aquifer. After several cycles, where oxygen-free Fe(II)-containing waters alternate with aerated waters, the augmented Fe-oxide coatings result in a larger retention of the Fe(II) in the aquifer.

Acknowledgement

We thank Stephan Hug for fruitful discussions and advices for the experimentpal work. Denis Mavrocordatos, Peter Weidler and Paul Wersin are thanked for their interest in this work and the hints they gave us. We are grateful to Lisa Salhi for technical support and to Hansjuergen Schindler for the introduction to the milling techniques.

Seite Leer /
Blank leaf

4

ADSORPTION AND OXYGENATION OF Fe (II) IN PRESENCE OF GOETHITE

4.1 Introduction

According to our hypothesis natural surfaces are gradually coated with Fe(III)-oxides in the precipitation zone of the aquifer. This process takes place at mineral surfaces, where Fe(II) is adsorbed and then oxidized by oxygen when aerated water is injected. The freshly formed Fe(III)-oxides are able to take up Fe(II) ions from the solution until saturation of the oxidic surfaces. Once saturated, a breakthrough of Fe(II) is observed in the pumped ground water. A new injection of aerated water is then required.

Goethite was chosen as a model for Fe(III)-oxides, to mimic iron removal processes in the precipitation zone, once the solid aquifer matrix has been coated with Fe-oxide. Goethite is a widespread crystalline Fe-oxide, which is formed by slow oxidation in neutral carbonate-buffered systems as they can be encountered in many Swiss ground waters (see Chap. 1).

The following chapter provides some information on the system Fe(II)-goethite regarding the partitioning between solution and surface, saturation capacity and reactivity toward oxygen in the presence of the major ionic background of ground waters (Ca^{2+}, Mg^{2+}, HCO_3^-). In addition the data presented here can be compared to the calcite system discussed in Chapter 3.

4.1.1 Ion adsorption on goethite

In laboratory systems goethite is often used as model Fe-oxide surface. Goethite is known to be a good sorbent for organic and inorganic pollutants, such as metallic cations (Ni, Co, Zn, Pb, Cd) or oxo-anions, (CrO_4^{2-}, SeO_4^{2-}, UO_4^-) or other organic or inorganic acids (Sigg and Stumm, 1994; Stumm and Morgan, 1996; Cornell and Schwertmann, 1996; Langmuir, 1997).

In the aqueous environment water binds to incompletely coordinated iron centers at the surface of the Fe-oxides. The water molecules hydrolyze to form surface bound >FeOH entities (Sigg and Stumm, 1994; Stumm and Morgan, 1996).

These surface >FeOH groups are involved in acid-base, ligand and cation exchange reactions. For goethite the following equilibrium reactions take place (Villalobos and Leckie, 2000):

$$>FeOH + H^+ \Leftrightarrow >FeOH_2^+ \qquad pK_{a1} = 6.9 \qquad (4\text{-}1)$$

$$>FeOH \Leftrightarrow >FeO^- + H^+ \qquad pK_{a2} = 10.9 \qquad (4\text{-}2)$$

$$>FeOH + Me^{2+} \Leftrightarrow >FeOMe^+ + H^+ \qquad \log K_{Me} \qquad (4\text{-}3)$$

$$>FeOH + HL^- \Leftrightarrow >FeL^- + H_2O \qquad \log K_L \qquad (4\text{-}4)$$

These reactions lead to charged surface species ($>FeOH_2^+$, $>FeO^-$, $>FeL^-$, $>FeOMe^+$). The overall charge of goethite in pure water (or in an inert electrolyte solution) is positive below pH 8.9. At higher pH, it is negatively charged (Villalobos and Leckie, 2001). In the vicinity of the surface, the ions in solution rearrange to compensate for the surface charge, building up a potential gradient. At the surface this potential is defined as Ψ_0.

Similar to reactions in aqueous solution surface reactions can be described by an equilibrium constant, K^s. However, additionally, electrostatic interactions at the surface have to be taken into account.

They depend on the pH, the saturation of the surface bonds and the concentration of the electrolytic background. Therefore, a chemical and an electrostatic contribution describe the surface equilibrium constant:

$$\text{Log } K^s = \text{Log } K^s_{,\text{chemical}} + 2.303\ F\ \Psi_0 / R\ T \qquad (4\text{-}5)$$

F ist the Faraday constant ($F = 96\ 485\ \text{C mol}^{-1}$), R the gas constant ($R = 8.31\ \text{J K}^{-1}\ \text{mol}^{-1}$) and T the temperature in ° Kelvin. The value of the surface chemical constant, K^s_{chemical}, corresponds to the situation of zero surface charge. Different surface complexation models (SCM) describe the electronic interactions at the surface based on the representations of the charge distribution at the interface. The most common are the constant capacitance (CC), the double layer (DLM) and the triple layer (TLM) models. The CD-MUSIC model considers, in addition, the crystallographic features of the surface (an overview of surface complexation modeling is given in Weirich, 2000; Venema, 1996; Stumm and Morgan, 1996). Surface equilibrium constants are determined by fitting the chemical and electrostatic parameters to the experimental data. It is not recommended to compare surface constants fitted with different electrostatic models.

Alternatively, the Langmuir and Freundlich isotherms are empirical models, which quantify adsorption of a solute onto a sorbent. They are based on a correlation function of the equilibrium concentration of the adsorbed concentration against the solute concentration. No mechanistic understanding can be gained from these models. The parameters determined with a Langmuir or Freundlich isotherm are valid only for the conditions, in which they were measured.

The Freundlich isotherm

The Freundlich isotherm results form a plot of the adsorbed concentration versus the dissolved concentration measured at equilibrium. It is formulated as :

$$\Gamma = K_F\ [A]^n \qquad \text{or} \qquad \log \Gamma = n \log [A] + \log K_F \qquad (4\text{-}6)$$

Γ is the adsorbed concentration in mol per mass of the sorbent, or mol per surface of the sorbent. [A] represents the concentration of the adsorbate in solution in mol / liter. The parameter K_F is the Freundlich constant and n a measure for the non-linearity of the correlation. In a logarithmic plot n results from the slope and K_F from the intercept of a straight line.

The Langmuir isotherm

The Langmuir isotherm allows determining a maximum adsorption capacity (Γ_{max}) of the sorbent for the solute (here A; the variables are the same as above):

$$\Gamma = \Gamma_{max} K_{ads} [A] / (1 + K_{ads} [A]) \qquad (4\text{-}7)$$

K_{ads} is the adsorption coefficient. The parameters K_{ads}, Γ_{max} can be determined by plotting the data in the reciprocal form:

$$\Gamma^{-1} = (\Gamma_{max})^{-1} + (K_{ads})^{-1} \ (\Gamma_{max})^{-1} [A]^{-1} \qquad (4\text{-}8)$$

4.1.2 Adsorption and oxidation of Fe(II) on goethite

With the help of comparative studies and surface complexation modeling the following affinity sequence has been determined between bivalent cations and goethite (Cornell and Schwertmann, 1996; Coughlin and Stone, 1995):

Cu(II) > Pb(II) > Zn(II) ≈ Fe(II) > Cd(II)> Co(II) > Ni(II) > Mn(II).

In general the binding strength of transition metals for ligands follows the "Irwing Williams" sequence (Cotton et al., 1987; Huheey, 1978):

Zn(II) < Cu(II) > Ni(II) > Co(II) > Fe(II) > Mn(II)

According to this sequence Fe(II) is expected to adsorb less strongly than the other divalent metals except for Mn(II), which is in contradiction to the experimental results. The binding strength of the divalent metals to Fe-oxides correlates best with the first hydrolysis constant of the metal (Dzombak and Morel, 1990).

$$Me(H_2O)_6^{2+} \Leftrightarrow Me(OH)(H_2O)_5^{+} + H^{+} \qquad K_H \qquad (4\text{-}9)$$

This reaction can also be formulated as the binding of the cation to the hydroxyl anion (OH^-). The hydrolysis constant (pK_H) of the divalent

Figure 4-1
pH-dependent adsorption of Fe(II) and other divalent metals on 1 g/L goethite (47.5 m^2/L). From Coughlin and Stone (1995).

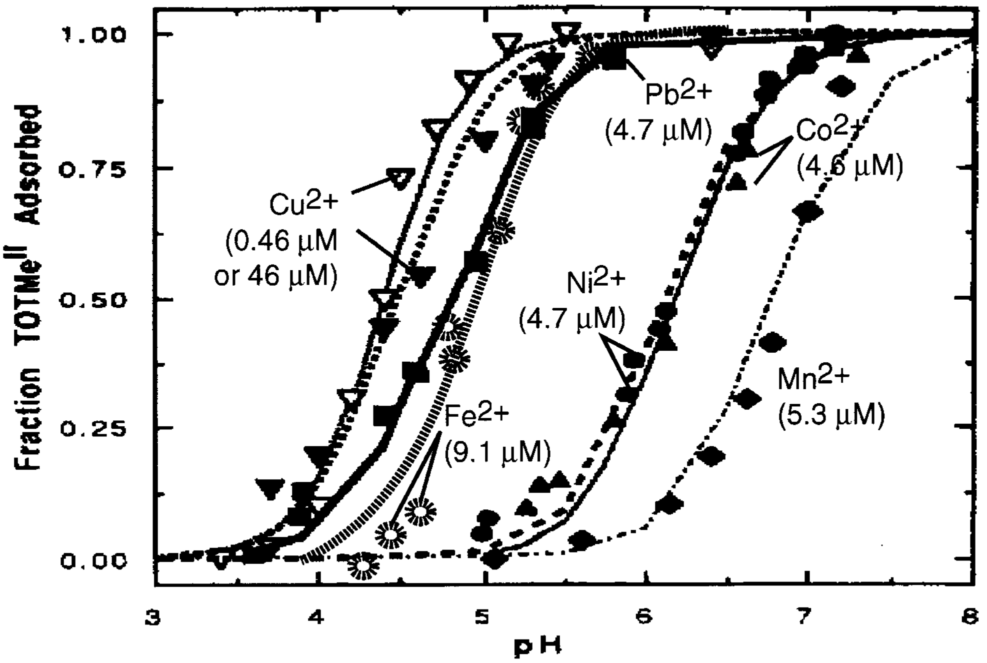

metals amounts in decreasing order to (Stumm and Morgan, 1996): $10^{-7.7}$(Cu) > $10^{-9.0}$(Zn) > $10^{-9.5}$(Fe) > $10^{-9.7}$(Co) > $10^{-9.9}$(Ni) > $10^{-10.6}$(Mn).

Figure 4-1 shows the pH-dependence of Me(II) adsorption on goethite. The increased adsorbed metal fraction with increasing pH goes along with the decreasing surface charge of the goethite surface. Fe(II) ranges between Pb and Cd (similar to Zn) regarding its affinity to goethite. In contrast to the other adsorbing metals, which exchange with a surface bound H^+ to produce the surface species >$FeOMe^+$, Fe(II) was best modeled forming a hydrolyzed, >FeOFe(OH), species. Therefore, the value of the equilibrium constants cannot be directly compared to the other metals.

Adsorption of Fe(II) on Fe-oxides has often been investigated conjointly with the redox reaction of the adsorbed Fe(II) species toward the reduction of a contaminant. Table 4-1 summarizes the studies on Fe(II) adsorption and its heterogeneous oxidation in presence of Fe-oxides

Table 4-1

Overview of the studies about Fe(II) adsorption and heterogeneous oxidation on Fe-oxides.

N°	Reference	Fe-oxide	Experimental conditions				
			Electrolytes	[Fe(II)]	[solid]	[Fe/nm^2]	pH
1	Tamura et al., 1980	α-FeOOH β-FeOOH γ-FeOOH Fe(OH)$_3$	0.1 M NaClO$_4$; 0.01 M NaHCO$_3$	0.18 mM	g/L; specific surface area no determined	-	6.7
2	Cougling and Stone, 1995	α-FeOOH	0.01 M NaNO$_3$; Acetic acid, HEPES	10 uM	1 g/L; 47.5 m^2/g	0.13	4.2-5.5
3	Haderlein and Pecher, 1998	Fe$_3$O$_4$ α-FeOOH α-Fe$_2$O$_3$ γ-FeOOH	25 mM MOPS, 7.5 mM NaCl	1 mM	Fe$_3$O$_4$: 3.1 g/L, 8.1 m^2/g α-FeOOH: 1.4 g/L, 17.5 m^2/g α-Fe$_2$O$_3$: 1.8 g/L, 13.7 m^2/g γ-FeOOH: 1.4 g/L, 17.6 m^2/g	24	7.2
4	Weidler et al.,	α-FeOOH	0.01 M KCl, 5.5 mM acetate	0.01M	0.026 g/L; 38.1 m^2/g	6030	4.8-4.9
5	Urrutia et al., 1998	α-FeOOH	0.01 M PIPES	4-650 μM	4.5 g/L; 55 m^2/g	0.01-16	6.9
6	Liger et al., 1999	α-FeOOH	0.1M NaNO$_3$	0.16 mM	α-FeOOH: 1.75 g/L, 1.38 m^2/g	40	5-9
		α-Fe$_2$O$_3$			α-Fe$_2$O$_3$: 0.53 g/L, 1.67 m^2/g	109	
		Fe$_5$HO$_8$ .4H$_2$O			Fe$_5$HO$_8$ .4H$_2$O: 0.21 g/L, 1.88 m^2/g	244	
7	Hofstetter et al., 1999	α-FeOOH	25 mM MOPS	1.5 mM	0.64 g/L; 17.5 m^2/g	81	7.2
8	Amonette et al., 2000	α-FeOOH	10 mM PIPES	0-3 mM	5 g/L ; 55 m^2/g	6.6	4.1-8.2
9	Zachara et al., 2000	α-FeOOH	3 mM Ca(ClO4)2	10 μM	0.5 g/L; 2.17 m^2/g	5.6	3-7
10	This study	α-FeOOH	0.01 M NaCl; 1-5 mM NaHCO$_3$	< 50 μM	0.3 g/L; 17.5 m^2/g	6	7.0; 8.0
11	Tamura et al., 1976	Fe(OH)$_3$	0.1 NaClO4; 0.01M NaHCO$_3$	18 μM	0.1-0.5 g Fe(III)/L, >200 m^2/g	ca. 0.1	6.8
12	Zhang et al., 1992	γ-FeOOH	0.6M NaCl	0.2-0,5 mM	10 g/L; 17.1 m^2/g	0.7-1.8	6
13	Klausen et al., 1995	Fe$_3$O$_4$	36 mM MES, PIPES, MOPS	1.5 mM	0.1-0.9 g/L; 56 m^2/g	18-16	5.5-8.2
14	Jeon et al., 2001	α-Fe$_2$O$_3$	0.01M NaCl, Na$_2$SO$_4$, NaNO$_3$, PIPES, acetate	0.125-0.25 mM	10 g/L; 9.04 m^2/g	0.8-1.6	3.7-7.5

Results			Focus, Comments
Saturation [Fe(II)/nm^2]	species	Model and parameters (log K^s)	
not determined	not determined	Equilibrium constant K	Heterogeneous oxygenation of Fe(II)
2.8	>FeOH +Fe +H_2O = >FeOFeOH +2H	-5 Triple layer model	Adsorption of bivalent metals
Fe_3O_4: 9.4 α-FeOOH: 3.1 α-Fe_2O_3: 1.13 γ-FeOOH: 2.55	not determined	adsorption-precipitation model	Reduction of nitro-aromatic and chlorinated aliphatic compounds with Fe(II).
10 (assumed)	not determined		Heterogeneous oxygenation of Fe(II) with SFM
2.73	not determined	Freundlich isotherm K_F= 0.57 mol/kg, n = 0.158	Effect of Fe(II) adsorption on the activity of Fe(II) reducing microorganisms
1.68	>FeOH + Fe = >FeOFe + H	0.11 constant	Reduction of UO_4^{2+}
	>FeOH + Fe +H_2O = >FeOFeOH + H	-7.64 capacitance	
2.07	>FeOH + Fe = >FeOFe + H	1.15	
	>FeOH + Fe +H_2O = >FeOFeOH + H	-10.05	
2.27	>FeOH + Fe = >FeOFe + H	-2.98	
	>FeOH + Fe +H_2O = >FeOFeOH + H	-11.96	
3.1	not determined	Langmuir isotherm	Reduction of nitro-aromatic compounds
1.6	not determined	Γ_{max} = 0.144 mmol/g Langmuir isotherm	Reduction of carbon tetrachloride
1.93 (pH 6.5)	not determined	repartition: Kd	Adsorption of Fe(II), Co(EDTA)
2.9 (pH7) 10.2 (pH8) 6.1 (Ca,Mg)	not determined	5.4(pH7) 6.2; 5.7 (pH8; Ca,Mg) Langmuir isotherms	Heterogeneous oxygenation of Fe(II)
not determined	>FeOH + Fe = >FeOFe + H	-9.6; repartition, Kd	Exchange reaction for given conditions
1.67	>FeOH + Fe = >FeOFe + H	-2.13 double Layer	Adsorption of Fe(II) and Al(III)
	>FeOH + Fe +H_2O = >FeOFeOH + H	-8.53 model	
9.8 (pH7)	2 surface species	-	Reduction of nitro-aromatic compounds
1.5-5.7 (pH 6.6)	2 sites strong ads pH 4-5 (10% of total sites); 2 surface species	Langmuir isotherm	Adsorption of Fe(II) with several electrolytes

along with some results. Haderlein and Pecher (1998), Hofstetter et al. (1999). Klausen et al. (1995) and Amonette et al. (2000) studied the reductive degradation of nitro-aromatic or chlorinated aliphatic compounds. Whereas Charlet et al. (1998), Liger et al. (1999) and Buerge and Hug (1999) investigated the reductive transformation of the chromate (CrO_4^{2-}) or the uranyl ions (UO_2^{2+}). Others studies focused on the adsorption of Fe(II) by Fe-oxides (Zachara et al., 2000; Zhang et al., 1992) or determined its effect on the activity of Fe-oxides reducing microorganisms (Urrutia et al., 1998). Two studies only address the oxygenation of the adsorbed Fe(II): Tamura et al. (1976; 1980) investigated the oxygenation of Fe(II) in presence of Fe-oxides, and Weidler et al. (1998) observed the growth rate of goethite crystals caused by the oxygenation of Fe(II) at its surface using scanning force microscopy. The studies are listed in Table 4-1 by order of chronology, the first ten (N° 1-10) used goethite as Fe-oxide. The studies were performed under different experimental conditions: organic or inorganic pH buffers were used, the ionic strengths ranged between 0.01 and 0.1M. In the different experimental studies a broad range of surface loadings were used, which varied from 0.01 to 6'030 Fe/nm^2. Generally, the largest loadings are found in studies about contaminant reduction. This ensures constant experimental conditions with regard to available electrons (Haderlein and Pecher, 1998; Hofstetter et al., 1999; Klausen, 1995; Liger et al., 1999). Despite the large range of the experimental Fe(II) loadings, a similar concentration of Fe(II) surface sites is reported for goethite: 1.7 to 3.1 sites/nm^2. One case of surface precipitation has been reported by Haderlein and Pecher (1998), which resulted in even faster reduction rates. Precipitation took place at elevated pH (pH> 7.5) and after longer equilibration times of the Fe(II) with the solid (Fe(II) in millimolar concentration).

Fe(II) adsorption on goethite was best modeled forming one hydrolyzed adsorbed species, >FeOFe(OH) (Coughlin and Stone, 1995) or the two surface species, >FeOFe$^+$ and >FeOFe(OH) (Liger et al., 1999). Liger et al. (1999) lists several formation constants K^s of the adsorbed Fe(II) species on different Fe-oxides (see Table 4-1). From the comparison of the data, Fe(II) has the highest affinity to goethite. Therefore, the >FeOFe(OH) species is probably already of some importance at near neutral pH.

If Fe(II) is adsorbed to Fe(III)-oxides, then it is oxidized far more readily than the Fe^{2+} species. Wehrli, (1990) and Buerge (1999) demonstrated that the rate constant of the Fe(II) oxygenation correlates with the thermodynamic equilibrium of the reactive Fe(II) species /Fe(III) couple. Charlet et al. (1998) showed that the rate constant of the contaminant transformation correlated with the concentration of the surface species >FeOFe(OH). Consequently, this species is responsible for the fast reduction of nitro-aromatic compounds and of the uranyl ion. This species resembles the dihydroxy-aquo Fe(II) ion, which is responsible for the fast reaction of O_2 in water (Chap. 1). Thermodynamically, the surface Fe(II) species is probably close to the dihydroxo Fe(II), $Fe(OH)_2$ (Eh = 0.031 V; Stumm and Morgan, 1996). $Fe(OH)_2$ reacts almost 10^{12} times faster with oxygen than Fe^{2+}_{aq}. However, it represents such a small fraction of the total Fe(II) in water (ca. 10^{-7}, pH 7) that it contributes only a few percent to the overall oxygenation rate at pH 7 (see also Chap 1, Fig.1-2). In presence of goethite the fraction of the adsorbed Fe(II) is in the order of a few percent. Therefore, the adsorbed Fe(II) determines the oxidation kinetics of Fe(II) at pH 7 in this case.

4.1.3 Fe(II) adsorption kinetics

Adsorption of metals onto Fe-oxides is a fast reaction (Stumm, 1992: Haderlein and Pecher, 1998). In general the kinetics of adsorption depends both on the metal and on the solid concentration according to:

$$-d[Fe(II)] / dt = k^S_{ads} [Fe(II)] [goethite] \qquad (4\text{-}10)$$

k^S_{ads} being the rate coefficient for adsorption. In reality, adsorption kinetics is a function of the combined surface and solution species, moreover it is affected by the surface charge. For one species (e. g. Fe^{2+}) the following relation has been proposed (for more details see Wehrli et al, 1990; Stumm, 1992):

$$k^S_{ads} = K_{OS} \bullet k_{ads} \qquad (4\text{-}11)$$

K_{OS} is an equilibrium constant, which depends on both the surface charge and the charge of the adsorbing species; k_{ads} is the intrinsic adsorption rate constant. For an uncharged species $k^S_{ads} = k_{ads}$.

k_{ads} of various metals have been compared and they have been found to correlate with the rate of exchange of coordinated water (Hachiya et al., 1984; Wehrli et al., 1990; Stumm, 1992: Grossi, 1994):

$$Me(H_2O)_5\,(H_2O)^* + (H_2O) \leftrightarrows Me(H_2O)_5\,(H_2O) + (H_2O)^* \qquad (4\text{-}12)$$

The kinetics rate constants of the back and the forth reactions can be symbolized by k_{+w}, and k_{-w}, respectively. The intrinsic adsorption rate constant correlates to the rate k_{-w}, according to (55.6 M is the concentration of H_2O in water):

$$\log k_{ads} = -2.42 + 0.92 \log (k_{-w} / 55.6) \qquad (4\text{-}13)$$

The equation results in an intrinsic rate constant, k_{ads}, for Fe^{2+} of ca. 90 $M^{-1}\ s^{-1}$ ($\log k_{-w} = 6.5\ s^{-1}$; Bennetto and Caldin, 1971).

The correlation of the adsorption rate constant k_{ads} with k_{-w} is due to the rate determining loss of coordinated water, which precedes the coordination with the surface ligand, >FeOH. It assumes the formation of an innersphere coordination of the metal with the ligand.

4.1.4 Sorption reversibility

Sorption is considered to be a reversible process (see Eq. 4.3). During desorption the metal ion exchanges with H^+ at larger proton concentration. Desorption, however, can be slower than adsorption and possibly a fraction of the adsorbed metal ion remains associated with the Fe-oxide (Cornell and Schwertmann, 1996; Coughlin and Stone, 1995). It is important to differentiate possible consecutive reactions (redox, surface precipitation) from the irreversibility of the adsorption. This is very significant for Fe(II), because it can be easily oxidized.

Coughlin and Stone (1995) investigated the reversibility of Fe(II) adsorption. The Fe(II) and the goethite were equilibrated for 28 hours at pH above 4.5. After acidifying the suspension to pH 1.9, they recovered less than half of the initial Fe(II). They gave several possible explanations: diffusion of the Fe(II) in small pores of the solid (crystal defects); particle aggregation as consequence of the adsorption; rearrangement of the surface, involving surface precipitation reactions.

Jeon et al. (2001) conducted adsorption experiments of Fe(II) onto hematite with three different electrolyte solutions: NaCl, $NaNO_3$ and Na_2SO_4. They observed the smallest desorption of Fe(II), when Na_2SO_4 was used. They interpreted their findings as coprecipitation of a new solid phase at the goethite surface. With the other electrolytes, less Fe(II) was recovered, with increasing pH. Haderlein and Pecher (1998) reported the formation of a blue-green precipitate at pH above 7.5, which can be attributed to green rusts (mixed Fe(II)-Fe(III) oxides). Because adsorbed Fe(II) is readily oxidized to Fe(III), desorption experiments were conducted in our system to verify the absence of oxygen and exclude possible surface precipitation.

4.1.5 Effect of the major ions HCO_3^-, Ca^{2+} and Mg^{2+}

The major ions, HCO_3^-, Ca^{2+} and Mg^{2+}, are ubiquitous and the prevalent species in aqueous, carbonaceous environment. They are present in millimolar concentration, which is close to 100 times the Fe(II) and Mn(II) concentrations in a reduced aquifer (Stumm and Morgan, 1996; Langmuir, 1997).

Recent studies showed that bicarbonate (HCO_3^-) efficiently sorbs to goethite forming a monodentate surface species (van Geen, 1994; Villalobos and Leckie, 2000; Villalobos and Leckie, 2001; Winja and Schulthess, 2001):

$$>FeOH + HCO_3^- \Leftrightarrow >FeOCOO^- + H_2O \qquad (4\text{-}14)$$

Villalobos and Leckie (2000 and 2001) determined a carbonate coverage of the goethite of 0.3 to 1 μmol/m^2 at atmospheric CO_2 concentration (0.033%) between pH 6 and 8, which represents 8-25% of the surface sites (available total site concentration on goethite 2.3

sites/nm^2). In confined aquifers CO_2 partial pressure can reach several percents, resulting in partial covering of the sites by carbonate.

Carbonate adsorption on goethite decreases its overall surface charge. The presence of bicarbonate resulted in a lower adsorption of the oxyanions CrO_4^{2-} and UO_2^{2-} by goethite due to the competition for surface sites and to electrostatic repulsion (Duff and Amrhein, 1996; Villalobos et al., 2001). The positively charged Pb(II), however, was adsorbed in larger concentration than in the absence of bicarbonate by formation of an additional ternary carbonato-complex (Villalobos et al., 2001). An important increase of Ca^{2+} adsorption could be explained by the electrostatic interaction due only to the conjoint adsorption of negatively charged phosphate (Rietra et al., 2001). A similar, but weaker effect is expected with adsorbed carbonate for cation adsorption onto goethite (Weirich, 2000).

In presence of the positively charged Ca^{2+} and Mg^{2+} a competitive effect on cation adsorption has mostly been observed. However, compared to other metals, Ca^{2+} and Mg^{2+} do not bind to Fe-oxides strongly (Dzombak and Morel, 1990; Rietra et al., 2001). Nevertheless, in presence of Ca^{2+} and Mg^{2+} reduced adsorption of Cd^{2+} was observed on amorphous Fe-oxide (Laxen, 1985). A similar effect was observed for the adsorption of the positively charged U(VI) species on goethite (Duff and Amrhein, 1996). Similarly, Weirich (2000) noted a competition of Ca^{2+} and Mg^{2+} on the adsorption of Cd and Ni onto goethite. This reduced the sorption by 30 to 50 % at neutral pH, compared to systems without Ca^{2+} and Mg^{2+}. On the other hand, copper adsorption was not affected.

Major cations (Ca^{2+} and Mg^{2+}) also affect the speciation of other metals in the aqueous phase. Fe(II), Ca^{2+} and Mg^{2+} all form aqueous (bi)carbonate complexes. In saturated $CaCO_3$ solution at pH 7 and with 10 μM Fe(II) 30 % of the carbonate is bound by Ca^{2+} and less than 0.1% by Fe(II) (Chap. 1, Figure 1-2). Consequently, a competition of cations for ligands is observed both in solution and at the surface.

In summary, the presence of major ions possibly affects the heterogeneous catalysis of the Fe(II) oxygenation by goethite. In particular the following interactions could take place:

- Competition of Ca^{2+} and Mg^{2+} with Fe(II) for the sorption sites on goethite.
- Competition of Ca^{2+} and Mg^{2+} with Fe(II) for the carbonate ligands in solution. The species $Fe(CO_3)_2^{2-}$ and $Fe(CO_3)(OH)^-$, $FeCO_3$, and $FeHCO_3$ account altogether for 94% of the oxygenation rate constant under our experimental conditions (pH 7, saturated $CaCO_3$ solution; see Chap 1; Figure 1-2).
- Increased adsorption of Fe(II) by co-adsorbed bicarbonate on goethite (electrostatic interaction).

The possible effect of the major ions on the Fe(II) adsorption and oxygenation was tested in the present study. For this purpose, experiments of (i) adsorption kinetics, (ii) Fe(II) isotherms on goethite and (iii) oxygenation kinetics were performed in solution of varying concentration of bicarbonate (1 or 5 mM) and in absence or in presence of Ca^{2+} and Mg^{2+} (with 0.9 mM $CaCl_2$ and 0.09 mM $MgCl_2$ in addition to 1 mM HCO_3^-). The electrolytic background corresponds to the electrolytic background used for the experiments with calcite.

4.2 Materials and methods

4.2.1 Reagents

All chemicals used were at least reagent grade. Solutions were prepared with deionized water (Q-H_2O, Barnstead nanopure) to which defined volumes of the electrolyte solutions were added ($CaCl_2$, $MgCl_2$, NaCl and $NaHCO_3$) to achieve final salt concentrations of 0.9 mM $CaCl_2$, 0.09 mM $MgCl_2$, 0.1 or 0.5 mM $NaHCO_3$ and 0.01M NaCl. Experiments with $CaCO_3$ -saturated water were performed at pH 7 only. For this, synthetic calcite powder (Merck, Suprapur) was equilibrated at the requested CO_2 partial pressure for 4 days. Afterward it was filtered and kept at the same pCO_2 (4.5-4.9 %; pH 7) until use. Fe(II) was added as solution prepared from the $FeSO_4.7H_2O$ salt (Riedel de Haehn; 0.01M, pH 4).

Synthetic goethite was purchased from Bayer (Bayferrox 910). The mean grain size ranged between 1 and 2 μm (determined with laser diffraction). A specific surface area of 17.5 m^2/g was measured by BET-N_2 adsorption. The goethite suspension was prepared from a stock solution (675 m^2/L): goethite stock suspension was diluted to a final goethite concentration of 5.25 m^2/L and equilibrated 15 hours before the experiment was started.

All experiments with Fe(II) were performed in an anoxic glove box containing a palladium catalyst to remove oxygen (Coy Laboratory Products Inc., Michigan). The atmosphere of the glove box consisted of 97-98% N_2 and 2-3 % H_2; O_2 was below 1 ppm (v/v).

Gas flows of the desired volume % of CO_2 were mixed with flow meters (Brooks Instruments) from gas bottles (100 % N_2; 20 % CO_2 / 80% N_2 and 8 % O_2 / 92 % N_2). The purity of the gases ranged between, 99.99 % and >99.999 %).

4.2.2 Analytical and experimental methods

4.2.2.1 Analytical methods

Fe(II) was measured photometrically with the Ferrozine method at 562 nm with a detection limit of 3 x10^{-7} M in a 1 cm cell (Stookey, 1970; Gibbs, 1976. Spectrophotometer Uvikon, Bio-Tek Kontron Instruments). To stabilize the pH in the acidic range, an acetic acid / acetate buffer was used (2M/2M; pH 4.5); in the neutral–basic range suspensions were buffered by bicarbonate/carbonate. The pH was checked with a pH glass electrode (Orion) calibrated with buffer solutions (Merck, Titrisol; pH 7 and pH 9).

4.2.2.2 Sorption experiments

For the *isotherms* various volumes of the $FeSO_4$ stock solution were added to 100 ml of a goethite suspension (5.25 m^2/L) and equilibrated for 80 minutes to 24 hours under constant stirring. After the equilibration time, samples were filtered through 0.2 μm nylon filters and measured for Fe(II). Adsorbed Fe(II) was calculated from the difference between added and measured Fe(II). The recovery of the total Fe(II) in the suspension was tested by acidifying the suspension to $3.5 < pH < 4$ with dilute hydrochloric acid (1M), this was followed by the same procedure to measure Fe(II) in solution (filtration 0.2 μm, ferrozine).

Adsorption kinetics were carried out similarly: to a 250 or 500 ml batch containing goethite (5.25 m^2/L), $FeSO_4$ was added to a final concentration of 1×10^{-5} M. Samples were taken as a function of time, filtrated and measured for Fe(II).

4.2.2.3 Desorption kinetics of Fe(II) upon acidification

At the end of the adsorption experiments, the batch containing the goethite suspension and the Fe(II) was acidified with HCl (1M) to $3.5 < pH < 4$. Samples were taken after various time intervals, filtered (0.2 μm) and measured for Fe(II).

4.2.2.4 Fe(II) oxygenation kinetics

For *homogeneous kinetics,* the experiments were conducted in a sealed batch under controlled $O_2/CO_2/N_2$ gas flow. The O_2 concentration was 3.8 % (v/v; equivalent to 2.4-2.6 mg/L O_2). Upon addition of Fe(II) to the sparged solution, 3-4 ml of sample were taken after certain reaction times, quenched in acetic acid/sodium acetate buffer (2M, pH 4.5), filtered and measured for remaining Fe(II).

For the *heterogeneous kinetics,* experiments (in presence of goethite) a similar procedure was followed. However, the oxidation was stopped by addition of HCl with a resulting pH of 4. The acidified samples were left for 15 hours (desorption). Afterwards, ferrozine was added to bind the remaining Fe(II) and the samples were filtered in a buffer (acetic acid/ acetate) and measured by spectrophotometry.

4.3 Results and Discussion

4.3.1 Adsorption experiments

4.3.1.1 Adsorption kinetics

Adsorption was determined by the difference of the total added Fe(II) and the measured aqueous Fe(II):

$$[\mathrm{Fe(II)}]_{tot} - [\mathrm{Fe(II)}]_{aq} = [\mathrm{Fe(II)}]_{ads} \qquad (4\text{-}15)$$

The kinetics of adsorption were monitored by following the decrease of aqueous Fe(II) as a function of time (Figure 4-2):

$$-d[\mathrm{Fe(II)}]_{aq} / dt = d[\mathrm{Fe(II)}]_{ads} / dt. \qquad (4\text{-}16)$$

Figure 4-2 shows the adsorption kinetics of Fe(II) on goethite on a time scale of 5 hours with (a) various bicarbonate concentrations (1 and 5 mM [HCO_3^-]) and (b) in presence and absence of the major cations Ca^{2+} and Mg^{2+}. The adsorption of Fe(II) is a fast process. Close to half of the Fe(II) disappears from the solution in 30 seconds (first sampling point). Relative to the adsorbed Fe(II) concentration after 24 hours of equilibration time, 90% was adsorbed within 1 hour.

Figure 4-2 shows that (bi)carbonate does not affect the Fe(II) kinetics within the applied concentrations. In presence of Ca^{2+} and Mg^{2+}, however, the rate of adsorption is decreased. For longer equilibration times, the same adsorbed concentration is measured both with and without Ca^{2+} and Mg^{2+}.

In summary, no differences are observed for the different bicarbonate concentrations, whereas the presence of Ca^{2+} and Mg^{2} slightly slows down the kinetics. Under these experimental conditions no pseudo first order kinetics can be assumed, since neither Fe(II) nor the surface sites concentration of goethite are in excess (proportion $[>\mathrm{FeOH}]_0 / [\mathrm{Fe(II)}]_{tot} = 2.5$). Consequently, the data have to be analyzed according to a second-order rate law.

Figure 4-2

Measured Fe(II) decrease in solution as a function of time in presence of goethite (pH 7, 5.25 m^2/L 10 μM Fe(II), 10 mM NaCl). (**a**) With 1mM HCO_3^- (open symbols) and with 5 mM HCO_3^- (filled symbols). (**b**) In presence of Ca^{2+} and Mg^{2+} (▲) and without Ca^{2+} and Mg^{2+} (□).

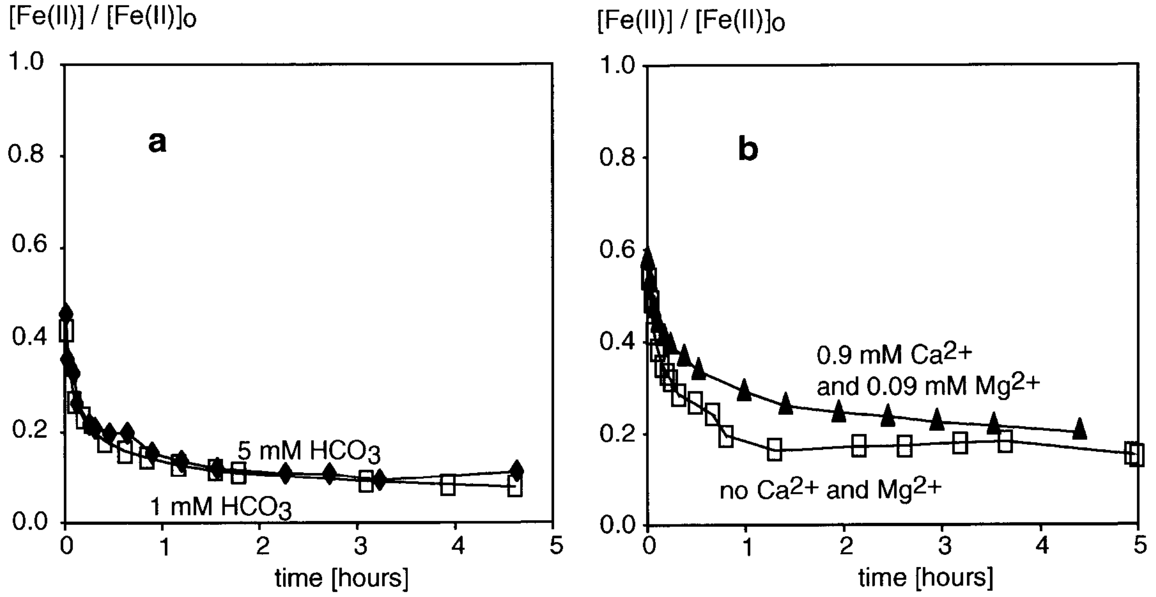

The second-order rate law expression is based on a defined initial concentration of goethite surface sites ($[>FeOH]_0 = 25\ \mu M$), which decreases simultaneously to the aqueous Fe(II) by adsorption of Fe(II) to these sites:

$$-d[Fe(II)]_{aq} / dt = -[>FeOH] / dt = k\,[Fe(II)]_{aq}\,[>FeOH]. \qquad (4\text{-}17)$$

The surface sites concentration is calculated from the goethite concentration (5.25 m^2/L) and the site density of goethite (2.9 sites/ nm^2. See below, 4.3.1.2). Thus, for each measured [Fe(II)], [>FeOH] can be calculated:

$$\begin{aligned}[>FeOH] &= [>FeOH]_o - [Fe(II)]_{ads} \\ &= [>FeOH]_o - \{\, [Fe(II)]_{tot} - [Fe(II)]_{aq} \,\} \qquad (4\text{-}18)\end{aligned}$$

Replacement of equation (4-18) in the kinetics rate equation, followed by integration results in:

$$\begin{aligned}[Fe(II)]_{aq} &= [Fe(II)]_{tot} \{\, [>FeOH] / [>FeOH]_0 \,\} \\ &\times \exp \{\, k\, t\, [Fe(II)]_{tot} / [>FeOH]_0 \,\} \qquad (4\text{-}19)\end{aligned}$$

Figure 4-3
Second order representation of the kinetics data (1mM HCO_3^-) shown in Figure 4-2a.

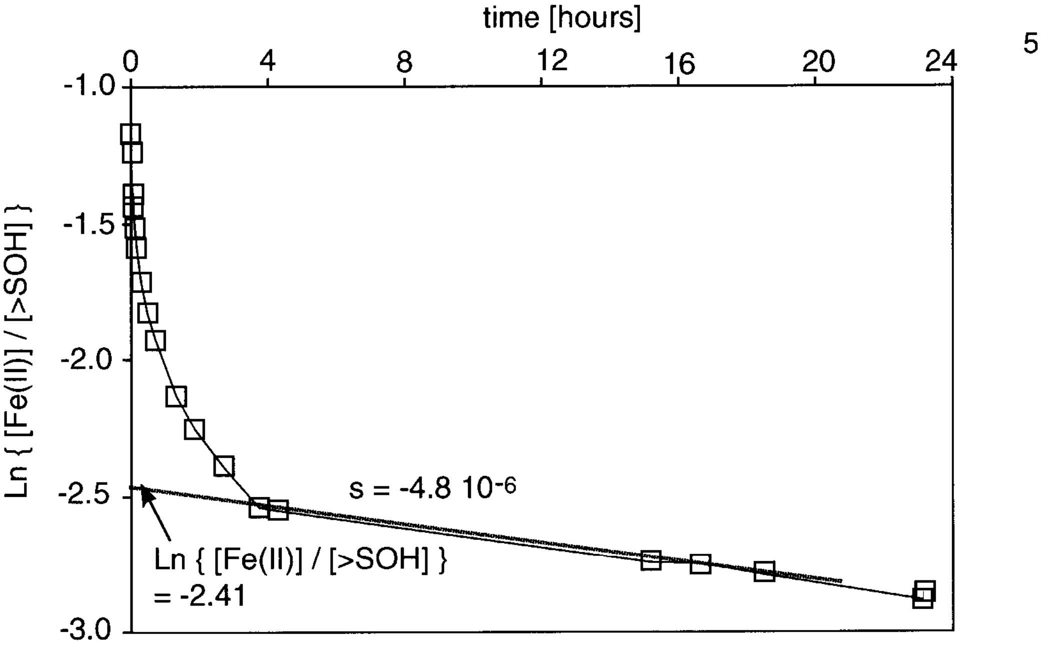

or in the logarithmic form:

$$\ln \{ [Fe(II)]_{aq} / [>FeOH] \} = \{ Fe(II)]_{tot} - [>FeOH]_0 \} k t + \ln \{ [Fe(II)]_{tot} / [>FeOH]_0 \} \qquad (4\text{-}20)$$

A second order plot of the data is depicted in Figure 4-3. The curve cannot be linearized in the first section, where most of the adsorption takes place. Most probably there is a range of surfaces sites, >FeOH, with varying adsorption characteristics. This is in agreement with crystallographic evidence for diverse binding environments on goethite surfaces (Venema, 1996). The last section can be linearized, it gives a slope of 4.8 x10^{-6} and an intercept of –2.47. A second order rate constant of 0.2 $M^{-1}s^{-1}$ can be calculated from the slope. The intercept indicates the fraction of the initial Fe(II) and surface site concentrations, which take part in this slow adsorption: it amounts to 1.5 x10^{-6} M [Fe(II)] and 1.67 x10^{-5} M [>FeOH]. This slow adsorption is visible 4 hours after the start of the experiment. Then, adsorption was close to complete, more than 85% of the Fe(II) was already adsorbed.

In the time dependent decrease of Fe(II) (Figure 4-2) 50 % of the Fe(II) was adsorbed within 5 to 7 minutes. For the slow adsorption (≥ 4 hours), a halftime of 1.8 days is calculated according to second order kinetics.

At pH 8, adsorption experiments were conducted at lower goethite concentrations to compensate for the larger site density at higher pH (10.3 sites/nm^2 at pH 8. See below). The resulting surface site concentration of the suspension was 44 μM, corresponding to a concentration ratio $[>FeOH]_0 / [Fe(II)]_0 = 4.4$. Under these conditions close to complete adsorption (>95 %) was observed within 30 minutes. In presence of both Ca^{2+} and Mg^{2+} 75% of the final adsorption was measured after 30 minutes. The final adsorbed fraction was lower in presence of Ca^{2+} and Mg^{2+} than without. No measurements were done at 5 mM bicarbonate, because of oversaturation with respect to siderite.

Adsorption kinetics can be described in two steps. The first adsorption step is fast, it takes place within minutes and is responsible for most of the adsorption (> 75 %). The consecutive adsorption step takes place within days. The presence of Ca^{2+} and Mg^{2+} delays the adsorption of Fe(II) on goethite by a factor of 1.5 to 2 at pH 7 and up to a factor of 5 at pH 8, when the first halftimes (50% adsorbed) are compared.

4.3.1.2 Langmuir isotherm

An analysis of the data by a Langmuir isotherm, yields the maximum adsorption density of goethite for Fe(II) as a function of the Fe(II) concentration at pH 7 and 8 with and without the major ions (Figure 4-4 and Figure 4-5).

Various bicarbonate concentration levels did not result in a measurable change of the adsorption. Although the presence of the Ca^{2+} and Mg^{2+} led to a time lag until the maximum adsorption capacity was reached, the final adsorption capacity was the same. This is illustrated in Figure 4-4 for the data with Ca^{2+} and Mg^{2+} obtained after 80 minutes and 24 hours, respectively. The fitted parameter of the Langmuir isotherm resulted in

Figure 4-4
Langmuir isotherm on goethite (5.25 m^2/L) at pH 7 and 10 mM NaCl in addition to 1mM HCO_3^- (□),5 mM HCO_3^- (♦), or with 1mM HCO_3^- and 0.9 mM Ca^{2+} and 0.09 mM Mg^{2+} (Δ). The lower line (dashed) represents an isotherm in presence of the major cations after 80 minutes of reaction. Arrows indicate the equilibrium Fe(II) concentration towards precipitation of siderite ($FeCO_3$) for the conditions stated.

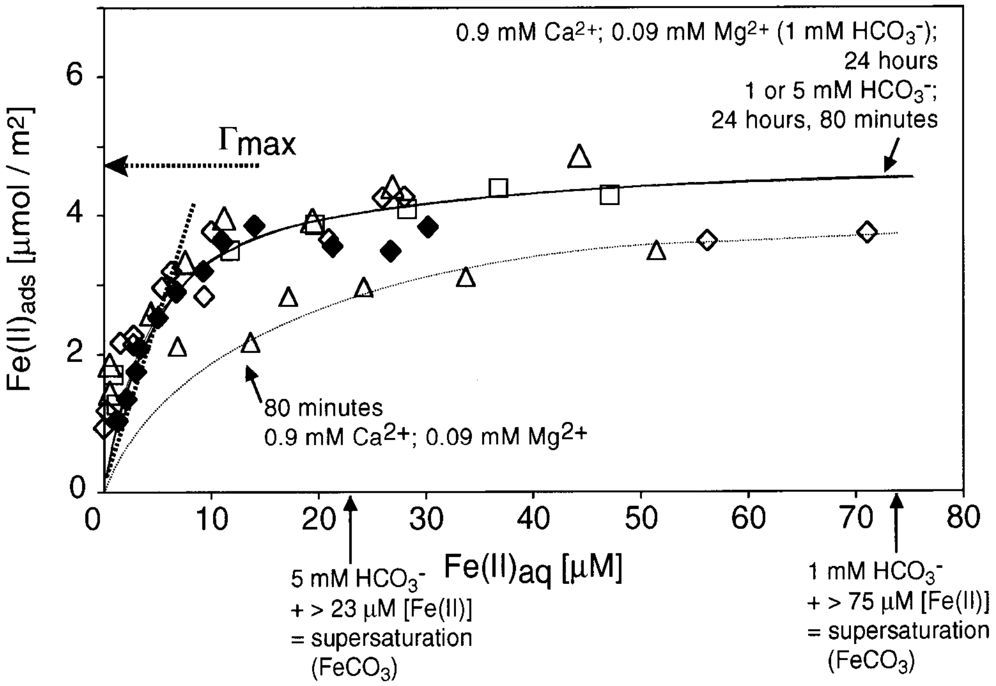

Γ_{max} = 4.8 µmol/m^2 and log K_{ads} of 5.4. The Γ_{max} corresponds to a site density of 2.9 sites / nm^2.

At pH 8 (Figure 4-5) a larger maximum sorption capacity is observed with a Γ_{max} of 17.0 µmol/m^2 and log K_{ads} of 6.2, which is equivalent to 10.3 sites / nm^2. Moreover, the presence of Ca^{2+} and Mg^{2+} visibly prevents adsorption: A smaller Γ_{max} of 10.1 µmol/m^2 with a log K_{ads} of 5.7 was determined for these conditions.

The results of the adsorption experiments at pH 7 are comparable to the kinetics experiments: no differences were found due to varying bicarbonate concentration in the applied concentration range (pH 7 only). In contrast, major cations retarded the time of the maximum adsorption. At pH 8 an increased maximum sorption capacity is observed. This can be related to a larger concentration of deprotonated

Figure 4-5
Langmuir adsorption isotherms at pH 8, 2.6 m^2/L goethite, 10mM NaCl and 1 mM HCO_3^-. in presence of Ca^{2+} and Mg^{2+} (▲ Δ) and without Ca^{2+} and Mg^{2+} (□). Arrow on the x-Axis indicate the equilibrium Fe(II) concentration towards precipitation of siderite ($FeCO_3$). Above 14µM Fe(II) siderite is likely to precipitate.

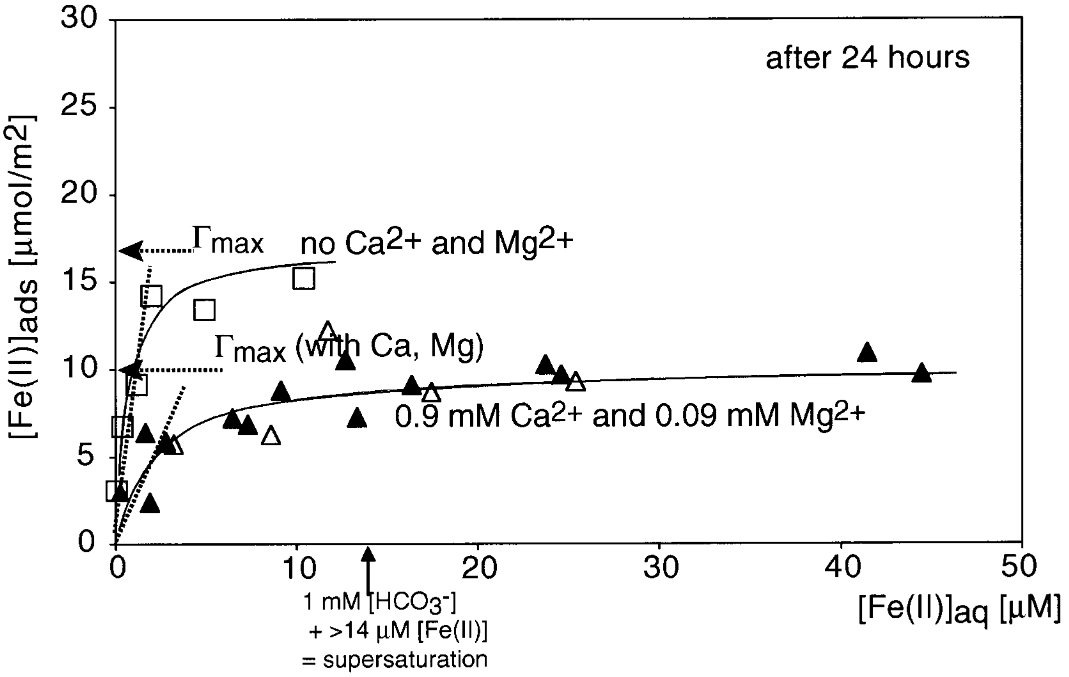

surface groups, >FeO⁻, compared to pH 7. The larger sorption capacity is compensated by an enhanced competition of Ca^{2+} and Mg^{2+}.

4.3.1.3 Desorption

The reversibility of the Fe(II) adsorption was tested by acidifying the Fe(II) carrying goethite suspensions to pH ≈ 4. Figure 4-6 shows the time dependent release of Fe(II). In Figure 4-6 (a), the equilibration pH before acidification was pH 7, whereas in Figure 4-6 (b), the equilibration pH was 8. The initially added Fe(II) is recovered almost entirely after 24 hours. In presence of Ca^{2+} and Mg^{2+} the recovery was slightly faster both at pH 7 and 8.The desorption characteristics of pH 7 and 8 show a similar pattern. This is an indication that the same adsorption mechanism takes place at pH 7 and 8, even though a larger sorption capacity is observed at pH 8.

Figure 4-6
Desorption kinetics of Fe(II) with acidification (HCl) to pH 4 after preliminary adsorption (10 μM Fe(II), 10 mM NaCl). (**a**) At pH 7 and 5.25 m^2/L goethite with 1mM HCO_3^- (◊), 5mM HCO_3^- (◆) or 1mM HCO_3^- and 0.9 mM Ca^{2+} (▲). (**b**) Adsorption pH 8 (2.6 m^2/L goethite) together with 1mM HCO_3^- (◊) or 1 mM HCO_3^- together with 0.9 mM Ca^{2+} and 0.09 mM Mg^{2+} (◆).

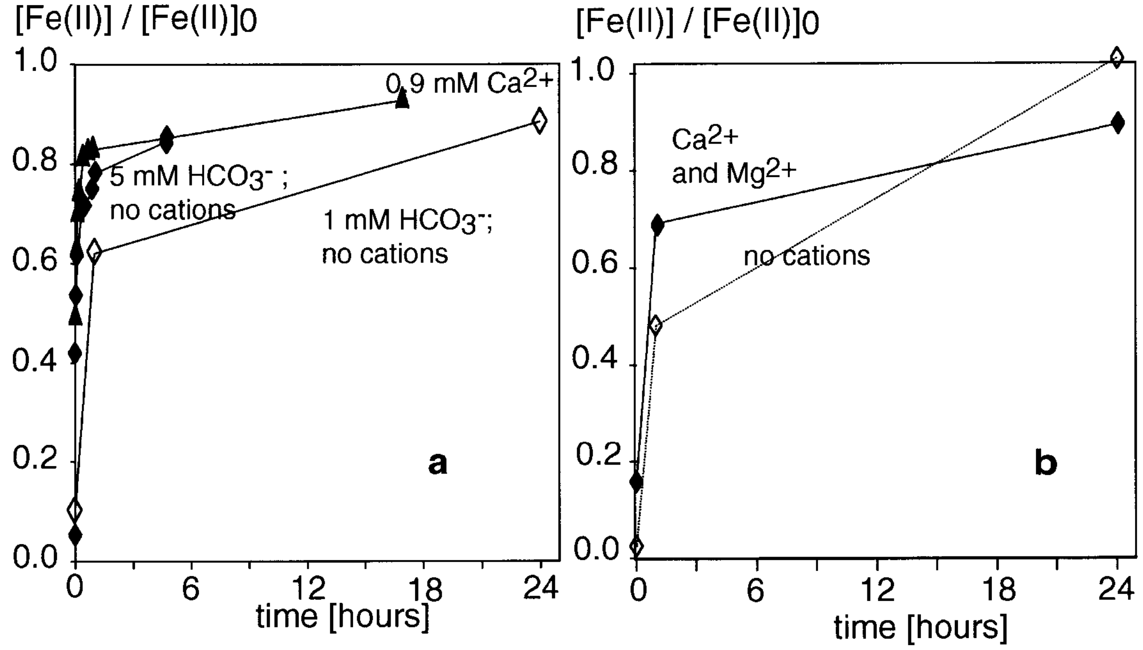

4.3.1.4 Summary

The results of the adsorption experiments can be summarized as follows. Adsorption kinetics at pH 7 and 8 take place rapidly, even in the presence of the major cations. A first fast adsorption is followed by a slower step. In the applied range of concentrations, varying bicarbonate concentrations had no effect. In contrast, the presence of the Ca^{2+} and Mg^{2+} slowed down the fast initial adsorption step. At pH 8, this effect is more pronounced with Mg^{2+} and Ca^{2+} than with Ca^{2+} alone.

The adsorption capacity for Fe(II) adsorption on goethite at pH 7 was determined as 2.9 sites / nm^2. This value is similar to adsorption densities of goethite found in the literature (1.68 - 3.1 sites / nm^2; see Table 4-1). At pH 8, we measured an adsorption capacity of 10.2 sites / nm^2. The range of adsorption densities found in the literature could be related to varying concentrations of solid goethite during the adsorption experiments. Amonette et al. (2000) noticed that the adsorption capacity of goethite changed depending on the solid concentration of the goethite suspension (1.6 sites/nm^2 to 3.6 sites/nm^2 for 5 mg/L and 1 mg/L goethite, respectively). They related it to coagulation of goethite particles at larger concentrations, which impedes the access of Fe(II) to the total surface of the solid. The lower adsorption correlated with a corresponding decrease of the oxidation rate.

Whereas at pH 7 no measurable effect of Ca^{2+} and Mg^{2+} was found on the amount of Fe(II) adsorbed, at pH 8 the maximum adsorption density was reduced by almost 60% of the value without the cations. Besides electrostatic effects (outersphere complexation), Ca^{2+} forms binuclear innersphere complexes at higher pH, which could block surface sites (Rietra et al., 2001). Magnesium has even a larger affinity than Ca^{2+} to goethite (Weirich, 2000).

Care was taken to avoid surface precipitation by using low Fe(II) surface loadings during the experiments. Compared to Coughlin and Stone (1995), more Fe(II) was recovered (>85 %) after 24 hours in our experiments. The presence of cations accelerated the recovery of the Fe(II), but not visibly increased the fraction recovered.

4.3.2 Fe(II) oxygenation

The kinetics of the homogeneous oxidation reaction was measured at a low O_2 concentration (2.6 mg/L). The electrolytic background was the same as for heterogeneous reactions with calcite and goethite (saturated $CaCO_3$ solutions or 0.01M NaCl).

The oxygenation kinetics were based on measurements of the decrease of Fe(II) in solution according to:

$$-d[Fe(II)] / dt = d[Fe(III) / dt = k'_{hom} [Fe(II)] [O_2]$$

$$k_{hom} = k'_{hom} [O_2];\ pH = const = 7 \qquad (4\text{-}21)$$

Where k_{hom} and k'_{hom} stand for the first-order rate constant and the second-order rate constant, respectively. For the heterogeneous reactions similar conditions as for the adsorption experiments were applied (5.25 m^2/L or 0.3 g/L goethite, 10 μM Fe(II)). This allows a comparison between oxygenation and adsorption kinetics.

In Figure 4-7 the time-dependent decrease of Fe(II) due to homogeneous oxidation (X) is shown together with the decrease of Fe(II) due to its adsorption on goethite (open symbols), and to heterogeneous oxidation of Fe(II) on goethite (closed symbols). The time scale is 10 minutes. During this time about 20 % of the Fe(II) disappeared by homogeneous oxygenation, 60 % of the total Fe(II) was adsorbed, and mostly all of Fe(II) (> 90%) was oxidized in the presence of goethite.

The presence of calcium delays the oxidation reaction similarly to the way it affects the adsorption reaction. These observations show that the heterogeneous oxygenation kinetics depends on the rate of formation and on the type of the adsorbed Fe(II) species. A reduced rate of adsorption due to the presence of calcium results in a reduced rate of oxygenation. The adsorbed Fe(II) fraction, moreover, is oxidized within 1-2 minutes (compare open and filled symbols in Figure 4-7), but after this, the heterogeneous oxidation still continues with a higher rate than the oxidation in solution. This means that new promoting adsorption sites are produced consecutive to oxidation of Fe(II), generating a catalytic cycle (Figure 4-8). The oxygenation kinetics, however, is slower than observed initially. A possible explanation is that only a fraction, α, of the initial sites is regenerated, whereas the other one becomes less reactive. This is illustrated in Figure 4-8, where >FeO-Fe(II) represents adsorbed Fe(II) at a reactive goethite surface site, >FeOH. A fraction of the adsorbed Fe(II), α, is oxidized and precipitated to new reactive >FeOH sites at the goethite surface. The remaining fraction, (1-α), produces less reactive surface site, $>Fe(OH)_X$. The oxygenation reaction gets slower, due to only a partial reformation of the reactive sites.

To determine the second-order rate constant for the oxygenation of Fe(II) adsorbed to goethite, an experiment was conducted in excess of goethite (17.5m^2/L) and the same initial Fe(II) concentration (10 μM). Figure 4-9 shows a logarithmic plot of the data (pseudo-first order

Figure 4-7

Decrease of Fe(II) (10 μM) due to adsorption and heterogeneous oxygenation in presence of goethite (5.25 m^2/L) at pH 7 and 2.6 mg/L oxygen. Open symbols: Adsorption in presence (Δ) or in absence of Ca^{2+} (◊). Filled symbols: oxygenation in presence (▲) or in absence of Ca^{2+} (◆). For comparison homogeneous oxygenation is shown as (x).

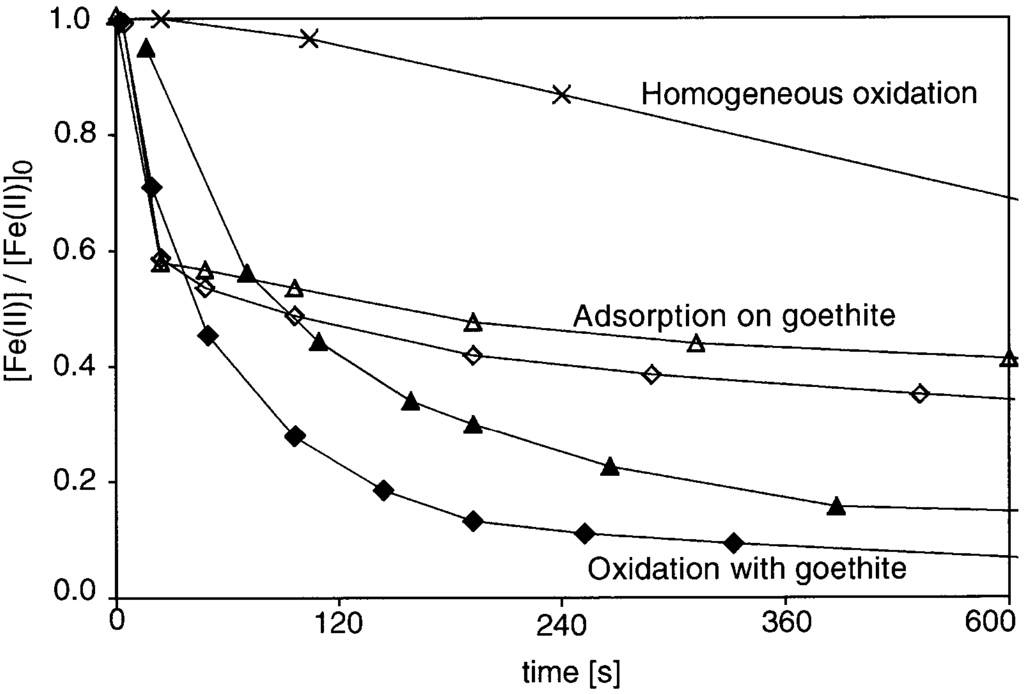

Figure 4-8

Schematic model of the catalytic cycle: partial (α) regeneration of the reactive surface sites at the goethite (>FeOH) or the calcite surface (>$CaCO_3$). >*$CaCO_3$ and >$Fe(OH)_x$ represent surface sites, with a lower reactivity than the original surface sites.

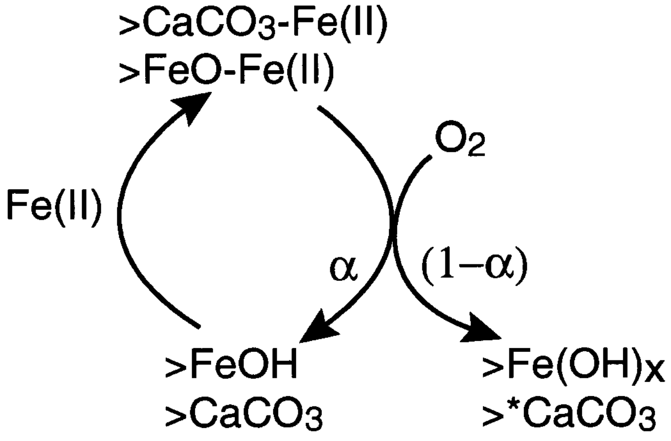

Figure 4-9
Logarithmic representation of the homogeneous (x) compared to heterogeneous (■) Fe(II) oxygenation (17.5 m^2/L) at pH 7, with 10 μM initial Fe(II), and 2.6 mg/L oxygen. The slopes of the dashed lines correspond to the pseudo first order rate constants.

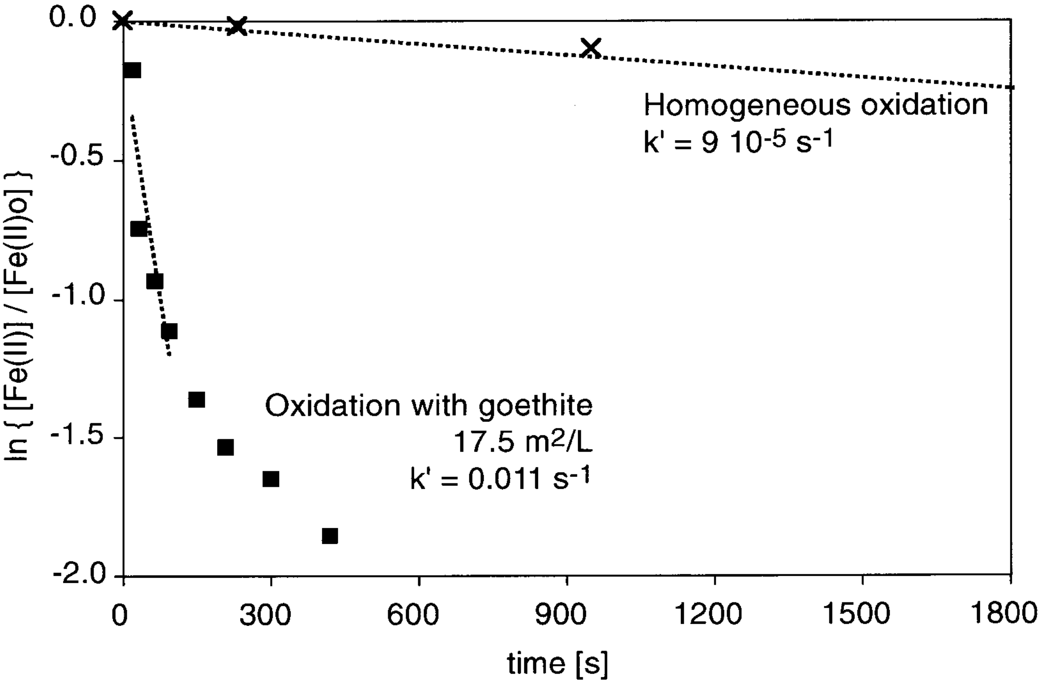

kinetics), as well as the experiments without goethite (homogeneous oxidation in solution).

For the homogeneous oxidation kinetics, a second-order rate constant of 1.2 $M^{-1} s^{-1}$ is determined from the straight line (pH 7, 2.5 mg/L O_2). In presence of goethite the initial oxygenation step (< 230 sec.) results in a rate constant of 193 $M^{-1} s^{-1}$. A third order rate constant of 0.30 L mg^{-1} M^{-1} s^{-1} is calculated if the goethite concentration is accounted for (in mg/L Fe(III)).

The rate constants determined in this study are in the range of the reported values for the homogeneous and heterogeneous oxidation of Fe(II). The homogeneous rate constant amounts to (9 ± 5) $x10^{13}$ $M^{-3}s^{-1}$, which has to be compared to 2 $x10^{14}$ $M^{-3}s^{-1}$ (Stumm and Lee, 1961; Millero et al. 1987; Millero and Miguel. 1989; Chap. 1). Whereas our heterogeneous rate constant can be compared to data obtained by

Tamura et al. (1980). These authors measured rate constants of 0.097 L mg^{-1} M^{-1} s^{-1} for amorphous $Fe(OH)_3$ and 0.021 L mg^{-1} M^{-1} s^{-1} for goethite at pH 6.4 (the rates are given as L mg^{-1} M^{-1} s^{-1}, which means with respect to Fe(III) in mg/L and dissolved oxygen, M). Extrapolated to pH 7 this yields 0.16 L mg^{-1} M^{-1} s^{-1}, respectively 0.033 L mg^{-1} M^{-1} s^{-1}. Given the possible variabilities of the experiments, these values are in reasonable agreement with our findings ($k = 0.3$ L mg^{-1} M^{-1} s^{-1}). In the heterogeneous oxidation experiments presented in Figure 4-8, the Fe(II) decrease from solution is caused by the combination of adsorption and oxidation. Adsorption equilibrium was not reached before the oxygen addition. In such a system, there is a pronounced competition effect of Ca^{2+} and Mg^{2+} adsorption. If the system is left long enough to equilibrateprior to oxygen addition (See Figure 4-4, Langmuir isotherm), the presence of Ca^{+} and Mg^{2+} does not decrease the fraction of the adsorbed Fe(II) but its rate of formation. Therefore, the same kinetics should be measured initially at pH 7 with and without Ca^{+} and Mg^{2+}. However, this is not the case at pH 8, because Ca^{+} and Mg^{2+} prevent some adsorption of Fe(II) (Figure 4-5).

Based on the catalytic effect of goethite, regeneration of the goethite surface allows a significantly higher amount of Fe(II) to be rapidly adsorbed and oxidized than the amount measured separately by adsorption only. Amonette et al. (2000) observed that they were able to reduce an amount of carbon tetrachloride, which corresponded to the equivalent of 124 % of the initially adsorbed Fe(II) concentration. Klausen et al. (1995) reduced an equivalent of 165 % of nitro-aromatic compounds relative to the adsorbed Fe(II). Similar observations were made by other authors (Hofstetter et al., 1999 and Buerge and Hug, 1999). Therefore, new adsorption sites have been generated at the goethite surface according to the catalytic cycle (Figure 4-8), which allowed the reduction of a surplus of oxidant. Weidler et al. (1998) conducted Fe(II) oxygenation experiments in presence of goethite at pH 4.5, where the oxidation in solution is negligible compared to oxidation catalyzed by the surface. The measured growth of the goethite crystal can only be explained by the formation of fresh binding sites for Fe(II) consecutive to the precipitation of Fe(III). With ongoing oxidation a deviation of the initial oxidation rate was noticed. A similar deviation was found by Klausen et al. (1995), as well as Hofstetter et al. (1999) and Amonette et al. (2000). This corresponds to the parallel formation of less reactive sites, which leads to a decrease of the heterogeneous oxidation rate.

4.3.3 Heterogeneous oxidation of Fe(II): Comparison of the goethite with the calcite system

Figure 4-10 shows a comparison of the first order decrease of Fe(II) by oxygenation in a homogeneous system, in a system with 1 g/L calcite, and with 1 g/L goethite.

Table 4-2 is a summary of Figure 4-10. It presents the maximum adsorption capacities of the solids and the rate coefficient of the oxidation kinetics at pH 7. Goethite has a five times larger adsorption capacity than calcite with respect to the surface (mol/m^2). However, co-precipitation of Fe(II) may occur on calcite, leading to a larger uptake of Fe(II) after several days, although part of the incorporated Fe(II) is not accessible to oxygenation anymore (see Chapter 3).

The presence of goethite accelerates the oxidation kinetics by a factor of hundred compared to calcite. If the rate constants are transformed with respect to maximum surface site concentration of the solid at pH 7 (goethite 84 μmol/g; calcite 2.4 μmol/g), the rate constants result in 8.3 x10^5 M^{-2} s^{-1} for calcite and 2.3 x10^6 M^{-2} s^{-1} for goethite. The difference between the rate is reduced to a factor of 3. This allows the conclusion that, the higher reactivity of goethite is mostly related to its large adsorption capacity for Fe(II).

Figure 4-11 compares the adsorption kinetics of Fe(II) on calcite and on goethite at the same surface site concentration for both solids (25.2 μM [>FeOH] and [24.0 μM [>CaCO$_3$], which corresponds to 0.3 g/L goethite and 10 g/L calcite). The figure shows that adsorption kinetics of Fe(II) on calcite and goethite is similar, if it is normalized to the surfaces site concentration.

Figure 4-10

First order representation of the oxygenation kinetics of Fe(II) (10 μM Fe(II), 2.6 mg/L oxygen) at pH 7 (saturated $CaCO_3$ solution) under varying conditions: No solid (O); with 1 g/L calcite (♦); with 1 g/L goethite (▲).

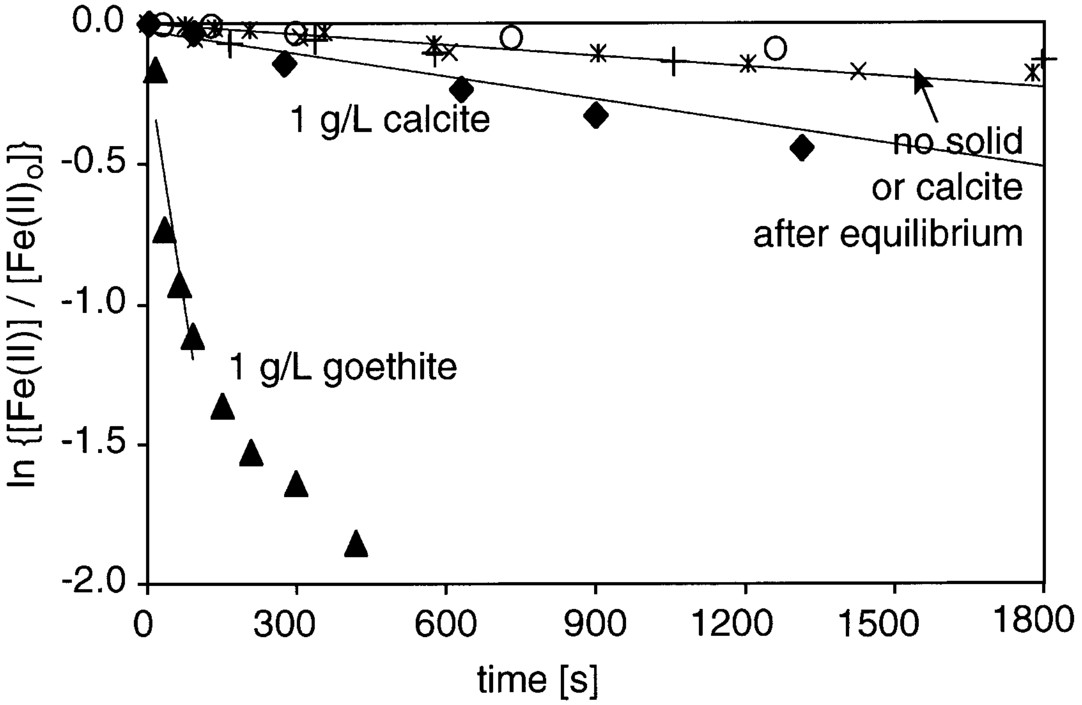

Table 4-2

Measured rate constants and one standard deviation (±) for the homogeneous oxidation experiments at pH 7 assuming the following rate law: -d[Fe(II)] / dt = k [Fe(II)] [solid] [O_2], the solid being calcite or goethite.

Conditions	**Γ_{max} (24h)** [μmol/m^2]	**Rate constant*** [M^{-1} s^{-1}]
No solid	-	1.2 ± 0.5
Calcite	1.0	2 ± 1.5
Goethite	4.8	193 ± 13

*Second order rate constant measured with 1 g/L solid

For adsorption of Fe(II) on goethite or calcite, a maximum rate constant can be estimated from the first measured points (60 seconds) assuming first order kinetics. Rates constants of 0.012 s^{-1} and 0.010 s^{-1} are estimated for calcite and goethite, respectively. Considering the

Figure 4-11
Adsorption kinetics of Fe(II) (10 μM) at pH 7 on calcite (◇) and on goethite (Δ, ▲). (Δ) only bicarbonate; (▲) bicarbonate with Ca^{2+} and Mg^{2+}.

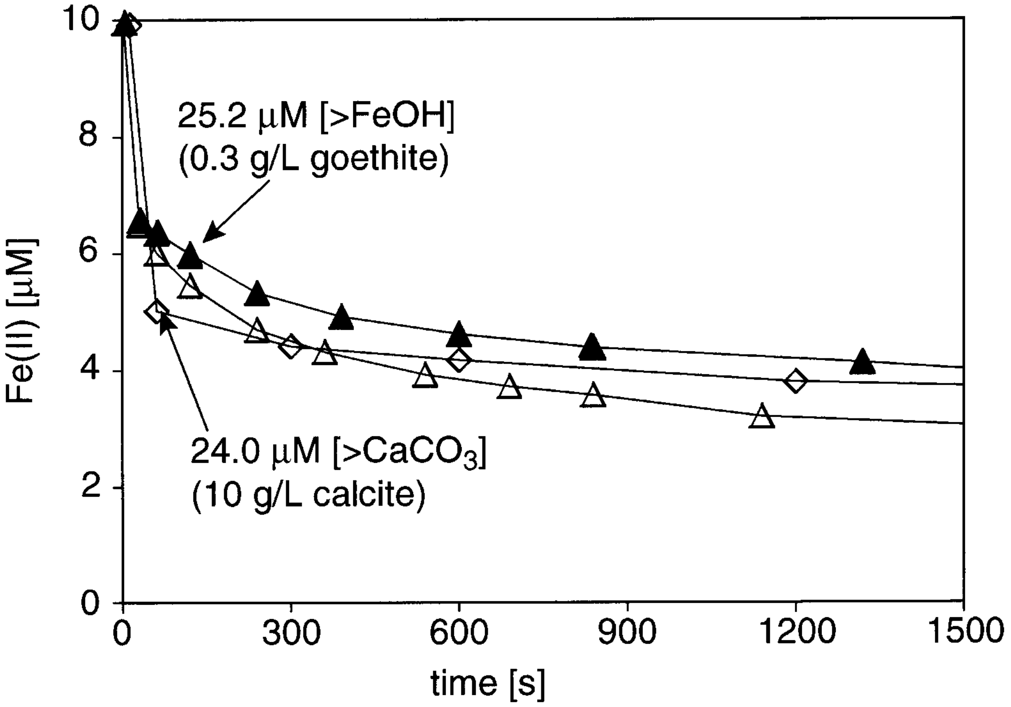

heterogeneous oxidation with the same solid concentration (25 μM surface site concentration) and an oxygen concentration of 2.6 mg/L, the resulting pseudo-first order constants are 1.7 10^{-3} s^{-1} and 4.7 10^{-3} s^{-1}. For calcite the rate constant for adsorption is ten times faster then the rate constant for oxygenation, whereas for goethite it is only a factor of two. Doubling the oxygen concentration results in a rate coefficient on the order of the rate constant for adsorption. Therefore, in both systems the oxidation kinetics seems to be the rate-limiting step. However, under large oxidant concentrations, adsorption could become limiting, to a larger extent for goethite than for calcite.

In both systems with calcite (Figure 3-11) and with goethite (Figure 4-7) continuous formation of new adsorbing sites is observed. In presence of calcite a maximum of reactive surface sites are regenerated (α close to 1; Figure 4-8). In consequence, oxygenation kinetics can be linearized by a first-order kinetics approach (Figure 3-11: small or no excess of surface sites; ratio [>CaCO3] / [Fe(II)] = 2.4 or 0.24). In contrast, with goethite the fraction of the reactive surface sites regenerated is not maximal, ($\alpha < 1$), the remaining fraction is transformed to less reactive sites, which results in a decrease of the rate compared to the initial conditions.

In addition, the regeneration mechanism is most probably not the same at the surface of both solids. With calcite, a calcium carbonate unit is dissolved locally; the calcite surface, thus, buffers the protons produced by the hydrolysis, following the oxidation of Fe(II) to Fe(III) (Figure 3-12). With goethite, the Fe(III) produced at the surface, hydrolyses and forms a new >FeOH adsorption site.

4.4 Conclusions

The adsorption and oxygenation experiments of Fe(II) in presence of goethite allow the following conclusions in relation to in situ deferrisation:

Varying concentrations of bicarbonate (1 to 5 mM) have no measurable effect on the adsorption kinetics and the adsorption capacity at pH 7. The presence of Ca^{2+} and Mg^{2+} in proportion of 100:1 (Ca^{2+}) and 10:1 (Mg^{2+}) with respect to Fe(II) concentration delays the adsorption kinetics both at pH 7 and pH 8. Compared to the kinetics without Ca^{2+} and Mg^{2+} the adsorption kinetics decrease by a factor of ca.2 at pH 7.

The adsorption isotherm (Langmuir) yields a maximum adsorption capacity for Fe(II) on goethite at pH 7 of 4.8 μmol / m^2 (2.9 sites /nm^2) and an adsorption constant of $10^{5.4}$, independent of the presence of Ca^{2+} and Mg^{2+}. At pH 8, the maximum adsorption capacity increases to 17.0 μmol / m^2 with an adsorption constant of $10^{6.2}$. The presence of Ca^{2+} and Mg^{2+} (100:1 and 10:1 with respect to Fe(II)) reduced this value by 60% to 10.1 μmol/m^2 and an adsorption coefficient of $10^{5.7}$.

In Switzerland the pH of the aquifers seldom surpasses pH 7.5, it varies usually between 6.8 and 7.3 (see Table1-2). Under these conditions the effect of the major ions, HCO_3^-, Ca^{2+}, and Mg^{2+}, can be considered as negligible and an average uptake capacity of goethite for Fe(II) of 5 μmol/m^2 can be used. For comparison, at the calcite surface a maximum adsorption capacity of 1 μmol / m^2 was measured at pH 7.

In addition to the larger adsorption capacity of Fe(II) on goethite, the oxygenation of Fe(II) in presence of goethite is about two orders of magnitude faster than on calcite or in homogeneous systems (Table 4-2.). Already small increases of goethite in a solid matrix of carbonate result in a noticeable change of the system with respect to Fe(II) oxygenation kinetics. It is exemplified in Table 4-3 that increasing proportion of goethite (w/w %) result in oxygenation kinetics several fold faster than pure calcite.

Table 4-3
Increasing reactivity of a suspension relative to plain calcite with increasing goethite content

Calcite (w/w) %	Goethite (w/w) %	Multiplication factor -
100	0	1
99	1	2
95	5	4
92	8	9
85	15	15

The rate of Fe(II) oxygenation is an important factor in reduced ground waters, where the injected oxygen can also be consumed by other processes (aerobic respiration, nitrification). Therefore the efficiency of the process depends on the relative rates of the reactions. It has been observed in a field system that the injection of small amounts of oxygen leads to a stoichiometric oxygenation of Fe(II) (von Gunten et al., 2002). It showed that the oxygenation of Fe(II) adsorbed to Fe(III) oxides is faster than the consumption of oxygen by other biological processes.

5

CONCLUSIONS AND OUTLOOK

5.1 Fe(II) removal from ground water by heterogeneous oxidation and precipitation

As a result of this study heterogeneous oxidation and precipitation is the proposed mechanism for the Fe(II) removal during in situ ground water treatment. The oxidation reaction of Fe(II), is highly facilitated by the presence of natural surfaces (quartz, aluminum oxide, clay minerals: Klausen et al., 1995; Schultz and Grundl, 2000; Buerge and Hug, 1999; Hofstetter, 1999), in particular by Fe-oxides, the products of Fe(II) oxidation (Jeon et al., 2001; Liger et al., 1999; Tamura et al., 1976).

Heterogeneous oxidation-precipitation takes place in two steps: First Fe(II) is adsorbed on a natural surface of the aquifer matrix (quartz, aluminum oxide, clay, calcite, etc.), which leads to the adsorbed Fe(II) species. This reactive Fe(II) species is then rapidly oxidized to Fe(III), which hydrolyses to Fe(III)-oxides. The produced Fe(III)-oxides (FeOOH), can anew adsorb Fe(II) from solution. Through oxygenation of the adsorbed Fe(II) a new layer of Fe(III)-oxides is formed. After several cycles of adsorption and oxygenation a coating of Fe-oxides forms at the surfaces, which very efficiently filters the Fe(II) from the reduced ground water, if water is pumped from the underground (see Figure 1-4).

To mimic these processes, which occur in engineered full-scale systems, laboratory experiments were performed with the model substances calcite and goethite. Calcite was taken to represent a reference aquifer system, corresponding to the system before treatment. Goethite was taken as model Fe-oxide for the coatings grown at the solid surfaces of the aquifer matrix. It represents the steady-state conditions of *in situ* deferrisation.

The adsorption capacity of goethite for Fe(II) is five times as high as for calcite (2.9 sites /nm^2 versus 0.6 sites /nm^2 at pH 7; respectively 35 times with respect to the masses 84 μM /g and 2.4 μM /g). Comparable adsorption capacity to Fe-oxides was measured for clay minerals (Buerge, 1999; pH 5). Based on the weight of the minerals, oxygenation kinetics of Fe(II) in the presence of goethite is 100 times faster than in the presence of calcite. The difference between goethite and calcite is a factor of 3, if the rates are compared with respect to the adsorption capacities of the minerals (8.3 x10^5 M^{-2} s^{-1} and 2.3 x10^6 M^{-2} s^{-1}, respectively).

Fe(II) addition to the calcite suspension and subsequent oxygenation was used to simulate the processes taking place during the start-up phase of in situ deferrisation, during which the calcite suspension is gradually enriched with Fe(III). The Fe(II) oxygenation was significantly faster for elevated Fe(III) concentrations (factor 5 to 6 relative to pure calcite). This enhancement can be explained with the formation of small clusters of Fe(III)-oxides on the calcite surface, which are very reactive because of their large specific surface area. Similar observations were made in a system, where Fe(II) was oxidized in presence of aluminum oxide (γ-Al_2O_3) (Klausen et al. 1995). The interpretation was also an enhanced reactivity due to the formation of Fe-oxide coatings of the surface of the aluminum oxide.

It was shown in Chapter 3 that calcite can also immobilize Fe(II) by co-precipitation to produce a mixed Fe(II)/Ca-carbonate with a relative mole ratio of 0.4 %. This co-precipitation can prevent a fraction of the Fe(II) associated with calcite from being oxidized. However, heterogeneous oxygenation of Fe(II) is by far faster than co-precipitation as carbonate. Therefore, Fe(II) oxygenation and its precipitation as Fe(III)-oxide is also the dominating removal process in this system.

In an anaerobic environment other redox transformation reactions, predominantly the aerobic respiration (DOC transformation. See 1.1.2.3 and Table 1-2) and to a lesser extent nitrification compete with Fe(II) and Mn(II) for a potential oxidants. These reduced species (DOC, NH_4^+) can rapidly consume the injected oxygen, the kinetics of the oxygenation reaction is then decisive. Therefore fast Fe(II) oxygenation kinetics ensures the oxidation and precipitation of Fe(II) and conjointly allows an efficient removal of Fe(II) from the ground water. Larger oxidant concentrations do not necessarily increase the efficiency of the Fe(II) removal, since it does not switch off the competition of the other reduced compounds for the oxidant. In a field study von Gunten et al. (2002) showed that diminishing the concentrations of injected oxygen resulted in the oxidation of the exact equivalent concentration of Fe(II). At larger oxidant concentration, however, the oxygen was also consumed by other redox processes, mostly by aerobic respiration.

Based on our laboratory experiments and findings in the field, Fe(II) removal by in situ ground water treatment is likely to happen by heterogeneous oxidation and precipitation at the surface of Fe-oxides. This does not infer that the microbiological Fe(II) oxidation is an impossible mechanism. However, at circumneutral pH in a well-buffered system, the chemical reaction is so fast, that Fe(II)-oxidizing microorganisms can hardly compete. Microorganisms probably play a role in the in situ Fe(II) removal of ground water, when the chemical reaction is inhibited, for example, in less buffered systems with lower pH, such as in silicaceous environment encountered in Scandinavia.

5.2 Manganese removal

The field study of La Neuveville showed that most of the manganese was not present in its oxidized form. Calculation showed that the injected groundwater was saturated with respect to $CaCO_3$, $FeCO_3$ and $MnCO_3$. The oxidation of Mn(II) is much slower than Fe(II). In contrast, Mn(II) has a larger affinity for carbonate than Fe(II) (Chap 3. Table 3-1). Therefore the incorporation of Mn(II) as mixed Mn/Ca-carbonate is a very possible immobilization process. It corresponds to the conclusions that Mn(II) was most likely associated with carbonate minerals.

Precipitation as Mn(II)/Ca-carbonate or rhodochrosite ($MnCO_3$) is certainly related to the particularities of the very carbonaceous site in La Neuveville. It also indicates, however, that the conditions for chemical oxidations of manganese were not satisfied. Further field investigations would allow more conclusions about the efficiency and the possible mechanisms of manganese removal.

5.3 In situ deferrisation and risk of clogging the aquifer

Heterogeneous oxidation and precipitation lead to a gradual growth of Fe-oxide coatings at the surface of the solid aquifer matrix. The coatings were mostly goethite and therefore in a very compact form. This ensures a long term operation without significant clogging of the aquifer. In contrast to these findings, homogeneous oxygenation would lead to more voluminous Fe(III)-oxides, that could affect the hydraulic conductivity of the aquifer.

In the field study of La Neuveville, the measured precipitated concentrations showed a significant dependence of the grain size, more so for iron than for manganese. The larger concentrations measured for the smaller particles correlate with the larger surface to volume ratio of the small particles. Such a pattern points to a heterogeneous mechanism, where precipitation is facilitated at the surface of the aquifer material. This is a further confirmation of the findings from the laboratory, which showed the catalytic role of natural surfaces.

Generally, the spatial variations of the iron and manganese concentration in the precipitation zone were small. This can be explained by a uniform distribution within the precipitation zone. Concentrations of precipitated iron and manganese amounted to twice the background concentration after 10 years of operation.

To guarantee a long-term operation of an in situ deferrisation plant, it is decisive to dimension the volume of the precipitation zone large enough. Based on our findings the dimensions of the precipitation zone can be optimized in relation to the expected volume of the precipitates if all the dissolved iron and manganese from ground water is precipitated to solid Fe-oxides and Mn-carbonates, and homogeneously distributed throughout the precipitation zone. In addition it can be assumed that the precipitation occurs as growth on surfaces rather than into the space between particles.

5.4 Outlook

In situ ground water treatment is an applied topic, which includes aspects of hydrology, mineralogy, microbiology, engineering sciences. The manageable dimensions of the *in situ* ground water treatment system allow a careful investigation. More fundamental hydrological aspects can be brought in for a better understanding of possible changes occurring in the aquifer due to the precipitated iron and manganese. These could be small scale studies (like column) in defined model systems about changes of the hydraulic conductivity with varying saturation of the pore volume or investigations regarding the time-variable heterogeneity of the underground under larger flow conditions.

Natural surfaces play an important role as catalyst for transformation reactions in the environment. Conjointly to transformations processes, changes take place at the surface, which lead to the dissolution of the solid or to the precipitation of a new mineral. There is scarce knowledge about consecutive transformations of the solid, like re-crystallization to solid intermediates, finally leading to a stable mineral. Transformation of the solid may go along with changing reactivity of its surface with respect to sorption and transformation reactions. Combining both wet chemistry studies with surface specific microscopy and spectroscopy (Atomic Force Microscopy, electron diffraction, X-ray Absorption Spectroscopy, etc.) could be interesting means to better understand these processes.

Depending on the prevalent conditions (oxygen and nitrate concentrations, pH) microbiologically mediated iron oxidation potentially controls the oxidation of Fe(II) beyond some threshold. Microorganisms can develop mechanisms to outcompete chemical oxidation and establish themselves in the niche (Benz et al., 1998; Emerson and Moyer, 1997). There is little knowledge about the habitat and the surviving strategies of these organisms.

The mechanisms of the oxidation and precipitation of manganese by *in situ* ground water treatment is not explained. Microorganisms most probably play a key role. There is likely more information required for removal of manganese, which apparently represents a possible health risk for a sensible fraction of the population (European Commission, 2000; Valezquez and Du, 1994).

APPENDIX

Binding constants

Equilibrium constants used to calculate the species concentrations. After King (1998) and Wersin (1990).

N°	Species	Equilibrium constant T = 25° C; I = 0.0 M
1	$H_2O \Leftrightarrow OH^- + H^+$	-14.00
2	$H_2CO_3 \Leftrightarrow HCO_3^- + H^+$	-6.35
3	$HCO_3^- \Leftrightarrow CO_3^{2-} + H^+$	-10.33
4	$Fe^{2+} H_2O \Leftrightarrow FeOH^+ + H^+$	-9.51
5	$Fe^{2+} +2\ H_2O \Leftrightarrow Fe(OH)_2 + 2H^+$	-20.61
6	$Fe^{2+} + HCO_3^- \Leftrightarrow FeHCO_3^+$	1.47
7	$Fe^{2+} + CO_3^{2-} \Leftrightarrow FeCO_3$	5.69
8	$Fe^{2+} + 2\ CO_3^{2-} \Leftrightarrow Fe(CO_3)_2^{2-}$	7.45
9	$Fe^{2+} + CO_3^{2-} + OH^- \Leftrightarrow Fe(CO_3)(OH)^-$	9.97
10	$FeCO_3\ (s) \Leftrightarrow Fe^{2+} + CO_3^{2-}$	-10.8

In situ treatment plants worldwide

After Waldburger (1994) Zienkiewicz (1984), Groth et al. (1988) and Mengis (2002).

Place	Since	Operation capacity [m^3/d]	Fe [mg/L]	Mn [mg/L]
Switzerland				
Sursee	1984	2 x 250	0.2	0.04
Sion	1985	2 x 12 000	0.15	0.04
La Neuveville	1988	2 x 3500	0.5-1.0	0.1-0.2
Büron	1990	2 x 300	1.95-3.2	0.12-0.2
Dübendorf	1991	2 x 850	0.1	0.09
Luzern	1991	3 x 1000	3.7-3.9	0.17-0.33
Menznau	1993	1400	6	0.6
Meisterschwanden	1993	3 x 1080	0.1	0.15
Bächau	1996	8600	< 0.7	< 0.17

Place	**Since**	**Operation capacity** [m³/d]	**Fe** [mg/L]	**Mn** [mg/L]
Germany				
Oberkirch	1997	430	> 0.1	1.2
Landringhausen	1973	7900	2.5	0.25
Isernhagen	1976	2900	20.0	2.0
Homberg	1978	36000	0.6	0.2
Wittingen	1980	1680	0.7	
Wahlstedt	1982	11500	0.3	0.19
France				
Chalon	1977	4800	0.08	0.15
Baleone	1979	6000	1.0-10.0	0.5
Denmark				
Orslevkloster	1976	5400	1.2	0.07
Trehje	1977	7200	0.7	0.07
Stoholm	1977	6480	0.6	0.08
Glyngøre	1978	6000	0.4	0.07
Billund	1978	5400	1.5	0.14
Karup	1980	3600	0.4	0.07
Rødkjaersbro	1980	3600	1.4	0.06
Sweden				
Grimsås	1971	960	3.9	0.07
Holmsjö	1971	240	5.2	0.16
Stallarsholmen	1973	1200	0.5	0.2
Värsås	1974	240	1.2	0.09
Hormantorp	1976	3360	4	1.2
Kärnsjön	1979	3600	0.5	0.05
Lönsboda	1979	1680	0.2	0.35
Ljungsarp	1980	480	2	0.25
Almesåsen	1981	1680	0.4	0.25
Hägasen	1982	19680	0.5	0.48
Yugoslavia				
Karlovac	1982	24000	10.5	0.43
USA				
Pembroke, MA	1981	2900	0.6	0.45
Columbus, IN	1982	31200	1.7	0.8

REFERENCES

1995. Fremd- und Inhaltsstoffe in Lebensmittel. Fremd- und Inhaltsstoffverordnung (FIV). *2 Liste der zugelassenen Höchstkonzentrationen (Toleranz- und Grenzwerte) für Metalle und Metalloïde*. SR 817.021.23.

Amirbahman A., Schönenberger R., Johnson A., and Sigg L. (1998) Aqueous- and solid- phase biogeochemistry of a calcareous aquifer system downgradient from a municipal solid waste landfill (Winterthur, Switzerland). *Environmental Science and Technology.* 32, 1933-1940.

Amonette J. E., Workman D. J., Kennedy D. W., Fruchter J. S., and Gorby Y. A. (2000) Dechlorination of carbon tetrachloride by Fe(II) associated with goethite. *Environment Science and Technology.* 34, 4606-4613.

Appelo C. A. J., Drijver B., Hekkenberg R., and Jonge M. D. (1999) Modeling in situ iron removal from ground water. *Ground Water.* 37 (6), 811-816.

Astilleros J. M., Pina C. M., Fernandez-Diaz L., and Putnis A. (2002) Molecular-scale surface processes during the growth of calcite in the presence of manganese. *Geochimica et Cosmochimica Acta.* 66 (18), 3177-3189.

Bargar J. R., Tebo B. M., and Villinski J. E. (2000) In situ characterization of Mn(II) oxidation by spores of the marine Bacilllus sp. strain SG-1. *Geochimica et Cosmochimica Acta.* 64 (16), 2775-2778.

Beers M. H. and Berkow R. (1999) The Merck manual of diagnosis and therapy. Merck & Co. Inc. *www.merck.com/pubs/mmanual/.*

Bennetto H. P. and Caldin E. F. (1971) Kinetics of solvent exchange and ligand substition reactions of metal ions in relation to structural properties of the solvent. *Journal of the Chemical Society (A)*, 2198.

Benz M., Brune A., and Schink B. (1998) Anaerobic and aerobic oxidation of ferrous iron at neutral pH by chemoheterotrophic nitrate-reducing bacteria. *Arch Microbiol.* 169, 159-165.

Bernard C. and Serieys J.-M. (1986) Déferrisation -Démanganisation biologique des eaux souterraines in situ. *L'Eau, l'Industrie, les Nuisances.* 99 (Mars), 44-46.

Braester C. and Martinell R. (1988) The Vyredox and Nitredox methods of in situ treatment of groundwater. *Water Science and Technology.* 20 (3), 149-163.

Bruno J., Stumm W., Wersin P., and Brandenberg F. (1992a) On the influence of carbonate in mineral dissolution: I. The thermodynamics and kinetics of hematite dissolution in bicarbonate solutions at T = 25°C. *Geochimica et Cosmochimica Acta.* 56, 1139-1147.

Bruno J., Wersin P., and Stumm W. (1992b) On the influence of carbonate in mineral dissolution: II. The solubility of $FeCO_3(s)$ at 25°C and 1 atm total pressure. *Geochimica et Cosmochimica Acta.* 56, 1149-1155.

Buerge I. J. (1999) Influence of pH, organic ligands, and mineral surfaces on the reduction of chromium(VI) by iron(II). Doctoral thesis. Swiss Federal Institute of Technology, Zürich.

Buerge I. J. and Hug S. J. (1999) Influence of mineral surfaces on Chromium(VI) reduction by Iron(II). *Environmental Science and Technology.* 33 (23), 4285-4291.

Burns R. G. and Burns V. M. (1979) Manganese Oxides. In: *Review in Mineralogy*, Vol. 6 (ed. R. G. Burns), pp. 1-47.

Charlet L., Silvester E., and Liger E. (1998) N-compound reduction and actinide immobilisation in surficial fluids by Fe(II): the surface >Fe(III)OFe(II)OH species as major reductant. *Chemical Geology.* 151, 85-93.

Clarke E. T., Loeppert R. H., and Ehrman J. M. (1985) Crystallization of iron oxides on calcite surfaces in static systems. *Clays and Clay Minerals.* 33 (2). 152-158.

Comans R. N. J. and Middelburg J. J. (1987) Sorption of trace metals on calcite: Applicability of the surface precipitation model. *Geochimica et Cosmochimica Acta.* 51, 2587-2591.

Cornell R. M. and Schwertmann U. (1996) *The iron oxides. Structure, properties, reactions, occurence and uses*. VCH. Weinheim.

Cotton F. A., Wilkinson G., and Gaus P. L. (1987) *Basic inorganic chemistry*. John Wiley & Sons. New York.

Coughlin B. R. and Stone A. T. (1995) Nonreversible adsorption of divalent metal ions (Mn^{II}, Co^{II}, Ni^{II}, Cu^{II} and Pb^{II}) onto goethite: Effects of acidification, Fe(II) addition, and piccolinic acid addition. *Environmental Science and Technology.* 29, 2445-2455.

Davies S. H. R. and Morgan J. J. (1989) Manganese(II) oxidation kinetics on metal oxide surfaces. *Journal of Colloids and Interface Science.* 129 (1), 63-77.

Davis J. A., Fuller C. C., and Cook A. D. (1987) A model for trace metal sorption processes at the calcite surface: adsorption of Cd^{2+} and subsequent solid solution formation. *Geochimica et Cosmochimica Acta.* 51, 1477-1490.

Davison W. and Seed G. (1983) The kinetics of the oxidation of ferrous iron in synthetic and natural waters. *Geochimica et Cosmochimica Acta.* 47, 67-69.

Diem D. and Stumm W. (1984) Is dissolved Mn^{2+} being oxidized by O_2 in absence of Mn-bacteria or surface catalysts? *Geochimica et Cosmochimica Acta.* 48, 1571-1573.

Dove P. M. and Hochella Jr. M. F. (1993) Calcite precipitation mechanisms and inhibition by orthophosphate: *In situ* observation by Scanning Force Microscopy. *Geochimica et Cosmochimica Acta.* 57, 705-714.

Dromgoole E. L. and Walter L. M. (1990) Iron and manganese incorporation into calcite: effect of growth kinetics, temperature and solution chemistry. *Chemical Geology.* 81, 311-336.

Duff M. C. and Amrhein C. (1996) Uranium(VI) adsorption on goethite and soil in carbonate solutions. *Journal of Soil Science Society of America.* 60, 1393-1400.

Dzombak D. A. and Morel F. M. M. (1990) *Surface complexation modeling hydrous ferric oxide.* Wiley. New York.

Emerson D. and Moyer C. (1997) Isolation and characterization of novel iron-oxidizing bacteria that grow at circumneutral pH. *Applied and Environmental Microbiology.* 63 (12), 4784-4792.

Emmenegger L. (1999) Light-induced redox cycling of iron in lakes. Doctoral Thesis. Swiss Federal Institute of Technology, Zürich.

Emmenegger L., King D. W., Sigg L., and Sulzberger B. (1998) Fe(II) Oxidation kinetics in an Eutrophic Swiss Lake. *Environmental Science and Technology.* 32, 2990-2996.

European Commission. (2000) Opinion of the Scientific Comittee on Food on the tolerable upper intake level of manganese. Health & Consumer Protection Directorate-General. Brussels.

European Union. (1998) Richtlinie 98/83/EG des Rates.

Faust S. D. and Aly O. M. (1998) *Chemistry of water treatment.* Ann Arbor Press, Inc. Chelsea, Michigan.

Fenter P., Geissbühler P., Di Masi E., Srajer G., Sorensen L. B., and Sturchio N. C. (2000) Surface speciation of calcite observed in situ by high-resolution X-ray reflectivity. *Geochimica et Cosmochimica Acta.* 64 (7), 1221-1228.

Fisler D. K. and Cygan R. T. (1999) Diffusion of Ca and Mg in calcite. *American Mineralogist.* 84, 1392-1399.

Franklin M. L. and Morse J. W. (1983) The interaction of manganese(II) with the surface of calcite in dilute solutions and seawater. *Marine Chemistry.* 12, 241-254.

Friedl G. (1995) Die Mineralogie des Mangankreislaufs in eutrophen Seen: Eine Untersuchung mit EXAFS-Spektroskopie. Doctoral thesis. Swiss Federal Institute of Technology, Zürich.

Friedl G., Wehrli B., and Manceau A. (1997) Solid phases in the cycling of manganese in eutrophic lakes: New insight from EXAFS spectroscopy. *Geochimica et Cosmochimica Acta.* 61 (2), 275-290.

Ghosh M. M., Connor J. T. O., and Engelbrecht R. S. (1966) Precipitation of iron in aerated ground waters. *Journal of the Sanitary Engineering Division.* 92, 199-213.

Gibbs C. R. (1976) Characterization and application of Ferrozine iron reagent as a ferrous iron indicator. *Analytical Chemistry.* 48 (8, July), 1197-1201.

Graham R. D., Hannam R. J., and Uren N. C. (1988) Manganese in soils and plants. *Developments in Plant and Soil Sciences;* Adelaïde, Australia. Kluwer Academic Publishers, Dordrecht, The Netherland.

Greenwood N. N. and Earnshaw A. (1990) *Chemie der Elemente.* VCH. Weinheim.

Griffith R. (2002) Health and Age. Novartis Foundation for Gerontology. *www.healthandage.com/index.jsp.*

Grossi P. R., Sparks, D. L., Ainsworth, C. C. (1994) Rapid kinetics of Cu(II) adsorption/desorption on goethite. *Environment Science and Technology.* 28 (8), 1422-1429.

Groth P., Bühring F., Dannöhl R., Liessfeld R., Olthoff R., and Rott U. (1988) Unterirdische Enteisenung und Entmanganung -ein Statusbericht. *Das Gas- und Wasserfach.* 129 (5), 321-339.

Hachiya K., Sasaki M., Ikeda T., Mikami N., and Yasunaga T. (1984) Static and kinetic studies of adsorption-desorption of metals ions on a γ-Al_2O_3 surface. Kinetics study by means of pressure-jump technique. *Journal of Physical Chemistry.* 88, 27-31.

Haderlein S. B. and Pecher K. (1998) Pollutant reduction in heterogeneous Fe(II)/Fe(III) systems. In: *Kinetics and mechanisms of reaction at the mineral/water interface*, pp. 342-357. American Chemical Society. Washington, DC.

Hallberg R. O. and Martinell R. (1976) Vyredox - In situ purification of ground water. *Ground Water.* 14 (2), 88-93.

Hao O. J., Davis A. P., and Chang P. H. (1991) Kinetics of manganese(II) oxidation with chlorine. *Journal of Environmental Engineering.* 117 (3), 358-375.

Hauck S., Benz M., Brune A., and Schink B. (2001) Ferrous iron oxidation by denitrifying bacteria in profundal sediments of a deep lake (Lake Constance). *FEMS Microbiology Ecology.* 37, 127-134.

Hem J. D. and Lind C. J. (1983) Nonequilibrium models for predicting forms of precipitated manganese oxides. *Geochimica et Cosmochimica Acta.* 47, 2037-2046.

Heron G., Crouzet C., Bourg A. C. M., and Christensen T. H. (1994) Speciation of Fe(II) and Fe(III) in contaminated aquifer sediments using chemical extraction techniques. *Environmental Science and Technology.* 28, 1698-1705.

Hoffmann U. and Stipp S. L. S. (2001) The behavior of Ni^{2+} on calcite surfaces. *Geochimica et Cosmochimica Acta.* 65 (22), 4131-4139.

Hofstetter T. B. (1999) Reduction of polynitroaromatic compounds by reduced iron species - coupling biogeochemical processes with pollutant transformation. Doctoral thesis. Swiss Federal Institute of Technology, Zürich.

Hofstetter T. B., Heijman C. G., Haderlein S. B., Holliger C., and Schwarzenbach R. P. (1999) Complete reduction of TNT and other (poly)nitroaromatic compounds under iron reducing subsurface conditions. *Environmental Science and Technology.* 33 (9), 1479-1487.

Hoigné J. and Bader H. (1994) Kinetics of reactions of chlorine dioxide (OClO) in water - I. Rate constants for inorganic and organic compounds. *Water Research.* 28 (1), 45-55.

Hoigné J., Bader H., Haag W. R., and Staehelin J. (1985) Rate constants of reactions of ozone with organic and inorganic compounds in water - III Inorganic compounds and radicals. *Water Research.* 19 (8), 993-1004.

Huheey J. E. (1978) *Inorganic Chemistry. Principles of structure and reactivity.* Harper & Row. New York.

Jacobsen F., Holcman J., and Sehested K. (1998) Oxidation of manganese(II) by ozone and reduction of manganese(III) by hydrogen peroxide in acidic solution. *International Journal of Chemical Kinetics.* 30, 207-214.

Jeon B.-H., Dempsey B. A., Burgos W. D., and Royer R. A. (2001) Reactions of ferrous iron with hematite. *Colloids and Surfaces. A: Physiochemical and Engineering Aspects.* 191, 41-55.

Junta J. J. and Hochella Jr. M. F. (1994) Manganese(II) oxidation at mineral surfaces: A microscopic and spectroscopic study. *Geochimica et Cosmochimica Acta.* 58 (22), 4985-4999.

Katz J. L., Reick M. R., Herzog R. E., and Parsiegla K. I. (1993) Calcite growth inhibition by iron. *Langmuir.* 9, 1423-1430.

King W. (1998) Role of carbonate speciation on the oxidation rate of Fe(II) in aquatic systems. *Environmental Science and Technology.* 32, 2997-3003.

Klausen J. (1995) Abiotic redox transformations of aromatic nitro and amino compounds in suspensions of soil minerals. Doctoral thesis. Swiss Federal Institute of Technology, Zürich.

Klausen J., Tröber S. P., Haderlein S. B., and Schwarzenbach R. P. (1995) Reduction of substituted nitrobenzenes by Fe(II) in aqueous mineral suspensions. *Environmental Science and Technology.* 29, 2396-2404.

Knocke W. R., Benschoten J. E. V., Kearney M. J., Soborski A. W., and Reckhow D. A. (1991a) Kinetics of manganese and iron oxidation by potassium permanganate and chlorine dioxide. *Journal of the American Water Work Association.* 83 (6), 80-87.

Knocke W. R., Hamon J., and Thompson C. P. (1988) Soluble Manganese removal on oxide-coated filter media. *Journal of the America Water Work Association.* 80 (12), 65-70.

Knocke W. R., Occiano S. C., and Hungate R. (1991b) Removal of soluble manganese by oxide-coated filter media: Sorption rate and removal mechanism issues. *Journal of the America Water Work Association.* 83 (8), 64-69.

Kölle W. and Schneider B. H. (1992) Die unterirdische Wasseraufbereitung. *Neue DELIWA-Zeitschrift.* 43 (6), 272-278.

Kostka J. E. and Luther III G. W. (1994) Partitioning and speciation of solid phase iron in saltmarsh sediments. *Geochimica et Cosmochimica Acta.* 58 (7), 1701-1710.

Lahav N. and Bolt G. H. (1964) Self-diffusion of Ca^{45} into certain carbonate. *Soil Science.* 97 (5), 293-299.

Langmuir D. (1997) *Aqueous environmental geochemistry.* Prentice-Hall, Inc. Upper Saddle River, New Jersey.

Laxen C. P. H. (1985) Trace metal adsorption/coprecipitation on hydrous ferric oxide under realistic conditions. *Water Research.* 19 (10), 1229-1236.

Letterman R. D. (1999) *Water quality and treatment. A handbook of community water supplies.* Mc Graw Hill. New York.

Liger E., Charlet L., and Capellen P. V. (1999) Surface catalysis of uranium(VI) reduction by iron(II). *Geochimica et Cosmochimica Acta.* 63 (19/20), 2939-2955.

Loeppert R. H. and Hossner L. R. (1984) Reactions of Fe^{2+} and Fe^{3+} with calcite. *Clays and Clay Minerals.* 32 (3), 213-222.

Loeppert R. H., Hossner L. R., and Amin P. K. (1984) Formation of ferric oxyhydroxides from ferrous and ferric perchlorate. *Soil Science Society of America Journal.* 48, 677-683.

Logager T., Holcman J., Sehested K., and Pedersen T. (1992) Oxidation of ferrous ions by ozone in acidic solutions. *Inorganic Chemistry.* 31, 3523-3529.

Lorens R. B. (1981) Sr, Cd, Mn and Co distribution coefficient in calcite as a function of calcite precipitation rate. *Geochimica et Cosmochimica Acta.* 45, 553-561.

Lovley D. R. (1987) Organic matter mineralization with the reduction of ferric iron: a review. *Journal of Geomicrobiology.* 5, 375-399.

Lovley D. R. and Phillips E. J. P. (1988) Novel mode of microbial energy metabolism: Organic carbon oxidation coupled to dissimilatory reduction of iron and manganese. *Applied and Environmental Microbiology.* 54 (6), 1472-1480.

Luther III G. W. (1990) The frontier-molecular-orbital theory approach in geochemical processes. In: *Aquatic chemical kinetics* (ed. W. Stumm), pp. 173-198. John Wiley & Sons, Inc. New york.

Mandernack K. W., Fogel M. L., Tebo B. M., and Usui A. (1995a) Oxygen isotope analyses of chemically and microbially produced manganese oxides and manganates. *Geochimica Cosmochimica Acta.* 59 (21), 4409-4425.

Mandernack K. W., Post J., and Tebo B. M. (1995b) Manganese mineral formation by bacterial spores of the marine Bacillus, strain SG-1: Evidence for the direct oxidation of Mn(II) to Mn(IV). *Geochimica et Cosmochimica Acta.* 59, 4393-4408.

Marcus Y. (1994) A simple empirical model describing the thermodynamics of hydration of ions of widely varying charges, sizes, and shapes. *Biophysical Chemistry.* 51, 111-127.

Mengis H. (1984) Vyredox - Eine wirtschaftliche Methode zur Enteisenung und Entmanganung von Grundwasser. *Gas-Wasser-Abwasser.* 9, 595-598.

Mengis H. (2002) Referenzanlagen (Vyredox). Gebrüder Mengis, AG. Personal communication.

Mettler S., Abdelmoula M., Hoehn E., Schoenenberger R., Weidler P. G., and Von Gunten U. (2001) Characterization of iron and manganese precipitates from an in situ ground water treatment plant. *Ground Water.* 39 (6), 921-930.

Meyer H. J. (1984) Influence of impurities on growth rate of calcite. *Journal of Crystal Growth.* 66, 639-646.

Meyerhoff R. (1995) Anwendungsmöglichkeiten der in situ-Aufbereitung von eisen- und manganhaltigen Grundwässern. *Aktuelle Entwicklungen in der Wasserversorgung aus Grund- und Oberflächenwässern;* Stuttgart. 149-162.

Millero F. J. and Miguel I. (1989) Effect of ionic strength and ionic interactions on the oxidation of Fe(II). *Journal of Solution Chemistry.* 18 (6), 585-599.

Millero F. J., Sotolongo S., and Izaguirre M. (1987) The oxidation kinetics of Fe(II) in seawater. *Geochimica Cosmochimica Acta.* 51 (4), 793-801.

Möller P. and Sastri C. S. (1974) Estimation of the number of surface layers of calcite involved in Ca-^{45}Ca isotopic exchange with solution. *Zeitschrift für Physikalische Chemie. Neue Folge.* 89, 80-87.

Morgan J. J. (1967) Chemical equilibria and kinetics properties of manganese in natural waters. *Rudolfs Research Conference Rutgers;* New Brunswik, New Jersey.

Mouchet P. (1992a) From conventional to biological removal of iron and manganese in France. *American Water Works Association* (April), 158-167.

Mouchet P. (1992b) Iron and manganese removal in France: from conventional to biological process. Degrémont. Rueil-Malmaison, F-92508.

Mozeto A. A., Fritz P., and Reardon E. J. (1984) Experimental observations on carbon isotope exchange in carbonate-water systems. *Geochimica et Cosmochimica Acta.* 48, 495-504.

Müller R. (1998) Einfluss elektromagnetischer Felder auf Kristallisationsvorgänge: Praktische Anwendungen in der Schlammbehandlung von Kläranlagen und in Trinkwassersystemen. Doctoral thesis; Eidgenössische Technische Hochschule. Zürich.

Murray J. W., Balistrieri L. S., and Paul B. (1984) The oxidation state of manganese in marine sediments and ferromanganese nodules. *Geochimica et Cosmochimica Acta.* 48, 1237-1247.

Murray J. W., Dillard J. G., Giovanoli R., Moers H., and Stumm W. (1985) Oxidation of Mn(II): initial mineralogy, oxidation state and ageing. *Geochimica et Cosmochimica Acta.* 49, 463-470.

O'connor J. T. (1971) Iron and manganese. In: *Water quality and treatment. A handbok of public water supplies* (ed. A. W. W. Association). McGraw-Hill. New York.

Olthoff R. (1986) Die Enteisenung und Entmanganung vom Grundwasser im Aquifer. Doctoral thesis. Universität Hannover, Hannover.

Olthoff R. (1987) Erkenntnisse zur Errichtung und zum Betrieb einer unterirdischen Wasseraufbereitungsanlage- Eisen und Mangan. *bbr.* 4, 158-165.

Paquette J. and Reeder R. J. (1995) Relationship between surface structure, growth mechanism, and trace element incorporation. *Geochimica et Cosmochimica Acta.* 59 (4), 1995.

Piper D. Z., Basler J. R., and Bischoff J. L. (1984) Oxidation state of marine manganese nodules. *Geochimica et Cosmochimica Acta.* 48, 2347-2355.

Postma D. (1981) Formation of siderite and vivianite and the pore-water composition of a recent bog sediment in Denmark. *Chemical Geology.* 31, 225-244.

Reckhow D. A., Knocke W. R., and Kearney M. J. (1991) Oxidation of iron and manganese by ozone. *Ozone Science and Engineering.* 13, 675-695.

Reeder R. J. (1996) Interaction of divalent cobalt, zinc, cadmium, and barium with the calcite surface during layer growth. *Geochimica et Cosmochimica Acta.* 60 (9), 1543-1552.

Reeder R. R. (1983) Carbonates: Mineralogy and Chemistry. In *Reviews in Mineralogy*, Vol. 11. Mineralogical Society of America.

Rey J.-P. and Schindler B.-A. (1984) Essai de déferrisation d'eau de fond par la méthode Vyredox à La Neuveville (BE). *Gas-Wasser-Abwasser.* 9, 599-603.

Rietra R. P. J., Hiemstra T., and Riemsdijk W. H. V. (2001) Interaction between calcium and phosphate adsorption on goethite. *Environmental Science and Technology.* 35 (16), 3369-3374.

Rimstidt D., Balog A., and Webb J. (1998) Distribution of trace elements between carbonate minerals an aqueous solutions. *Geochimica et Cosmochimica Acta.* 62 (11), 1851-1863.

Rosenberg P. E. (1963) Subsolidus relations in the system $CaCO_3$-$FeCO_3$. *American Journal of Science.* 261, 683-690.

Rott U. and Meyerhoff R. (1993) Wasseraufbereitung im Untergrund. *Neue Deliwa Zeitschrift.* 3, 102-105.

Rott U. and Meyerhoff R. (1994) Physical, chemical and biological processes in consequence of in-situ treatment of groundwater. *Groundwater Quality Management;* Tallinn. IAHS. 439-447.

Rundell B. D. and Randtke S. J. (1987) In-situ groundwater treatment for iron and manganese: fundamental, practical and economic consideration. *Annual Conference. American Water Works Association;* Kansas City, MO. American Water Works Association. 513-533.

Schosseler P. M., Wehrli B., and Schweiger A. (1999) Uptake of Cu^{2+} by the calcium carbonates vaterite and calcite as studied by continuous wave (CW) and pulse electron paramagnetic resonance. *Geochimica et Cosmochimica Acta.* 63 (13/14), 1955-1967.

Schultz C. A. and Grundl T. J. (2000) pH dependance on the reduction rate of a 4-Cl-nitrobenzene by Fe(II)/montmorillonite systems. *Environment Science and Technology.* 34 (17), 3641-3648.

Schwertmann U. and Cornell R. M. (2000) *Iron oxides in the laboratory. Preparation and characterization.* Weinheim.

Sigg L. and Stumm W. (1994) *Aquatische Chemie.* VDF / B. G. Teubner Verlag. Zürich, Stuttgart.

Singer P. C. and Stumm W. (1970) Acidic mine drainage: The rate-determining step. *Science.* 167, 1121-1123.

Sivan O., Erel Y., Mandler D., and Nishri A. (1998) The dynamic redox chemistry of iron in the epilimnion of Lake Kinneret (Sea of Galilee). *Geochimica et Cosmochimica Acta.* 62 (4), 556-576.

Søgaard E. G., Aruna R., Abraham-Peskir J., and Koch C. B. (2001) Conditions for biological precipitation of iron by *Gallionella ferruginea* in a slightly polluted ground water. *Applied Geochemistry.* 16, 1129-1137.

Stipp S. and Hochella Jr. M. F. (1991) Structure and bonding environment at the calcite surface as observed with X-ray photoelectron spectroscopy (XPS) and low energy electron diffraction (LEED). *Geochimica et Cosmochimica Acta.* 55, 1723-1736.

Stipp S. L., Hochella M. F., Parks G. A., and Leckie J. O. (1992) Cd^{2+} uptake by calcite, solid-state diffusion, and the formation of solid-solution: Interface processes observed with near-surface sensitive techniques (XPS, LEED, and AES). *Geochimica et Cosmochimica Acta.* 56, 1941-1954.

Stipp S. L. S., Konnerup-Madsen J., Franzreb K., Kulik A., and Mathieu H. J. (1998) Spontaneous movement of ions through calcite at standard temperature and pressure. *Nature.* 396, 356-359.

Stookey L. L. (1970) Ferrozine - A new spectrophotometric reagent for iron. *Analytical Chemistry.* 42 (7), 779-81.

Straub K. L., Benz M., and Schink B. (2001) Iron metabolism in anoxic environments at near neutral pH. *FEMS Microbiology Ecology.* 34, 181-186.

Stumm W. (1992) *Chemistry of the solid-water interface. Processes at the mineral-water and particle-water interface in natural systems*. John Wiley and Sons, Inc. New york.

Stumm W. and Lee G. F. (1961) Oxygenation of ferrous iron. *Industrial and Engineering Chemistry*. 53 (2), 143-146.

Stumm W. and Morgan J. J. (1996) *Aquatic Chemistry*. John Wiley & Sons, Inc. New York.

Sung W. and Morgan J. (1980) Kinetics and products of ferrous iron oxygenation in aqueous systems. *Environmental Science and Technology*. 14, 561-568.

Sung W. and Morgan J. J. (1981) Oxidative removal of Mn(II) from solution catalysed by the γ-FeOOH (lepidocrocite) surface. *Geochimica and Cosmochimica Acta*. 45, 2377-2383.

Tamura H., Goto K., and Nagayama M. (1976) The effect of ferric hydroxide on the oxygenation of ferrous ions in neutral solutions. *Corrosion Science*. 16, 197-207.

Tamura H., Kawamura S., and Hagayama M. (1980) Acceleration of the oxidation of Fe^{2+} ions by Fe(III)-oxyhydroxides. *Corrosion Science*. 20, 963-971.

Tebo B. M., Ghiorse W. C., Waasbergen L. G. V., Siering P. L., and Caspi R. (1997) Bacterially mediated mineral formation: insights into manganese(II) oxidation from molecular genetic and biochemical studies. In: *Geomicrobiology: Interactions between Microbes and Minerals*, Vol. 35 (ed. K. H. N. J. F. Banfield), pp. 226-265. Mineralogical Society of America. Blacksburg, Virginia.

Temmam M., Paquette J., and Vali H. (2000) Mn and Zn incorporation into calcite as function of chloride aqueous concentration. *Geochimica et Cosmochimica Acta*. 64 (14), 2417-2430.

Urrutia M. M., Roden E. E., Fredrickson J. K., and Zachara J. M. (1998) Microbial and surface chemistry controls on reduction of synthetic Fe(III) oxide minerals by the dissimilatory iron-reducing bacterium Shewanella alga. *Geomicrobiology*. 15, 269-291.

USEPA. (2001) Office of Water. National secondary drinking water regulations. In *Code of Federal Regulation* pp. 612-614.

Valezquez S. F. and Du J. T. (1994) Derivation of the reference dose for manganese. In: *Risk of Essential Elements* (ed. C. O. A. W. Mertz, and S. S. Olin). International Life Sciences Institute Press. Washington D. C.

Van Beek C. G. E. M. (1985) Experience with underground water treatment in the Netherlands. *Water Supply.* 3(1), 1-11.

Van Benschoten J. E., Lin W., and Knocke W. R. (1992) Kinetik modeling of manganese(II) oxidation by chlorine dioxide and potassium permanganate. *Environmental Science and Technology.* 26, 1326-1333.

Van Geen A., Robertson, A. P., Leckie, J. O. (1994) Complexation of carbonate species at the goethite surface: Implications for adsorption of metal ions in natural waters. *Geochimica et Cosmochimica Acta.* 58 (9), 2073-2086.

Veizer J. (1983) Trace elements and isotopes in sedimentary carbonates. In: *Carbonates: mineralogy and chemistry. Reviews in Mineralogy* (ed. R. J. Reeder), pp. 265-299. Mineralogical Society of America. Washington D. C.

Venema P. (1996) Charging and ion adsorption behaviour of different iron (hydr)oxides. Doctoral thesis. Wageningen Agricultural University. Wageningen, The Netherlands.

Villalobos M. and Leckie J. O. (2000) Carbonate adsorption on goethite under closed and open CO_2 conditions. *Geochimica et Cosmochimica Acta.* 64 (22), 3787-3802.

Villalobos M. and Leckie J. O. (2001) Surface complexation modeling and FTIR study of carbonate adsorption to goethite. *Journal of Colloid and Interface Science.* 235 (1), 15-32.

Villalobos M., Trotz M. A., and Leckie J. O. (2001) Surface complexation modeling of carbonate effects on the adsorption of Cr(VI), Pb(II) and U(VI) on goethite. *Environmental Science and Technology.* 35 (19), 3849-3856.

Von Gunten U. (2002) Ozonation of drinking water: Part I. Oxidation kinetics and product formation. *Water Research.* submitted.

Von Gunten U., Salhi E., Hoehn E., Haderlein S., and Stengel C. (2002) In situ deferrisation of groundwater: a field study. *Ground Water.* submitted.

Von Gunten U. and Schneider W. (1991) Primary products of the oxygenation of the iron(II) at an oxic-anoxic boundary: nucleation, aggregation and aging. *Journal of Colloids and Interface Science.* 145 (1), 127-139.

Von Gunten U. and Zobrist J. (1993) Biogeochemical changes in groundwater-infiltration systems: Column studies. *Geochimica et Cosmochimica Acta.* 57, 3895-3906.

Von Langen P. J., Johnson K. S., Coale K. H., and Elrod V. A. (1997) Oxidation kinetics of manganese(II) in seawater at nanomolar concentrations. *Geochimica et Cosmochimica Acta.* 61 (23), 4945-4954.

Wajon J. E., Ho G.-E., and Murphy P. J. (1985) Rate of precipitation of ferrous ion and formation of mixed iron-calcium carbonates by naturally occurring carbonate minerals. *Water Research.* 7, 831-837.

Waldburger J. (1994) Unterrirdische Grundwasseraufbereitungsanlage. Planung und Bau. *GWA.* 10, 828-834.

Wehrli B. (1990) Redox reactions of metal ions at mineral surfaces. In: *Aquatic Chemical Kinetics* (ed. W. Stumm), pp. 311-37. Wiley. New York.

Wehrli B., Friedl G., and Manceau A. (1995) Reaction rates and products of manganese oxidation at the sediment-water interface. In: *ACS Advances in Chemistry Series 244*, pp. 111-138. Washington DC.

Wehrli B., Ibric S., and Stumm W. (1990) Adsorption kinetics of vanadyl (IV) and chromium to aluminium oxide: evidence for a two step mechanism. *Colloids and Surfaces.* 51, 77-89.

Weidler P. G., Hug S. J., Wetche T. P., and Hiemstra T. (1998) Determination of growth rates of (100) and (110) faces of synthetic goethite by scanning force microscopy. *Geochimica et Cosmochimica Acta.* 62 (21/22), 3407-3412.

Weirich D. (2000) Influence of organic ligands on the adsorption of copper, cadmium, and nickel on goethite. Doctoral thesis. Swiss Federal Institute of Technology, Zürich.

Wersin P. (1990) The Fe(II)-CO_2-H_2O system in anoxic natural waters: equilibria and surface chemistry. Doctoral thesis. Swiss Federal Institute of Technology, Zürich.

Wersin P., Höhener P., Giovanoli R., and Stumm W. (1991) Early diagenetic influences on iron transformations in a fresh-water lake sediment. *Chemical Geology.* 90, 233-252.

Winja H. and Schulthess C. P. (2001) Carbonate adsorption mechanism on goethite studied with ATR-FTIR, DRIFT, and proton coadsorption measurements. *Journal of the Soil Science Society of America.* 65, 324-330.

Xu N., Hochella Jr. M. F., Brown Jr. G. E., and Parks G. A. (1996) Co(II) sorption at the calcite-water interface: I. X-ray photoelectron spectroscopic study. *Geochimica et Cosmochimica Acta.* 60 (15), 2801-2815.

Zachara J. M., Cowan C. E., and Resch C. T. (1991) Sorption of divalent metals on calcite. *Geochimica et Cosmochimica Acta.* 55, 1549-1562.

Zachara J. M., Cowan C. E., and Resch C. T. (1993) Metal cation/anion adsorption on calcium carbonate: implications to metal ion concentrations in groundwater. In: *Metals in Groundwater* (ed. M. P. H. Allen, D. Brown), pp. 37-71. Lewis Publishers. Chelsea, MI.

Zachara J. M., Kittrick J. A., Dake L. S., and Harsh J. B. (1989) Solubility and surface spectroscopy of zinc precipitates on calcite. *Geochimica et Cosmochimica Acta.* 53, 9-19.

Zachara J. M., Kittrick J. A., and Harsh J. B. (1988) The mechanism of Zn^{2+} adsorption on calcite. *Geochimica et Cosmochimica Acta.* 52, 2281-2291.

Zachara J. M., Smith S. C., and Fredrickson J. K. (2000) The effect of biogenic Fe(II) on the stability and sorption of $Co(II)EDTA^{2-}$ to goethite and a subsurface sediment. *Geochimica et Cosmochimica Acta.* 64 (8), 1345-1362.

Zhang Y., Charlet L., and Schindler P. W. (1992) Adsorption of protons, Fe(II) and Al(III) on lepidocrocite (γ-FeOOH).

Zienkiewicz A. W. (1984) Removal of iron and manganese from ground water with Vyredox. *Second international conference on ground water quality research;* Stillwater, Oklahoma. University Printing Services. 74-77.

Curriculum Vitae

SUZANNE B. METTLER
born November 17th, 1968 in Geneva, SWITZERLAND.

1975 – 1984	Elementary school in Troinex and Pinchat, Switzerland
1984 – 1988	High school at Collège de Staël, Carouge, Switzerland
1988 – 1989	University of Heidelberg, Germany. (Theology, German)
1989 – 1993	Temporary jobs (e.g. survey engineer consulting)
1991 – 1997	Diploma in Environmental Sciences, Swiss Federal Institute of Technology (ETH), Zürich, Switzerland.
1994 – 1995	Internship, Electrowatt Ingenieurunternehmung AG, Zürich, Switzerland (Waste incineration).
1997 – 2000	Teaching Assistant, Department of Chemistry and Department of Environmental Sciences, ETH Zürich.
1997 – 2002	Doctoral Studies, Swiss Federal Institute of Environmental Sciences and Technlogy (EAWAG) and Swiss Federal Institute of Technology (ETH) Zürich, Switzerland.